Jet Propulsion Laboratory
California Institute of Technology

Exoplanet Exploration Program

Technology Plan Appendix

2016

Nick Siegler
NASA Exoplanet Exploration Program Chief Technologist
Jet Propulsion Laboratory, California Institute of Technology

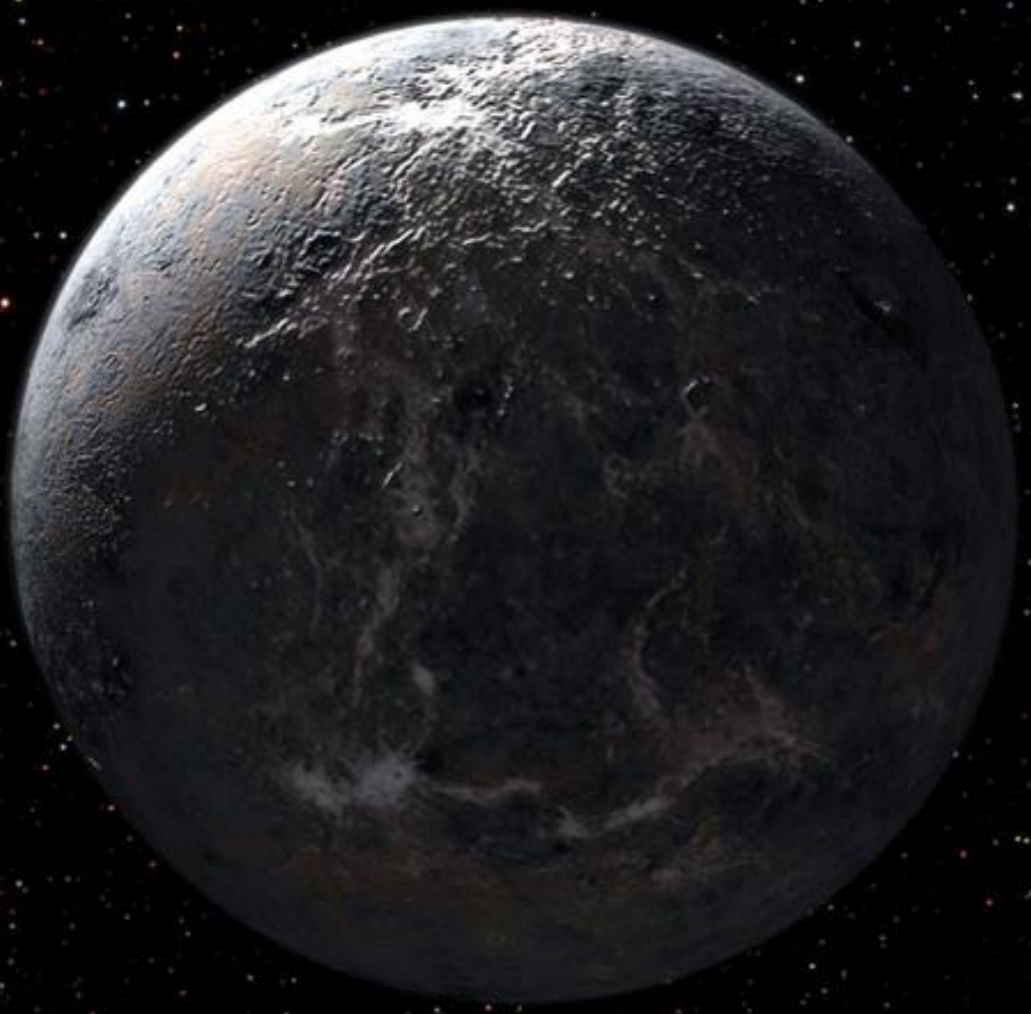

JPL Document No: 1513240

Acknowledgment

Important contributions were made from Doug Hudgins (NASA ExEP Program Scientist and TDEM Program Officer at NASA HQ), Phillip Stahl (NASA-MSFC), Matthew Bolcar (NASA-GSFC), Remi Soummer (Space Telescope Science Institute), Bernie Rauscher (NASA-GSFC), Stuart Shaklan (JPL), Rhonda Morgan (JPL), Doug Lisman (JPL), Bertrand Mennesson (JPL), Rick Demers, (JPL), Ilya Poberezhskiy (JPL), and Steve Warwick (Northrop Grumman).

This document has been cleared for public release (CL#16-0271).

This research was carried out at the Jet Propulsion Laboratory, California Institute of Technology, under a contract with the National Aeronautics and Space Administration.

Reference herein to any specific commercial product, process, or service by trade name, trademark, manufacturer, or otherwise, does not constitute or imply its endorsement by the United States Government, or the Jet Propulsion Laboratory, California Institute of Technology.

© 2016 California Institute of Technology. Government Sponsorship acknowledged.

APPROVALS

Approved by:

_____ _____

Dr. Nicholas Siegler
Program Chief Technologist
Exoplanet Exploration Program
NASA/Jet Propulsion Laboratory
California Institute of Technology

Date

_____ _____

Dr. Gary Blackwood
Program Manager
Exoplanet Exploration Program
NASA/Jet Propulsion Laboratory
California Institute of Technology

Date

Concurred by:

_____ _____

Dr. Douglas Hudgins
Program Scientist for Programs
Exoplanet Exploration Program
Science Mission Directorate
NASA Headquarters

Date

CONTENTS

A INTRODUCTION 1
A.1 Program Goals 1
A.2 Previously Funded Efforts 2
A.3 Technology Gap Prioritization Criteria 4
B CORONAGRAPH TECHNOLOGY NEEDS 6
B.1 Coronagraph Architectures (CG-2) 11
B.1.1 Hybrid Lyot Coronagraph 14
B.1.2 Shaped Pupil Coronagraphs 16
B.1.3 Hybrid Pupil Plane Masks: Apodized Pupil Lyot Coronagraph (APLC) / Shaped Pupil Coronagraph (SPC) 17
B.1.4 Phase-Induced Amplitude Apodization Coronagraph (PIAA) 18
B.1.5 Vector Vortex Masks 20
B.1.6 Visible Nulling Coronagraphs 22
B.2 Large Aperture Mirrors (CG-1) 23
B.2.1 Large Monolithic Mirrors 23
B.2.2 Large Segmented Mirrors 25
B.3 Ultra-Low Noise, Large-Format Detectors 26
B.3.1 Visible Detectors (CG-8) 27
B.3.2 Infrared Detectors (CG-9) 28
B.4 Segment Phasing Sensing and Control (CG-6) 29
B.5 Telescope Vibration Control (CG-7) 30
B.6 Deformable Mirrors (CG-3) 31
B.7 Low-Order Wavefront Sensing & Control (CG-5) 33
B.8 Post-data Processing (CG-4) 34
C STARSHADE TECHNOLOGY NEEDS 36
C.1 Optical Performance Demonstration and Model Validation (S-2) 39
C.1.1 Contrast vs Suppression 45
C.2 Solar Glint (S-1) 46
C.3 Petal Deployment (S-6) 47
C.4 Lateral Formation Flying Sensing (S-3) 48
C.5 Inner Disk Deployment (S-5) 50
C.5.1 Micrometeoroid Holes 52
C.6 Petal Shape (S-4) 53
D PRIORITIZATION 54
E CONCLUSION 55
F DOCUMENT CHANGE LOG 56
G ACRONYMS 57
H REFERENCES 59

A INTRODUCTION

The purpose of this Technology Development Plan Appendix is to guide near-term (1–5 year) technology development for future space observatories related to NASA's Exoplanet Exploration Program (ExEP or Program). A long-term goal of the Program is a New Worlds Mission, such as that envisaged by the 2010 Decadal Survey *New Worlds, New Horizons in Astronomy and Astrophysics* (NWNH)[1]—a mission capable of directly imaging terrestrial planets in the habitable zones (HZs) of stars in the solar neighborhood, and measuring their spectra to search for signs of life. Such a mission will require extreme starlight suppression and new technology developments.

In the near term, this technology development should also enable other missions, such as probe-class (life-cycle cost less than $1B) missions with compelling science that is essential to understanding the birth and evolution of planetary systems and the conditions that lead to life in the Universe.

This Appendix lists the enabling technology needs of the ExEP that support the efforts of NASA's Astrophysics Division to respond to the 2010 Decadal Survey recommendations. This response is captured in the Astrophysics Division Implementation Plan (updated in 2014).[2] The greatest emphasis is placed on technologies that enable direct imaging and characterization of Earth-like planets around Sun-like stars.

The two technology needs sections (Sections B and C) define the technology gaps and quantify, when possible, the difference between expected performance requirements and the current state of art. These sections also summarize recent key developments and communicate, when known, what is planned in the near future. Alternative technologies are also presented, as appropriate.

This 2016 Appendix includes a broader set of gaps for coronagraph technology than past appendices, which narrowly focused on the coronagraph instrument. Because achieving contrast ratios better than 10^{-10} represents a tremendous engineering challenge, it is no longer sufficient to assess the technology requirements of the coronagraph instrument in isolation. Instead, the coronagraph and its performance must be approached as part of an integrated telescope assembly, with noise sources and component requirements that extend beyond the coronagraph instrument. The coronagraph technology gap presented in this Appendix therefore reflects a more systems-level approach. Note that, while the ExEP will track all the listed technology gaps, a number of them are cross-cutting and important to all three Astrophysics Division science themes (Cosmic Origins, Physics of the Cosmos, and the ExEP).

Not all the technologies to fly a New Worlds mission listed here are currently solicited under the Research Opportunities in Space and Earth Sciences (ROSES) Strategic Astrophysics Technology (SAT) Program (ROSES 2015, Appendix D.8). The specific technologies that are solicited under the SAT Program are described in the call for proposals. In general, an effort is made to address the tallest tent poles within the limits of available funding. This Appendix communicates overall technology needs to aid scientists, engineers, and technology managers in academia, industry, research labs, and NASA centers in deciding which technology areas they are best suited to develop.

A.1 Program Goals

The 2010 Decadal Survey recommended the creation of a New Worlds Technology Development Program "to lay the technical and scientific foundation for a future mission to study nearby Earth-like planets" (pp. 215–217). The Technology Development for Exoplanet Missions (TDEM) element of the SAT Program was established to support the maturation of key technologies that will enable NASA to achieve that goal. For both cost and technical readiness reasons, infrared interferometry is currently a lower-priority technology area for a New Worlds mission. Conversely, previous work under the auspices of the SAT/TDEM Program, as well as the results of the Exo-Coronagraph (Exo-C) and Exo-Starshade

(Exo-S) probe studies,[3] which concluded in 2015, demonstrate that both coronagraphs and external occulters (starshades) are scientifically meritorious and their technology needs feasible for a future New Worlds mission.

The NASA Astrophysics Division response to the Decadal Survey's recommendations (2014 Astrophysics Implementation Plan Update) describes a path for implementing the Wide-Field Infrared Survey Telescope (WFIRST),[4] the top large-scale mission recommendation and the next strategic mission after the James Webb Space Telescope (JWST). It also recommended concept development for future strategic missions for consideration by the 2020 Decadal Survey.

At the time of the release of this Appendix, NASA is preparing to enter the formulation phase of an implementation of the WFIRST mission, which makes use of one of two 2.4-m-diameter Astrophysics Focused Telescope Assets (AFTA) donated to NASA by another Federal agency. A high-contrast exoplanet coronagraph with wavefront control has been baselined as part of the planned WFIRST-AFTA implementation. The development of technologies for a WFIRST-AFTA coronagraph instrument is the subject of a separate technology plan developed by the WFIRST-AFTA Study Office, which was published in early 2014. That WFIRST-AFTA technology plan describes many of the coronagraph technology needs called out in this Appendix. However, a WFIRST-AFTA coronagraph is not expected to directly image exo-Earths. Consequently, this Appendix describes technology devoted to instrument performance on missions capable of directly imaging and characterizing Earth-like planets and future (non-AFTA) NWNH missions.

Many of the exo-Earth detection technology needs described here are intended to support the exoplanet science objectives of the two NASA Astrophysics Division 2020 Decadal Survey large mission concept studies—the Large Ultra-Violet Optical InfraRed (LUVOIR) Surveyor and the Habitable Exoplanet Imaging (HabEx) Mission. Both telescope designs are expected to be driven by exo-Earth detection and characterization capabilities, and we assume that, unlike the case with WFIRST-AFTA, the coronagraph engineering requirements will drive the telescope requirements to meet the challenging contrast requirements. Both mission concept studies will commence in 2016 with approximately three-year durations. The studies will be led by Science and Technology Definition Teams (STDTs) and supported by NASA field centers for engineering and design work. Since their specific architectures are unknown at this time, we present the technologies we anticipate will be needed for the range of architectures likely to be considered by either mission.

NASA's ExEP supports activities that contribute to the maturation of key technologies that will enable these exoplanet mission concepts. The Program funds and facilitates experiments and analyses selected by NASA HQ through yearly solicitations issued through the omnibus ROSES NASA Research Announcement (NRA). The Program also provides support in the form of infrastructure, modeling, expertise, and test facilities to selected Principal Investigators (PIs).

As a part of ROSES, NASA currently funds technology development through the Astrophysics Research and Analysis (APRA) solicitation and the SAT/TDEM solicitations. APRA covers low Technology Readiness Level (TRL) technology research while SAT/TDEM covers maturation of mid-range TRL technologies. This two-stage approach supports the advancement of technology envisaged by the 2010 Decadal Survey. All the previous tasks funded under the 2009, 2010, 2012, 2013, and 2014 SAT/TDEM solicitations are listed in **Table 1**. Abstracts of funded APRA awards can be found online.[5]

A.2 Previously Funded Efforts

Table 1 lists the previously funded TDEM awards, grouped by research area. Final Milestone Reports for completed TDEMs as well as Milestone Whitepaper Reports for those still in process are posted on the ExEP Technology website.[6]

Table 1: TDEM awards for calls from 2009, 2010, 2012, 2013, and 2014. Each award nominally provides two years of funding although more years can be proposed as well.

Year	PI	Institution	Proposal Title
CORONAGRAPH STARLIGHT-SUPPRESSION DEMONSTRATIONS			
2009	Mark Clampin	NASA Goddard Space Flight Center	Visible Nulling Coronagraph Technology Maturation: High Contrast Imaging and Characterization of Exoplanets
2009	Olivier Guyon	Univ. of Arizona	Phase-Induced Amplitude Apodization Coronagraphy Development and Laboratory Validation
2009	John Trauger	JPL/Caltech	Advanced Hybrid Lyot Coronagraph Technology for Exoplanet Missions
2010	Olivier Guyon	Univ. of Arizona	Advances in Pupil Remapping (PIAA) Coronagraphy: improving Bandwidth, Throughput and Inner Working Angle
2010	Richard Lyon	NASA Goddard Space Flight Center	Compact Achromatic Visible Nulling Coronagraph Technology Maturation
2010	Jagmit Sandhu	JPL/Caltech	Visible Nulling Coronagraph (VNC) Technology Demonstration Program
2010	Eugene Serabyn	JPL/Caltech	Demonstrations of Deep Starlight Rejection with a Vortex Coronagraph
2013	Richard Lyon	NASA Goddard Space Flight Center	Segment Aperture Nulling Coronagraphy
2014	Matthew Bolcar	NASA Goddard Space Flight Center	Next Generation Visible Nulling Coronagraph
2014	Eugene Serabyn	JPL/Caltech	Broadband Light Rejection with the Optical Vortex Coronagraph
STARSHADE STARLIGHT-SUPPRESSION DEMONSTRATIONS			
2009	N. Jeremy Kasdin	Princeton Univ.	Starshades for Exoplanet Imaging and Characterization: Key Technology Development
2010	N. Jeremy Kasdin	Princeton Univ.	Verifying Deployment Tolerances of an External Occulter for Starlight Suppression
2012	Suzanne Casement	Northrop Grumman Aerospace Systems	Starshade Stray Light Mitigation through Edge Scatter Modeling and Sharp-Edge Materials Development
2012	Tiffany Glassman	Northrop Grumman Aerospace Systems	Demonstration of Starshade Starlight-Suppression Performance in the Field
2012	N. Jeremy Kasdin	Princeton Univ.	Optical and Mechanical Verification of an External Occulter for Straight Suppression
2013	Webster Cash	Univ. of Colorado	Development of Formation Flying Sensors
2013	N. Jeremy Kasdin	Princeton Univ.	Formation Flying for External Occulters
2014	Mark Thomson	JPL/Caltech	Optical Shield for the Starshades Inner Disc Subsystem

Year	PI	Institution	Proposal Title
WAVEFRONT SENSING AND CONTROL OF SCATTERED STARLIGHT			
2009	John Krist	JPL/Caltech	Assessing the Performance Limits of Internal Coronagraphs Through End-to-End Modeling
2009	M. Charley Noecker	Ball Aerospace	Advanced Speckle Sensing for Internal Coronagraphs and Methods of Isolating Exoplanets from Speckles
2010	Paul Bierden	Boston Micromachines	MEMS Deformable Mirror Technology Development for Space-Based Exoplanet Detection
2010	Michael Helmbrecht	Iris AO	Environmental Testing of MEMS Deformable Mirrors for Exoplanet Detection
2010	N. Jeremy Kasdin	Princeton Univ.	Integrated Coronagraph Design and Wavefront Control using Two Deformable Mirrors
OTHER TECHNOLOGIES			
2009	Donald Figer	Rochester Inst. of Technology	A Photon-Counting Detector for Exoplanet Missions
2010	Stuart Shaklan	JPL/Caltech	Coronagraph Starlight Suppression Model Validation: Coronagraph Milestone Report #3
2013	Eduardo Bendek	NASA Ames Research Center	Enhanced Direct Imaging Exoplanet Detection with Astrometric Mass Determination

A.3 Technology Gap Prioritization Criteria

The technology gaps for coronagraph and starshades are listed in **Table 3** and **Table 4**, respectively, in order of priority based on a set of criteria proposed by the ExEP Program Chief Technologist:

- Impact
- Urgency
- Trend

This criteria has been presented to the Exoplanet Program Analysis Group (ExoPAG) and its Executive Committee for review and feedback.

The higher the number within each criterion, the higher the contribution to the prioritization. Results of the prioritization effort can be found in Section D. These criteria are subjectively defined in Table 2:

Table 2: Technology gap prioritization criteria

Impact:	4: Critical and key enabling technology - required to meet mission concept objectives; without this technology, applicable missions would not launch
	3: Highly desirable - not mission-critical, but provides major benefits in enhanced science capability, reduced critical resources need, and/or reduced mission risks; without it, missions may launch, but science or implementation would be compromised
	2: Desirable - not required for mission success, but offers significant science or implementation benefits; if technology is available, would almost certainly be implemented in missions
	1: Minor science impact or implementation improvements; if technology is available would be considered for implementation in missions
Urgency:	4: In time for the Decadal Survey (2019); not necessarily at some TRL but reduced risk by 2019
	3: Possible launch date < 10 yr (< 2025)
	2: Possible launch date < 15 yr (< 2030)
	1: Possible launch date > 15 yr (> 2030)
Trend:	4: Very large perceived risk of not being ready in time: (a) no ongoing current efforts (b) little or no funding allocated
	3: Large perceived risk of not being ready in time: (a) others are working towards it but little results or their performance goals are very far from the need, (b) funding unclear, or (c) time frame not clear
	2: Medium perceived risk of not being ready in time: (a) others are working towards it with encouraging results or their performance goals will fall short from the need, (b) funding may be unclear, or (c) time frame not clear
	1: Small perceived risk of not being ready in time: (a) others are actively working towards it with encouraging results or their performance goals are close to need, (b) it's sufficiently funded, and (c) time frame clear and on time

B CORONAGRAPH TECHNOLOGY NEEDS

Exo-Earth detections will require starlight suppression that exceeds the current best ground-based performances by several orders of magnitude (**Figure 1**). Coronagraphs come in numerous architectures, each with its own strengths and weaknesses with respect to telescope aperture (monolithic, segmented), obscuration (unobscured, obscured by secondary mirror and its support struts), and wavefront error stability disturbances (e.g., line-of-sight jitter, telescope vibration, thermal gradients).

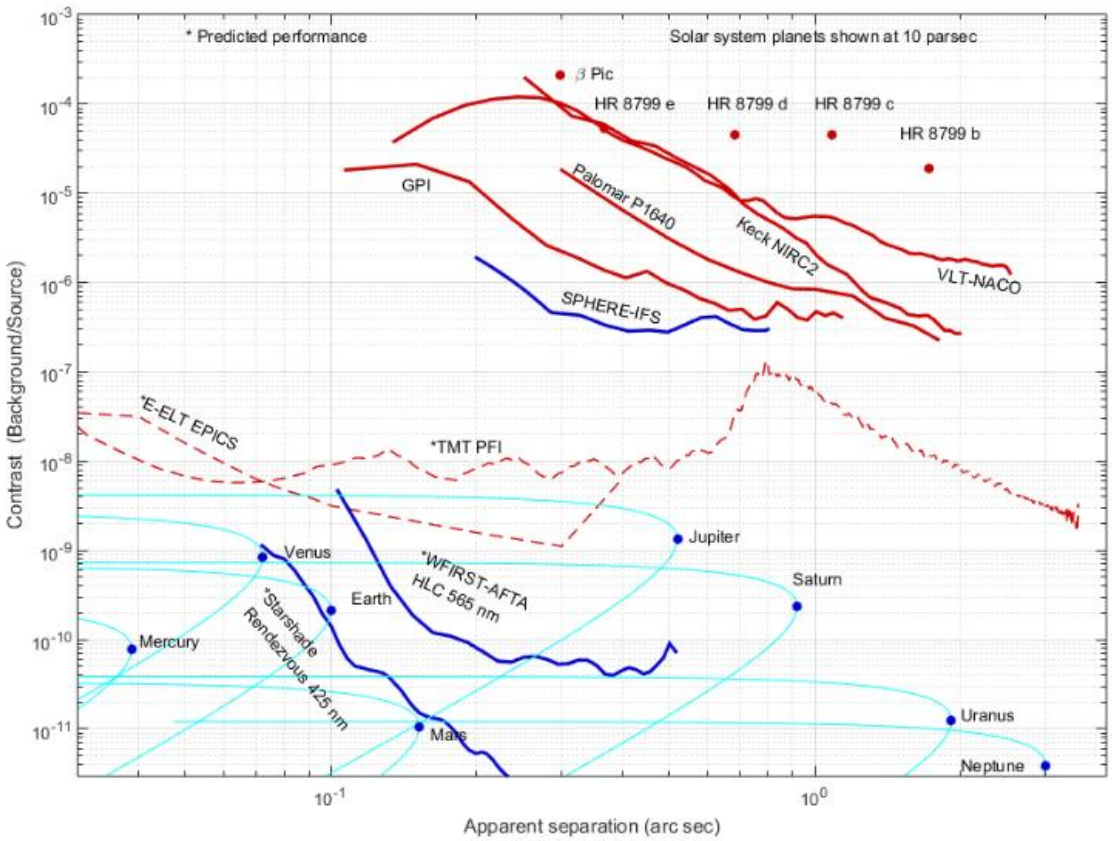

Figure 1: Contrast ratio versus apparent angular separation. The filled red circles indicate the direct imaging of young, self-illuminous gas giants in the near-infrared imaged by ground-based telescopes. The filled blue circles represent the planets of the Solar System placed 10 pc away, for reference. The solid red curves are current performance (SPHERE is temporarily in blue) in the near-infrared[7 8 9]; the dashed red curves are predicted performance of new or future coronagraphs on ground-based observatories. The predicted WFIRST-AFTA curve is at 565 nm and includes a factor of 10 contrast improvement from expected post-data processing gains. The predicted Starshade curve from the Exo-S study assumes a 34-m-diameter starshade flying 49,500 km away from a 2.4-m-diameter telescope at 425 nm. Contrast is based on a 5 sigma level; no post-processing contrast reduction was assumed. The starshade curve's profile requires vetting from the community.

The removal of diffraction is only part of the coronagraph's design goals. It must also remove the scattered light observed in the focal plane, appearing as speckles, due to imperfections in the optics. This is done through the control of deformable mirrors (Section B.4). As a final step, post-processing of the data images (Section B.8) further improves the effective contrast.

The most important recent development in coronagraph technology is the baselining of a coronagraph instrument on the WFIRST-AFTA space mission—it will be the first high-contrast coronagraph with wavefront control to fly in space. While both the Hubble Space Telescope (HST) and the JWST have onboard coronagraphs, neither have the corresponding wavefront sensing and control required to achieve better than 10^{-8} contrast sensitivity and close inner working angles (IWA) (< 3 λ/D). WFIRST will also have the first ultra-low noise visible detector and deformable mirrors to reach low-Earth orbit or beyond. When successful, the WFIRST-AFTA coronagraph will represent the state of the art.

The obscured pupil of the WFIRST-AFTA telescope (due to its on-axis secondary mirror and support struts) introduces complex diffraction features that are absent in designs with unobscured pupils. Consequently, the WFIRST-AFTA coronagraph architectures and optics have started the era of obscured pupil coronagraph design and demonstration that will serve on-axis and segmented telescope aperture designs of the future.

The ExEP coronagraph technology needs (**Table 3**) target the next generation coronagraphs beyond WFIRST-AFTA, which will be capable of directly imaging exo-Earths around Sun-like stars in the solar neighborhood. As mentioned earlier, the list of coronagraph technology needs has been broadened to include more of the telescope system since all contributing noise sources must be accounted for if contrasts of 10^{-10} are to be reached at 10^{-11} stability levels.

The nine coronagraph technology gaps listed in **Table 3** fall into four categories shown in Figure 2:

1. **Contrast** – the ability to block the on-axis light from a target star creating a dark region in the science focal plane where the faint off-axis reflected light of a planet could be detected.
2. **Contrast Stability** – the ability to sense and control the incoming starlight maintaining the desired contrast long enough for full science integration.
3. **Detection Sensitivity** – the ability to detect extraordinarily few photons dispersed across many pixels of a spectrograph and not be lost in the detector's read-out noise.
4. **Angular Resolution** – the ability to probe terrestrial regions around stars (e.g., the habitable zone) requires a minimum aperture size. The more distant the star, the larger the telescope aperture will need to be to probe these regions. Large apertures provide not just improved angular resolution but also improved sensitivity to faint objects (sharper point spread functions), higher throughput, lower integration times, and the capability to probe habitable zones of stars further away.

Note, funding levels in the near term are not expected to allow parallel technology advancement in all areas. Hence, prioritization based on programmatic considerations as well as impact, urgency, and trend will be taken into consideration in the selection of SAT/TDEM investigations that address the needs listed in **Table 3**

Figure 2: The four categories of coronagraph technology needs (in yellow font) to directly image and characterize exo-Earths around Sun-like stars.

Table 3: ExEP Coronagraph Technology Gap List. Gaps are listed in order of their prioritization scores according to the criteria in Section A.3.

ID	Title	Description	Current Capabilities	Needed Capabilities
CG-2	**Coronagraph Architecture**	Coronagraph optics and architecture that suppress diffracted starlight by a factor of $\leq 10^{-9}$ at visible and infrared wavelengths	6×10^{-10} raw contrast at 10% bandwidth across angles of 3-15 λ/D demonstrated with a linear mask and an unobscured pupil in a static vacuum lab environment (Hybrid Lyot) $< 8.8\times10^{-9}$ raw contrast at 10% bandwidth across angles of 4-11 λ/D demonstrated with a circularly-symmetric mask and obscured pupil in a static vacuum lab env't (WFIRST)	Coronagraph masks and optics capable of creating circularly symmetric dark regions in the focal plane enabling raw contrasts $\leq 10^{-9}$, IWA ≤ 3 λ/D, throughput ≥ 10%, and bandwidth ≥ 10% on obscured/ segmented pupils in a simulated dynamic vacuum environment.

ID	Title	Description	Current Capabilities	Needed Capabilities
CG-1**	**Large Aperture Primary Mirrors**	Large monolith and multi-segmented mirrors that meet tight surface figure error and thermal control requirements at visible wavelengths	Monolith: 3.5-m sintered SiC with <3 µm SFE (Herschel) 2.4-m ULE with ~10 nm SFE (HST) Depth: Waterjet cutting is TRL 9 to 14", but TRL 3 to >18". Fused core is TRL 3; slumped fused core is TRL 1. Segmented: 6 DOF, 1-m class SiC and ULE, < 20 nm SFE, and < 5 nm wavefront stability over 4 hrs with thermal control (100 nm/K material stability with 1 mK thermal control)	Aperture: 4–12 m; SFE < 10 nm rms (wavelength coverage 400–2500 nm) Wavefront stability better than 10 pm rms per wavefront control time step Segmented apertures leverage 6 DOF or higher control authority meter-class segments for wavefront control Environmentally tested
CG-8*	**Ultra-Low Noise, Large-Format Visible Detectors**	Low-noise visible detectors for faint exoplanet characterization with an Integral Field Spectrograph	1k×1k silicon EMCCD detectors provide dark current of 8×10^{-4} e-/px/sec; effective read noise < 0.2e- rms (in EM mode) after irradiation when cooled to 165.15K (WFIRST) 4k×4k EMCCD fabricated but still under development	Effective read noise < 0.1e- rms; CIC < 3×10^{-3} e-/px/fram; dark current < 10^{-4} e-/px/sec tolerant to a space radiation environment over mission lifetime ≥ 2k×2k format
CG-9**	**Ultra-Low Noise, Large Format Near-Infrared Detectors**	Near-infrared wavelength (900 nm to 2.5 µm), extremely low noise detectors for exo-Earth spectral characterization with Integral Field Spectrographs	HgCdTe photodiode arrays have read noise $\lesssim$ 2 e- rms with multiple nondestructive reads; dark current < 0.001 e-/s/pix; very radiation tolerant (JWST) HgCdTe APDs have dark current ~10–20 e-/s/pix, RN << 1 e- rms, and < 1k×1k format Cryogenic (superconducting) detectors have essentially no read noise nor dark current; radiation tolerance is unknown	Read noise << 1 e- rms, dark current noise < 0.001 e-/pix/s, in a space radiation environment over mission lifetime ≥ 2k×2k format

ID	Title	Description	Current Capabilities	Needed Capabilities
CG-6$^{\Delta}$	**Segment Phasing Sensing & Control**	Multisegment large-aperture mirrors require phasing and rigid-body sensing and control of the segments to achieve tight static and dynamic wavefront errors at visible wavelengths	6 nm rms rigid body positioning error and 49 nm rms stability (JWST error budget) SIM and non-NASA: nm accuracy and stability using laser metrology	Systems-level considerations to be evaluated but expect will require less than 10 pm accuracy and stability
CG-7$^{\Delta}$	**Telescope Vibration Control**	Isolation and damping of spacecraft and payload vibrational disturbances	80 dB attenuation at frequencies > 40 Hz (JWST passive isolation) Disturbance-free payload demonstrated at TRL 5 with 70 dB attenuation at "high frequencies" with 6-DOF low-order active pointing	Monolith: 120 dB end-to-end attenuation at frequencies >20 Hz Segmented: 140 dB end-to-end attenuation at frequencies > 40 Hz
CG-3*	**Deformable Mirrors**	Environment-tested, flight-qualified large-format deformable mirrors	Electrostrictive 64×64 DMs have been demonstrated to meet ≤ 10^{-9} contrasts and < 10^{-10} stability in a vacuum environment and 10% bandwidth; 48×48 DM passed random vibe testing	4 m primary: ≥ 96×96 DM 10 m primary: ≥ 128×128 DM Enable raw contrasts of ≤ 10^{-9} at ~20% bandwidth and IWA ≤ 3 λ/D Flight-qualified device and drive electronics (radiation hardened, environmentally tested, life-cycled including connectors and cables)
CG-5*	**Low-Order Wavefront Sensing & Control**	Sensing and control of line-of-sight jitter and low-order wavefront drift	< 0.5 mas rms per axis LOS residual error demonstrated in lab with a fast-steering mirror attenuating a 14 mas LOS jitter and reaction wheel inputs; ~100 pm rms sensitivity of focus (WFIRST) Higher low-order modes sensed to 10–100 nm WFE rms on ground-based telescopes	Sufficient fast line-of-sight jitter (< 0.5 mas rms residual) and slow thermally-induced (≤ 10 pm rms sensitivity) WFE sensing and control to maintain closed-loop < 10^{-9} raw contrast with an obscured/segmented pupil and simulated dynamic environment

ID	Title	Description	Current Capabilities	Needed Capabilities
CG-4*	**Post-data Processing Algorithms and Techniques**	Post-data processing techniques to uncover faint exoplanet signals from residual speckle noise at the focal-plane detector	Few 100× speckle suppression has been achieved by HST and by ground-based AO telescopes in the NIR and in contrast regimes of 10^{-4} to 10^{-5}, dominated by phase errors.]	A 10-fold contrast improvement in the visible from 10^{-9} raw contrast where amplitude errors are expected to be important (or a demonstration of the fundamental limits of post-processing)

*Coronagraph technologies that will be advanced through WFIRST are funded elsewhere and not eligible for TDEMs.

[Δ] Systems-level technology need, mission design–dependent; proposals for funding are not requested under the TDEM program at this time.

** SAT proposals are accepted through the Cosmic Origins Program.

B.1 Coronagraph Architectures (CG-2)

Specialized coronagraph optics suppress the on-axis starlight and allow the off-axis planet light to transmit through the instrument with a high contrast between the planet and star. A continuing program to advance the performance of masks, apodizers, and beam-shaping optics to better than WFIRST coronagraph performance requirements (< 10^{-8}, 3 λ/D, 10% bandwidth) is needed. This should include designs to improve inner working angles (< 3 λ/D), contrast performance (≤ 10^{-10}), bandwidth (≥ 10%), and core PSF throughput (≥ 10%), in dynamic vacuum environments on both obscured and segmented apertures.

Various architectures of coronagraphs have achieved contrasts in laboratory tests that begin to approach these requirements.[10] Demonstrated state-of-art results with unobscured pupils at monochromatic, 2%, 10%, and 20% bandwidths are shown in **Figure 3–6**. The deepest narrowband (2% bandwidth; **Figure 4**) simulated starlight suppression achieved is 1.2×10^{-10} raw contrast at 800 nm across angles of 3-16 λ/D; it was demonstrated in the High-Contrast Imaging Testbed (HCIT) with a Hybrid Lyot Coronagraph (HLC) linear mask on an unobscured pupil in a static vacuum lab environment.[11,12,13] "Static" demonstration here and throughout implies no intentionally introduced line of sight errors or other wavefront disturbances, while "dynamic" refers to the experiments where at least some of these disturbances expected on orbit were simulated in the testbed.

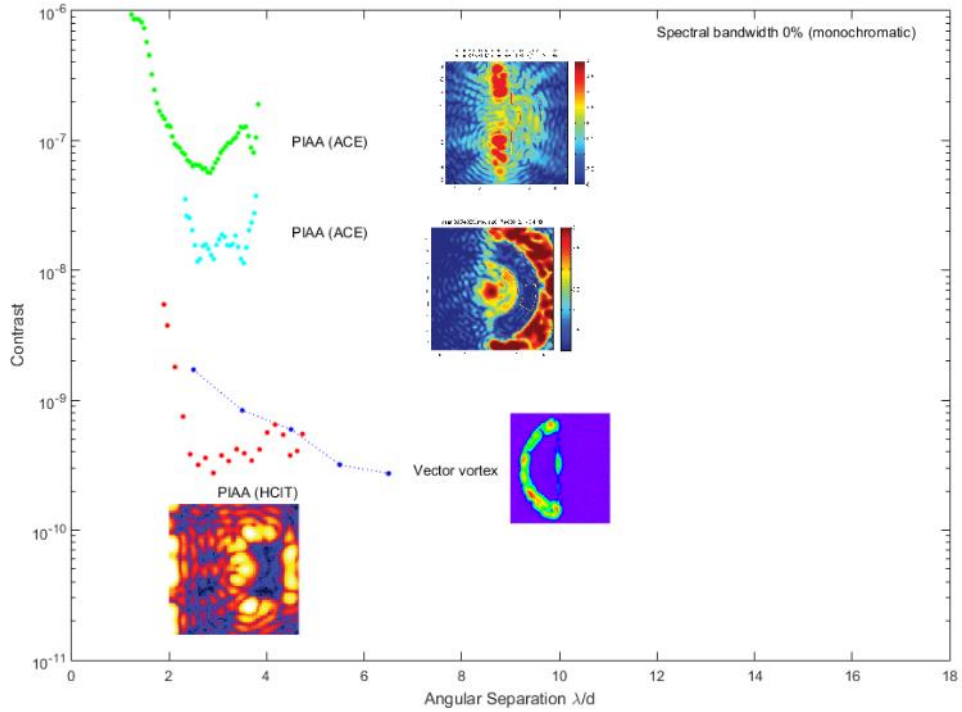

Figure 3: Coronagraph laboratory demonstrations using monochromatic spectral bandwidth with visible light.

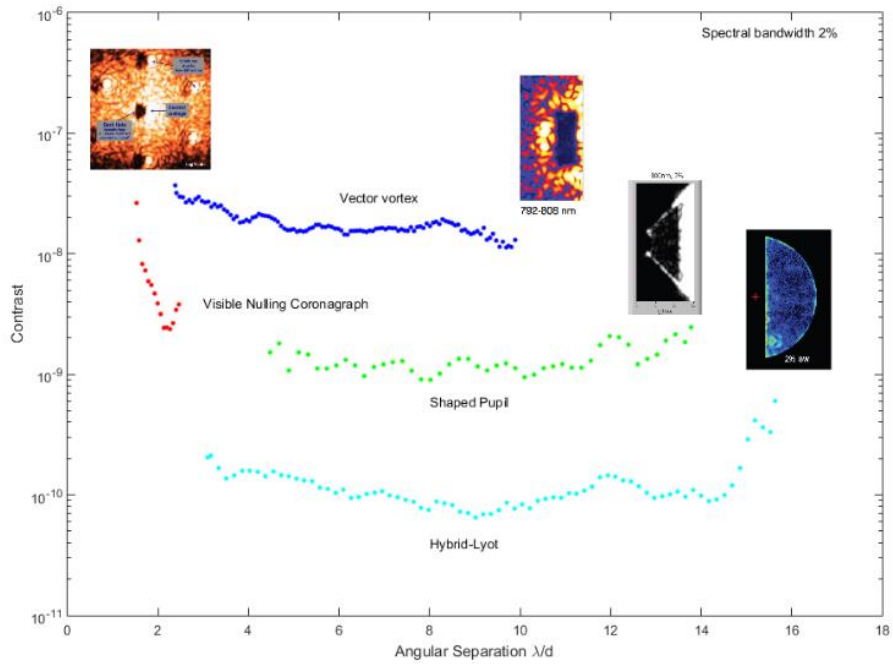

Figure 4: Coronagraph laboratory demonstrations using 2% bandwidth visible light.

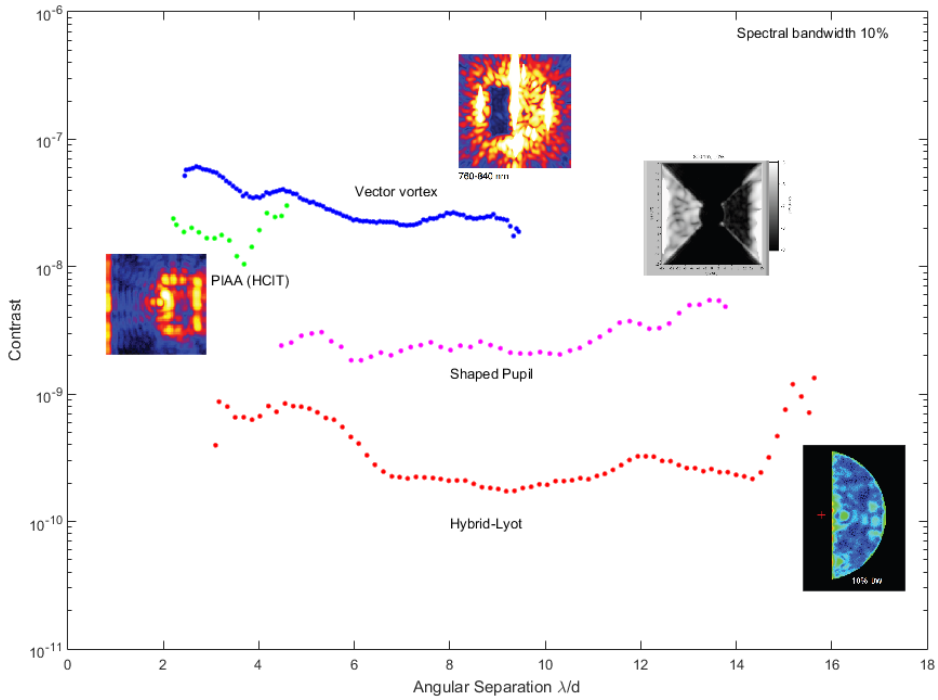

Figure 5: Coronagraph laboratory demonstrations using 10% bandwidth visible light.

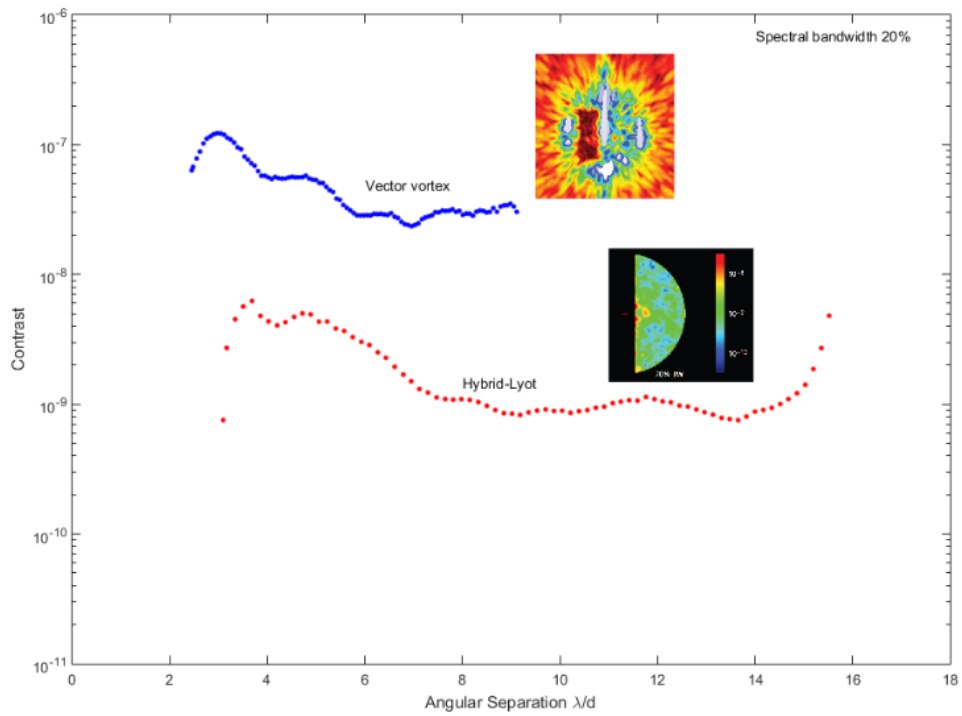

Figure 6: Coronagraph laboratory demonstrations using 20% spectral bandwidth visible light.

Demonstrated coronagraph contrast results as a function of optical bandwidth are shown in **Figure 7**.

The next level of difficulty for internal coronagraphs is working with obscured apertures. Pupil obscurations occur in on-axis design due to the secondary mirror and its structural supports. Pupil obscurations further diffract light making deep contrasts more challenging.

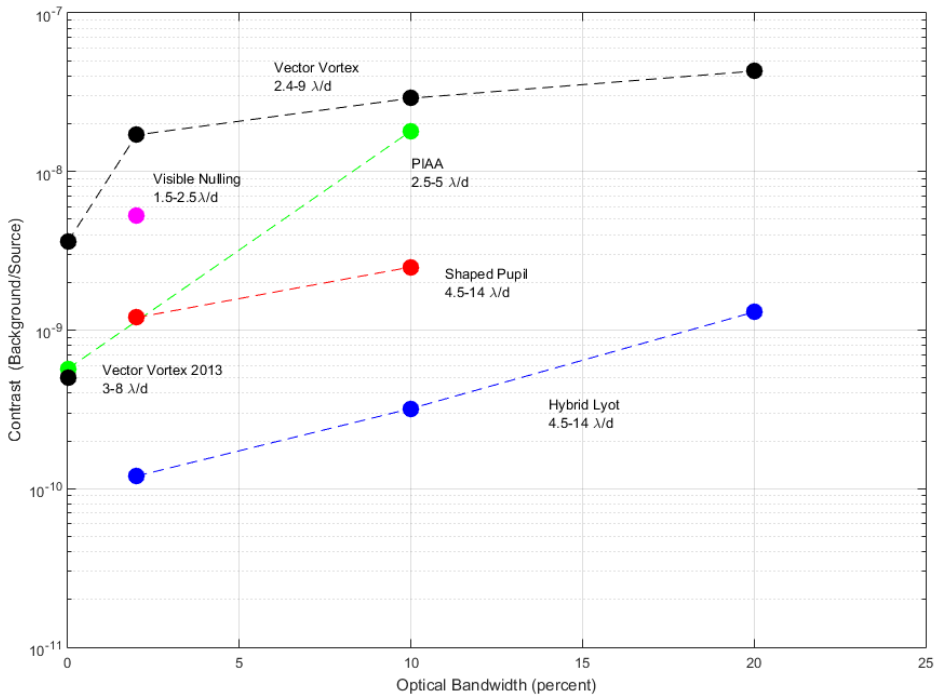

Figure 7: Demonstrated coronagraph contrast as a function of bandwidth. All experiments were conducted with unobscured pupils and demonstrated in vacuum chambers under static environment conditions at 800 nm to near-IR light.

B.1.1 Hybrid Lyot Coronagraph

The HLC is a modification of the classical Lyot coronagraph that consists of an occulting mask located at an intermediate focal plane followed by a Lyot mask at a subsequent pupil plane. In the HLC, the focal plane mask is a combination of a patterned amplitude modulator (usually a metal coating such as nickel) with an overlaid phase modulator (a patterned dielectric coating), hence the "hybrid". Both are simultaneously optimized to provide an optimal combination of IWA, contrast, bandwidth, and throughput with the wavelength-dependent characteristics of the materials included. The hybrid occulter provides better performance over broad spectral bands than previous amplitude-only designs.

John Trauger (JPL), with a 2009 TDEM award, demonstrated mean raw contrasts of 6×10^{-10} with a 10% bandwidth in a 284 $(\lambda/D)^2$ field extending from 3–15 λ/D (**Figure 5**). Raw contrasts of 1.3×10^{-9} were demonstrated with a 20% bandwidth (**Figure 6**). These results are the current state of the art for unobscured pupils.

Like other coronagraphic techniques, the performance of the HLC is seriously degraded by obscurations in the telescope, especially asymmetric ones such as the WFIRST secondary support struts. As part of the design optimization process, the deformable mirrors (DMs) were used to alter the wavefront to reduce the diffractive effects of these structures, resulting in a pattern of nominal actuator settings with relatively large strokes of ~0.2 µm peak-to-valley. The DM patterns are an inherent part of diffraction

control and would be used whether there were aberrations in the system or not. The occulter and DM patterns were optimized to provide reduced sensitivity to pointing errors assuming a pointing jitter as high as 1.6 mas rms per axis.[14]

The large DM strokes introduce significant mid-spatial-frequency wavefront variations that, while beneficial to achieving good overall contrast when combined with the occulter and Lyot stop, resulted in a degraded planet point spread function (PSF) with 4.3% total "PSF core" throughput (accounting for all instrument and telescope optical losses, as well as degraded Strehl).

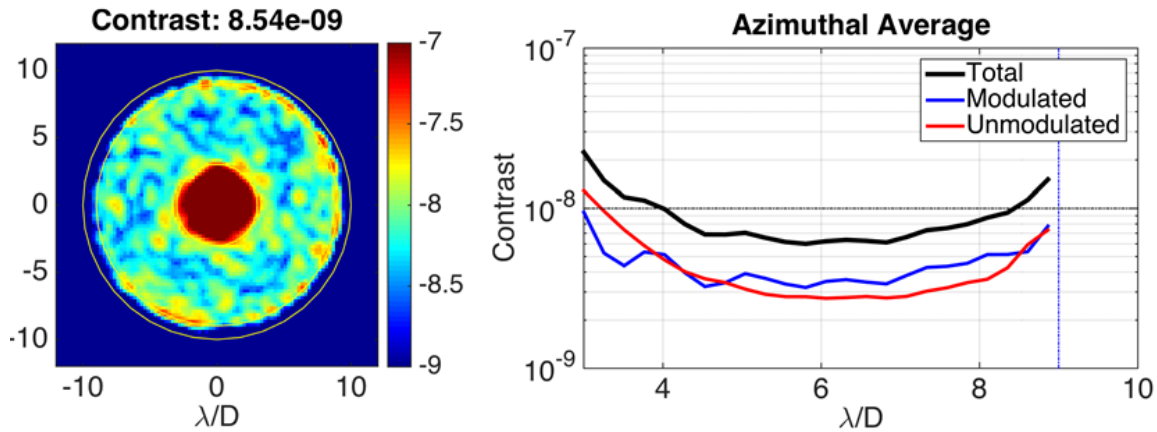

Figure 8: (Left) Focal-plane image from the WFIRST HLC testbed in HCIT-2 at JPL. (Right) Contrast curve achieved mean contrast of 8.5×10^{-9} at 10% broadband centered at 550 nm across a 3–9 λ/D dark hole (WFIRST; Milestone #5). The 10% bandwidth was achieved using five 2% bands averaged together; calibration uncertainty is ±2%.

Circularly symmetric masks (**Figure 9**) have been fabricated for the first time as a part of the WFIRST technology development and performance demonstrations with the simulated AFTA obscured pupil have already achieved a contrast of 8.5×10^{-9} at 550 nm with 10% bandwidth between angles 3 to 9 λ/D, as shown in **Figure 8** (WFIRST coronagraph technology Milestone #5). Wavefront control was achieved with two DMs and the dark hole region covered full annulus: 360 degrees.

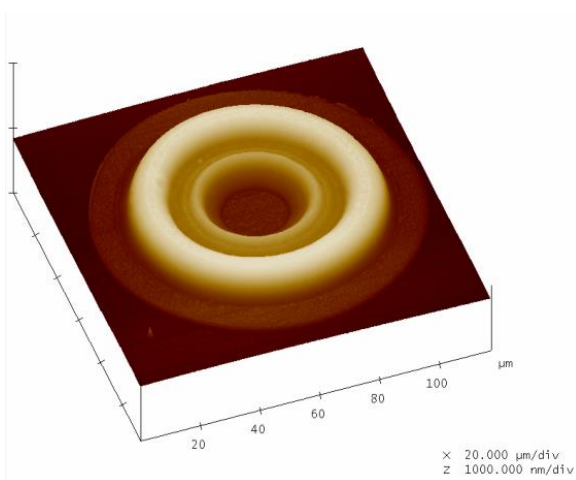

Figure 9: The WFIRST HLC focal plane mask is only 100 µm in diameter, composed of a flat nickel base layer and a super-imposed patternable dielectric layer made of PMGI (polymethylglutarimide). The mask was fabricated by e-beam lithography at JPL's Microdevices Laboratory.

B.1.2 Shaped Pupil Coronagraphs

A shaped pupil (SP) is a binary pupil-plane mask that blocks or passes light in different regions of the pupil and thus shapes the PSF of the coronagraph in the image plane to create dark, high-contrast regions. A field stop is usually placed at a focus between the SP and the camera to limit the dynamic range seen at the camera.

Early SP designs were optimized in 1D for open telescope apertures and could be manufactured as free-standing, through-hole masks. New designs for obstructed telescope apertures, such as that for WFIRST, require a 2-D optimization that produces non-freestanding opaque regions that must be placed on a substrate[15] (**Figure 10**). Ghosting and dispersion discouraged a transmissive glass substrate from being used for AFTA, so the new SPs act in reflection off a thick silicon wafer with aluminum-coated regions that reflect light and black silicon regions that absorb light. The main challenges of manufacturing reflective SPs are achieving sufficiently low specular reflectance in the black silicon regions and not damaging the aluminum sections during the cryogenic etching process that creates black silicon.

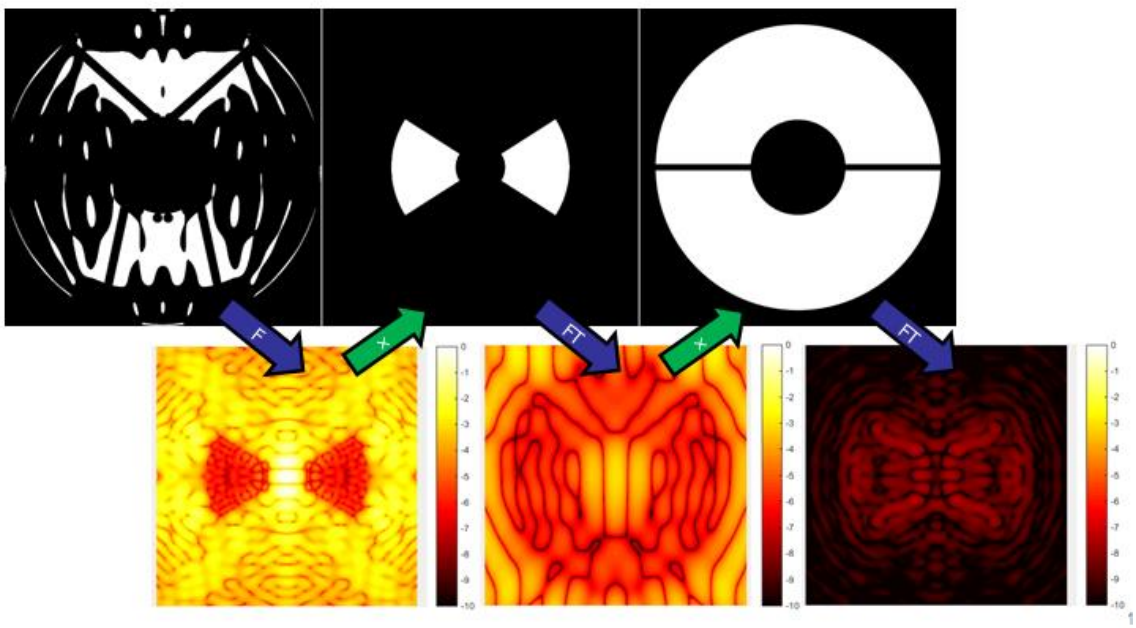

Figure 10: Shaped pupil coronagraph mask used to meet the < 10^{-8} contrast performance requirement on WFIRST. Demonstration was conducted in the HCIT-1 with the obscured WFIRST pupil under vacuum with no dynamic disturbances applied. The mask was fabricated at JPL's Microdevices Laboratory.

The SP used has a pupil transmission of 40% compared to the nominal obstructed aperture. No polarizers were used in these experiments.

Designs for WFIRST now include a diffractive focal plane mask and Lyot stop in a Shaped Pupil Lyot Coronagraph (SPLC)[16]. Such designs offer some of the robustness of a SP to low-order aberrations along with the improved performance (contrast, throughput, and/or inner working angle) of a Lyot-type coronagraph. WFIRST results with a reflective SPLC at 10% bandpass (five 2% filters) yielded a raw contrast of 8×10^{-9} in two bow-tie shaped regions between 2.8 and 8.8 λ/D (**Figure 11**).

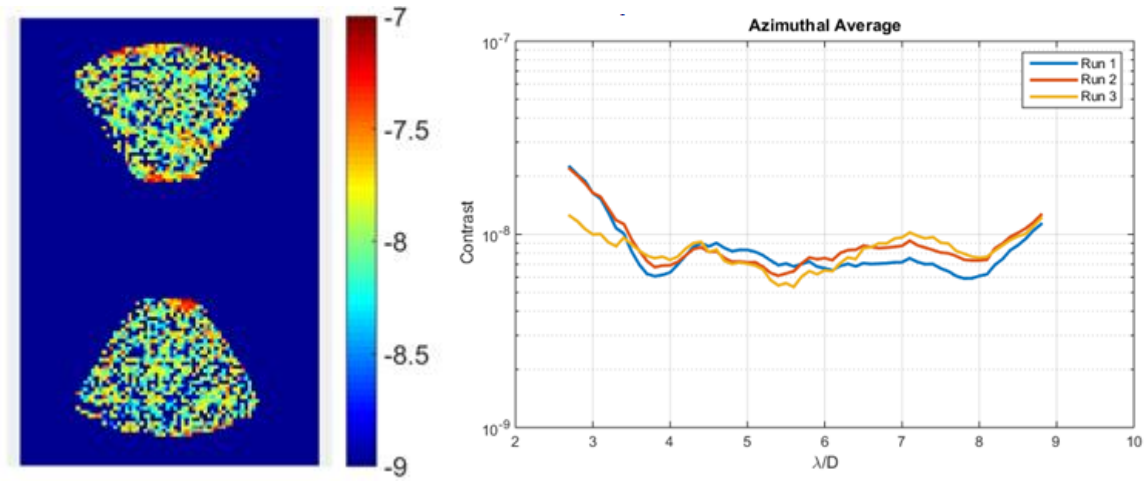

Figure 11: (Left) Focal-plane image from the WFIRST shaped pupil coronagraph testbed in HCIT-1 at JPL. (Right) 10% broadband result centered at 550 nm with mean contrast of 8×10^{-9} across a 3-9 λ/D two-sided 65° wedge dark hole (WFIRST; Milestone #5). The 10% bandwidth was achieved using five 2% bands.

B.1.3 Hybrid Pupil Plane Masks: Apodized Pupil Lyot Coronagraph (APLC) / Shaped Pupil Coronagraph (SPC)

The APLC/SPC hybrid approach is based on the general APLC design[17] implemented on several ground-based telescopes (Gemini, Very Large Telescope, Palomar) with a pupil apodizer, a hard-edged focal plane mask, and a Lyot stop.[18,19,20,21] N'Diaye and Zimmerman have developed a novel approach to introduce image plane contrast metrics as the target of the optimization as is done for shaped-pupil type optimizations.[22,23,24] APLC/SP designs are extremely interesting for their very high tolerance to low-order aberrations including jitter and focus. For instance, the gray-scales designs introduced in N'Diaye et al.[25] are virtually insensitive to jitter or tip/tilt up to ±10 mas in simulation.

Recently the Space Telescope Science Institute (STScI) team has identified two-dimensional apodizations for more complex aperture geometries (e.g., JWST-style segmented aperture) and a similar approach was developed by the Princeton team for the WFIRST coronagraph. A simulated proof of concept design in N'Diaye et al.[26] submitted reaches 10 orders of magnitude contrast as close a 4 λ/D with an 18% throughput in 10% spectral bandwidth, and it has a built-in oversized fast-steering mirror to limit its sensitivity to jitter, low-order aberrations, and stellar diameter (**Figure 12**). The proposed work will push the limits of the APLC/SP concept with an ideal goal of 10^{-10} contrast at 2-3 λ/D with 20% bandwidth and high throughput.

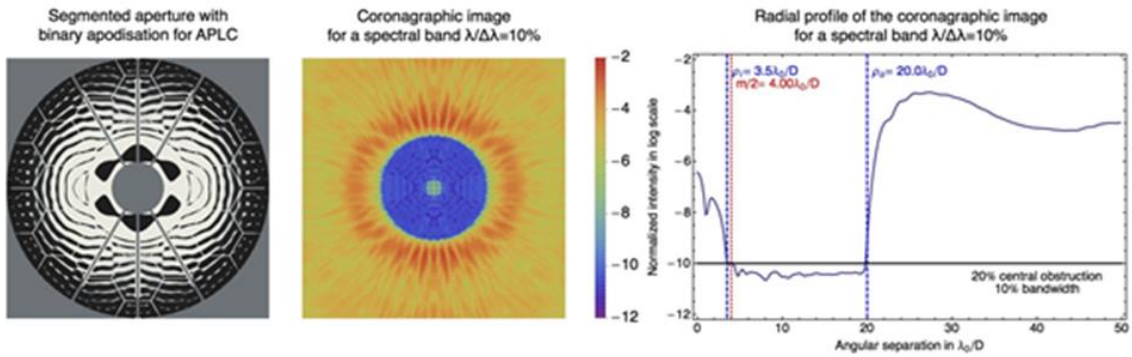

Figure 12: Left: Shaped pupil apodization for the APLC coronagraph for HDST/ATLAST-like segmented apertures. Middle: Coronagraph image obtained with the coronagraph for a 10% spectral bandwidth. A dark region with a 10^{-10} contrast level is produced with the segmented aperture. Right: Radial intensity profile with the size of the focal plane mask and the dimension of the high-contrast region delimited in the red and blue. The stellar image core is smaller than the mask, allowing an enlargement or a displacement within the mask without impact on the dark region, making the design virtually insensitive to low-order aberrations such as pointing errors and defocus drifts [N'Diaye et al. 2016, in prep].[27]

Performance advancement of the APLC is being conducted on the HiCAT (High-Contrast Imager for Complex Aperture Telescopes) testbed under development at STScI to integrate wavefront sensing and control with starlight suppression by coronagraphy for telescopes with complex aperture shapes (i.e., in the presence of central obstruction, support structures, or segmentation). The testbed design has the flexibility to enable studies with increasingly complex telescope aperture geometries from off-axis telescopes, to on-axis telescopes with central obstruction and support structures (e.g., WFIRST), up to on-axis segmented telescopes concepts such as the LUVOIR. Hardware procurement, optical alignment and preliminary DM calibrations were completed in 2015. The testbed will ultimately include two Boston Micromachine MicroElectroMechanical Systems (MEMS) DMs for wavefront control, as well as an Iris AO MEMS DM with 37 hexagonal segments to simulate a segmented aperture; it will also include a hybrid SP/APLC (N'Diaye et al. 2016; submitted)[28] with a reflective SP apodizer and a hard-edge circular focal plane mask. A staged development and integration is planned throughout 2016–2017. The testbed operates in air and is therefore intended to focus on a moderate-contrast, system-level integration to develop and demonstrate some of the key technologies for LUVOIR high-contrast imaging. The testbed will offer a flexible platform for system-level development and testing of LUVOIR high-contrast technologies, including segment phasing through a coronagraph, wavefront stability studies and segment vibration mitigation, low-order wavefront sensing (LOWFS), and optimization of broadband starlight suppression.

B.1.4 Phase-Induced Amplitude Apodization Coronagraph (PIAA)

Phase-Induced Amplitude Apodization (PIAA) is a technique for controlling diffraction that offers high throughput and small inner working angles.[29,30,31] Apodization of pupil amplitudes is achieved by a pair of aspheric mirrors absorbing no light aside from reflective losses. In a classic PIAA configuration, the mirrors have strong aspheric shapes and produce a PSF with very dark side lobes. PIAA designs have been further developed to incorporate diffraction at an occulting mask, producing the PIAA Complex Mask Coronagraph (PIAACMC), which can operate efficiently on obscured pupils[32] (see **Figure 13**). The PIAACMC under development as the backup design for WFIRST has much milder shaped mirrors than the classic PIAA designs, and the occulting masks have phase-only surface patterns suitable for nanofabrication.

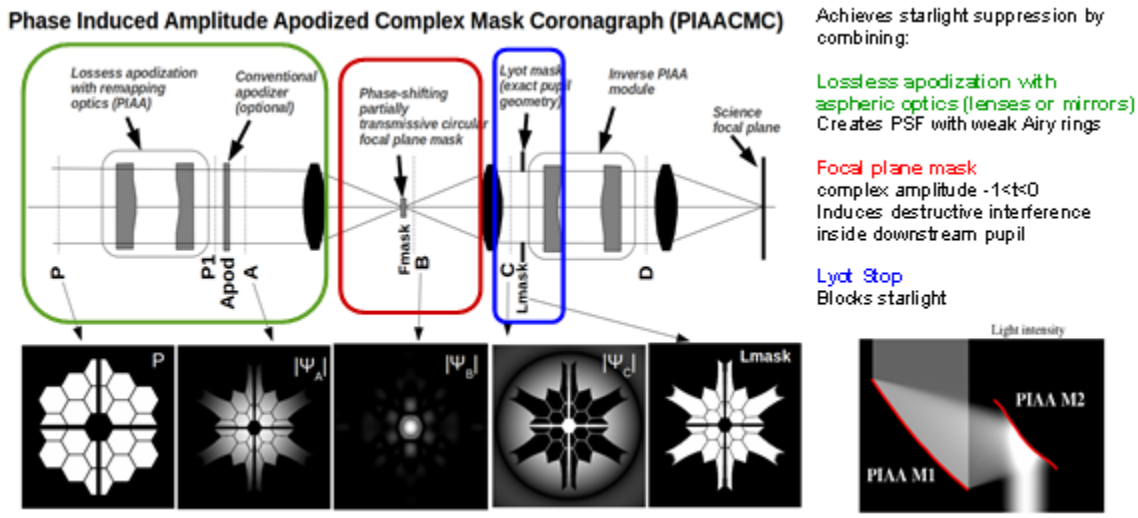

Figure 13: PIAACMC: The segmented input pupil is remapped into an apodized pupil. A phase focal plane mask creates a destructive interference inside the geometric pupil, moving all starlight outside the pupil.

Classic PIAA coronagraphs have been tested at the Subaru observatory in Hawaii, NASA Ames, and the ExEP's HCIT. In 2014, testing in the HCIT completed Guyon's TDEM-09 Milestone #1,[33] monochromatic contrast < 10^{-9}, and Guyon's TDEM-10 Milestone #3,[34] 10% broadband contrast < 10^{-9}. The monochromatic milestone was met with 6×10^{-10} contrast from 2–4 λ/D, while the broadband 10% milestone was not met but achieved 1×10^{-8} from 2–5 λ/D. Also in 2014, the WFIRST project completed its Milestone #3, which was fabrication and characterization of a PIAACMC mask (**Figure 14**) designed to meet the WFIRST coronagraph science requirements.

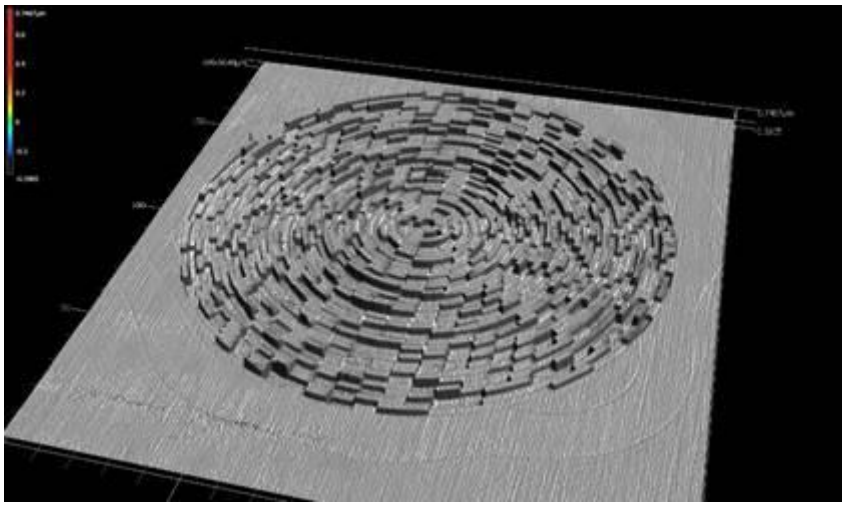

Figure 14: PIAACMC mask viewed by an atomic force microscope; designed by Brian Kern (JPL) and fabricated by JPL's Microdevices Laboratory. The Exo-TAC reviewed and passed the mask fabrication on 12/15/2014 as part of their technology Milestone #3.

The WFIRST-PIAACMC "Gen-3" design is the best-studied PIAACMC design for an obscured pupil. A full PIAACMC-based optical system has been evaluated taking into account chromatic diffractive propagation between optics, static and dynamic wavefront errors in the telescope, demonstrated level of manufacturing errors (including diamond turned PIAA optics and focal plane mask made at JPL's

MDL), and wavefront control (provided by a single 48×48 DM). Simulations show that it achieves a 1.3 λ/D IWA with high throughput, and delivers a 1.3×10^{-9} raw contrast in a 1-8 λ/D half dark hole in a 10% spectral band centered at 565 nm.

The raw contrast is currently dominated by manufacturing errors in the focal mask and telescope jitter (few mas per axis for the telescope, reduced to < 0.6 mas per axis after LOWFS correction). Expected advances in component manufacturing capabilities will improve the raw contrast. At longer wavelength, these errors are a smaller fraction of a wave, so contrast values are better. WFIRST has a planned Milestone #8 demonstration of < 10^{-8} raw contrast with 10% bandwidth centered at 550 ηm in a static lab environment by the end of September 2016. The PIAACMC design, the backup coronagraph on WFIRST, promises better optical throughput and improved IWA of just 1.3 λ/D. The latter creates the opportunity for probing more planets in the HZ of more distant stars.

As the PIAACMC concept design process and its performance are largely insensitive to aperture geometry, the WFIRST-PIAACMC performance numbers quoted above are good predictors of PIAACMC performance with current demonstrated technology on a segmented aperture, assuming a similar instrument design. An idealized PIAACMC design (assuming perfect optical components) was produced for the High Definition Space Telescope (HDST)[35] segmented pupil and predicted 1.2 λ/D IWA with a 70% throughput. The predicted raw contrast is 1×10^{-10} in monochromatic light, and will be limited by focal plane mask manufacturing errors and wavefront control agility in broadband light. A focal plane mask, consisting of a few hundred zones (consistent with current demonstrated manufacturing capabilities) was designed to offer 1×10^{-9} raw contrast in a 10% wide band.

Evaluation of the HDST-PIAACMC design showed that its predicted performance (especially its small IWA) enables imaging Earth-like planets around stars as far as 40 pc in visible light, and spectroscopic characterization into the near-IR for nearby exo-Earths, assuming a 12-m-diameter HDST pupil. The sensitivity is, however, limited by stellar angular size, which produces a significant leak, requiring PSF subtraction and increased exposure times to overcome the additional photon noise. Quantifying and reducing the PIAACMC's sensitivity to stellar angular size will therefore be a high priority.

B.1.5 Vector Vortex Masks

The Vector Vortex is an image-plane mask that adjusts the phase of the incoming field producing a rotational phase ramp of two or more even number of cycles to cancel the on-axis starlight. For the results shown in **Figure 15**, a liquid-crystal polymer vector vortex was used.

The Vortex coronagraph is in operation at major ground-based facilities. It has also demonstrated raw monochromatic rejections of 10^{-9} or better at angles of 2 λ/D in the HCIT[36] and an average contrast of 10^{-8} across 1.5–9.5 λ/D for 10% bandwidth light.

Eugene Serabyn (JPL), with a 2010 TDEM award, demonstrated mean raw contrasts of 3.2×10^{-8} with a 10% bandwidth in a 60 $(\lambda/D)^2$ field extending from 2.4–9.4 λ/D.[37] His team later demonstrated contrast performance 4.3×10^{-10} in monochromatic light. Serabyn was awarded a TDEM-14 to continue unobscured vacuum demonstrations at 10% and 20% broadband.

Due to its widespread implementation on various on-axis (and thus obscured) ground-based telescopes, the question of unfriendly apertures was considered early on. Several solutions have been proposed such as the multistage vortex coronagraph[38] and three types of amplitude apodizations: gray scale,[39] binary shaped-pupil,[40] phase-induced remapping.[41] These solutions provide leverage against the detrimental effect of obscured apertures (including spiders and segments). Both the multistage and ring-apodized vortex coronagraphs have been tested in the lab and on-sky.[42]

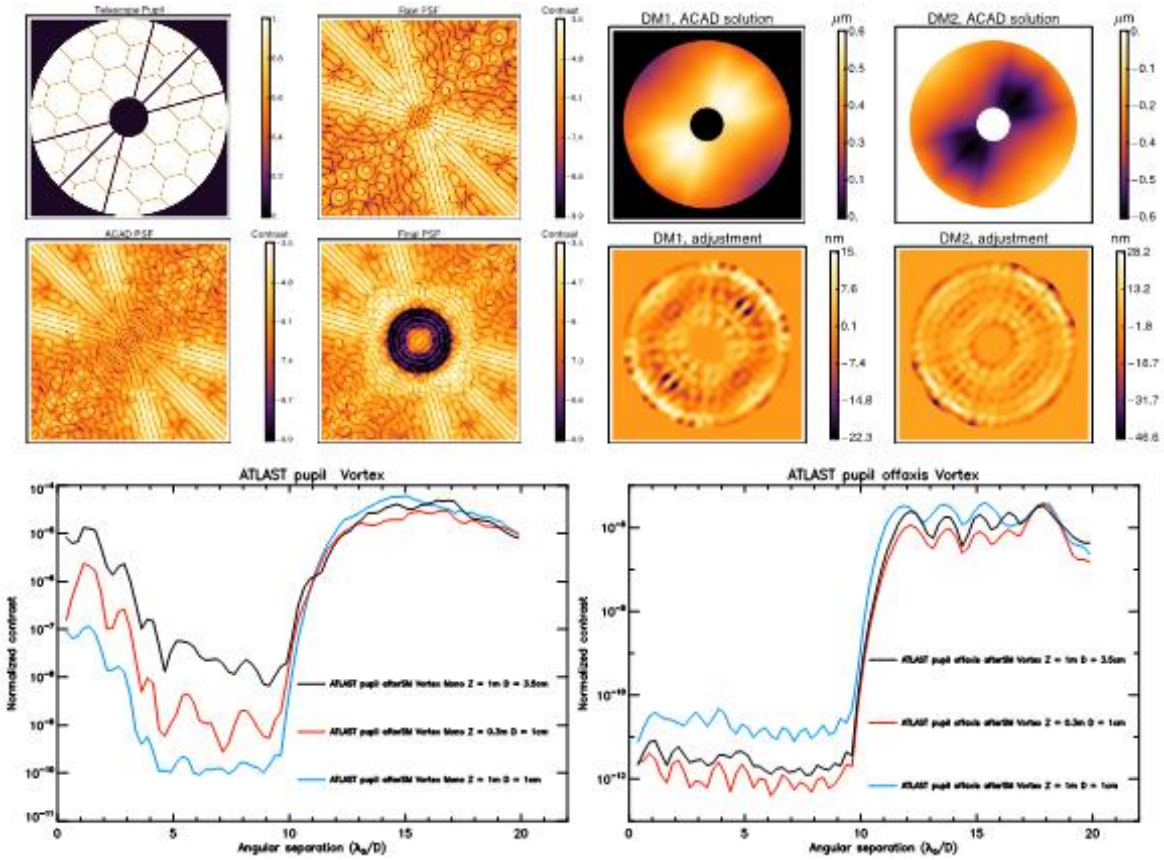

Figure 15: Preliminary ACAD (Adaptive Correction of Aperture Discontinuities) simulations from Mazoyer et al. 2015.[43] (Top left) ATLAST pupil stopped down by a circular mask, raw PSF, ACAD PSF, and final PSF after wavefront control. (Top right) DM shapes and strokes after the ACAD step (top) and after the adjustments by the stroke minimization method. (Bottom left) corresponding contrast for various DM configurations in 10% bandwidth. (Bottom right) corresponding contrast without central obscuration (off-axis telescope) in 10% bandwidth.

Recent work for the European Extremely Large Telescope combines vortex coronagraph phase corrector elements and ring-like entrance pupil apodization. The phase correction is in principle able to compensate for any aperture discontinuities perfectly, even missing segments.[44] The addition of pupil apodization and/or lossless remapping (ACAD, see **Figure 15**) dramatically relaxes manufacturing requirements for the vortex coronagraph corrector.

The optical configuration is essentially identical to that of the hybrid Lyot architecture, having only one DM for current testing, but using two for flight. No fundamental change to the mask design would be needed for flight (although material compatibility assessment in a radiation environment is still needed). The current limitation in performance is related to the ability to manufacture masks with a vortex pattern that is maintained to very small offsets from the center of rotation, and to extend the designs to broadband multilayer masks. For the current experiments, a polarizer is required prior to the pinhole of the source.

The throughput would ideally be 100%, but the Lyot stop was undersized to 85% for the monochromatic demonstrations and to 92% for the broadband demonstrations, yielding a 72% and 85% transmission, respectively. Additionally, a polarizer is used at the source (as mentioned above), and so the effective throughput is approximately 36% monochromatic and 43% broadband.

B.1.6 Visible Nulling Coronagraphs

A Visible Nulling Coronagraph (VNC) uses an interferometer back-end to reject starlight via interferometric nulling with a sheared pupil. This approach uses a segmented DM with piston, tip, and tilt actuation of each segment, sometimes in combination with an array of single-mode optical fibers.

In a flight configuration, two VNC combiners would be used in series, one for each of two orthogonal image axes. The results reported here involve use of only a single VNC combiner.

A larger outer working angle (OWA) than what is possible with the 163-segment DM presently in use would be achieved using a DM with at least 300, but preferably 925 segments. The lab demonstrations used a 163-segment DM (Iris AO) and produced a wedge-shaped dark hole in the region of 2–5 λ/D. Modeling will be required to determine if flight combiners would use 1) an array of single-mode fibers paired with a matched geometry DM, each having the same number of fibers and segments, respectively, or 2) two DMs. Both options allow simultaneous control of phase and amplitude errors over a circularly symmetric region of the focal plane. The fiber array was used to demonstrate coherent imaging, but was not used for the high-contrast demonstrations reported here.

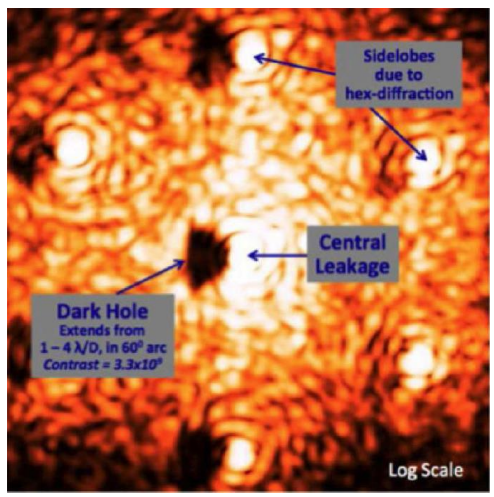

Figure 16: Focal plane image of Visible Nulling Coronagraph from TDEM-09 result by Mark Clampin and Richard Lyon (NASA-GSFC).

If the VNC uses a single shear of 25% of the pupil, with a secondary of obscuration zero (unobscured) or 0.25, geometric throughput is 69% or 60%, respectively. A linear polarizer was used for these experiments and so the effective throughput with these aperture geometries would be approximately 35% or 30%.

Mark Clampin and Richard Lyon (NASA-GSFC), with their 2009 TDEM (TDEM-09) award, demonstrated[45] mean raw contrasts of 5.7×10^{-9} with a 1.2 nm wide bandpass center on 632.8 nm (0.1% bandwidth) over a 1 λ/D circular field extending from 1.5–2.5 λ/D. The first broadband results (6%) are expected through Lyon's 2010 TDEM in the spring of 2016. A 2013 TDEM led by Lyon will enable the GSFC team to use their VNC with a segmented pupil consisting of controllable mirrors to demonstrate starlight suppression for a simulated segmented mirror telescope. A 2014 TDEM led by Matthew Bolcar (NASA-GSFC) intends to build the Next Generation Visible Nulling Coronagraph (NG-VNC), an evolution of the VNC concept that uses new phase occulting optics.[46] This architecture is a single nulling interferometer that delivers full-field observing disk suppression. By realizing high order stellar disk suppression with a single nuller and no lateral pupil shear, the number of optics is reduced, and effective throughput is increased.

B.2 Large Aperture Mirrors (CG-1)

The habitable zone of an exo-Earth at 10 pc has an angular resolution of 100 mas at planet quadrature (see **Figure 1**). To just detect such a planet at 400 nm, a telescope should have an angular resolution of 25 mas if we conservatively assume a 3 λ/D coronagraph. This telescope would then have a primary mirror aperture that is 3.3 m. However, our end objective is spectral biosignatures. Imposing the same parameters for detecting the planet at 760 nm (oxygen line) would then require a 6.3-m telescope; water at 940 nm would require a telescope aperture approaching 8 m. Improvements in inner working angle can help drive the aperture size down, as would investigations of our solar neighborhood limited to within 10 pc.

Large primary mirrors enable more than just improved angular resolution, they enhance planet sensitivity due to sharper PSFs, reduce science integration time due to greater collecting areas and throughput, and enable probing of a larger number of more distant stars' habitable zones. The telescope's primary mirror size and architecture (monolithic or segmented, obscured versus unobscured) is among the most important decisions a space telescope team will have to make, especially when considering optimizing the performance of a coronagraph.

The biggest unknown to date needed to select the telescope size is the fraction of Sun-like stars with Earth-size planets in their habitable zones, also known as η_{Earth}. As η_{Earth} increases, fewer planetary systems will need to be observed in order to build sufficient statistics about the habitability of exoplanets. If η_{Earth} is near 0.1, then a 10-m-class telescope is required to detect and characterize approximately 30 candidate habitable zones for exo-Earths[47]. If η_{Earth} is above 0.8 then only a 4 m-class telescope would be required to observe the same number of candidate habitable zones. η_{Earth} is expected to be better constrained in 2016, based on additional analysis of the Kepler data.

Although crucial for the implementation of a future exo-Earth imaging and spectroscopy mission, proposals for the development of large aperture mirror and associated technologies are not solicited under the TDEM element of the SAT 2015 call. Proposals in this area may be suitable under the Technology Development for the Cosmic Origins Program (TCOP) element of the SAT 2015 solicitation or under the APRA 2015 solicitation. Proposers should contact the cognizant program officer to confirm the suitability of their investigation for those programs in advance of submitting a proposal.

B.2.1 Large Monolithic Mirrors

The maximum size monolithic mirror has been limited to approximately 4 m by currently available 5-m-class launch vehicle fairings. For example, the largest monolithic space telescope ever flown is the Herschel Telescope and its primary mirror is 3.5 m. Fortunately, with the advent of NASA's Space Launch System (SLS) and its planned 8.4- and 10-m fairings, it is possible to consider monolithic 4- to 8 m-class mirrors. Mirror mass, along with diameter, have traditionally been key telescope design parameters, especially with respect to cost. This has led to light-weighting technologies that continue to this day. But the SLS's larger fairings and greater mass capacity may allow designers to reconsider the benefits of more mass in the overall system (greater stiffness, lower resonance frequencies, greater thermal inertia, etc.). It is expected that the 2020 Decadal Survey will consider large monolithic mirror (> 4 m) mission concept studies that can fit in 5-, 8.4-, and 10-m fairings.

While the HST 2.4-m-diameter primary mirror is the most well-known monolithic space mirror, the current state of art is represented by the Kepler and WFIRST mirrors—both of which were made from ultra-low expansion (ULE) glass using frit bonding technology. The HST primary mirror was fabricated from a 46-cm-thick square pattern core. It has a total mass of approximately 800 kg (180 kg/m^2). The Kepler primary mirror is 1.45 m in diameter with a water jet–cut hex core. Its mass is approximate 330 kg (200 kg/m^2).[48]

The 2.4-m primary mirror for the planned WFIRST-AFTA mission was fabricated using a different process. Its facesheets were water jet–pocket-milled and its cores were water jet cut. The mirror was then assembled using low-temperature fusion (LTF). The LTF process was developed and first demonstrated,[49] along with the low-temperature slumping (LTS) process on the Advanced Mirror System Demonstrator (AMSD) project (PI H. Philip Stahl/NASA-MSFC).

In response to this challenge, since 2012, the Cosmic Origins Program has funded the Advanced Mirror Technology Development (AMTD) project (PI Stahl). AMTD is developing a stacked core process that uses low-temperature fusing and slumping to enable fabrication of thick (40 to 50 cm) 4m-class (or larger) monolith ULE glass UVOIR space telescope mirrors. AMTD Phase 1 successfully produced a 43-cm diameter cut-out of a 4-m-diameter, 40-cm thick mirror substrate (**Figure 17**) using the new five-layer stack and fuse process. This mirror was polished to 5.5 nm rms (UVOIR quality) and characterized for thermal stability. (Note: water jet cutting of core elements is currently limited to approximately 30 cm thickness but can be upgraded to achieve 45 cm.)

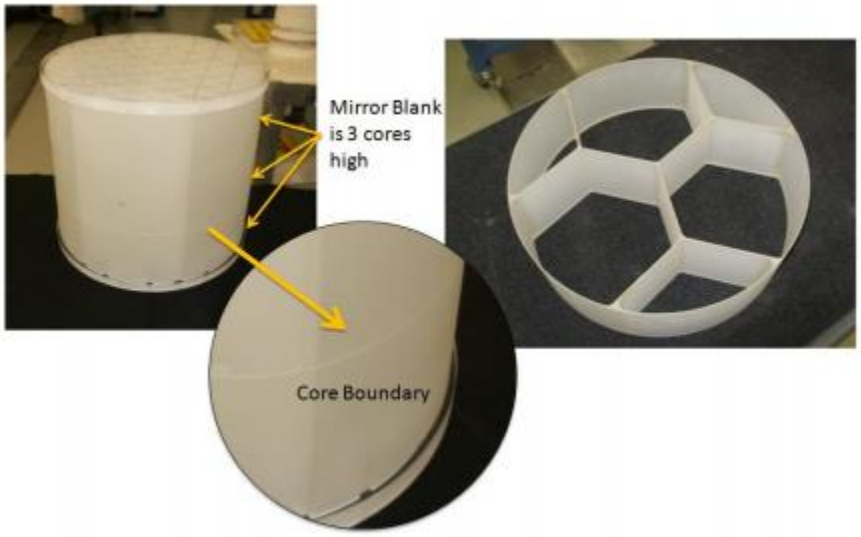

Figure 17: The 43-cm-diameter demonstration mirror blank shown consists of three independently cut cores sections and two facesheets that were co-fired to create the assembly.

AMTD Phase 2 is currently building a 1.5-m, 20-cm thick, 1/3rd scale model of a 4-m ULE mirror. The purpose of this mirror is to demonstrate lateral scalability of the stacked core process. When complete, AMTD-2 plans to characterize its static thermal wavefront error deformation. Additionally, AMTD Phase 2 is currently polishing a 1.2-m Zerodur mirror owned by Schott Corporation for the purpose of thermal wavefront error characterization.

Thermal stability and control is a key challenge for monolith mirrors. HST had the challenge of the diurnal thermal cycle of low-Earth orbit. While any future large space mission will probably be in the thermally stable Earth-Sun L2 Lagrange orbit, there will still be thermal load variations as a function of pointing angle relative to the Sun (as shown on JWST). Analysis indicates that exoplanet science requires a primary mirror that has a total wavefront error that is stable on the order of 10 pm per wavefront control step.[50]

Thermal control of the monolith depends on the material and architecture. ULE glass has a low coefficient of thermal expansion (CTE), which offers good passive thermal stability and could provide the required stability with precise thermal control. Silicon carbide has 100 times the CTE of glass, which

makes it 100 times more responsive than glass to precision thermal control (however, less stable to maintaining temperature). An open-back monolith mirror has a quicker response to thermal control but requires more mass than an equivalent closed-back mirror of the same material. Multiple material/architecture combinations exist with the potential to meet thermal stability requirements, but they have not yet been demonstrated at the required performance levels.

No previous space telescope has ever required < 10 pm wavefront stability. Historically, space telescopes use passive thermal control. JWST's telescope is in a Sun-shade shadow. HST's telescope is in a heated tube. And again, while not designed to meet the requirements of a UVOIR exoplanet science mission, JWST is predicted to have a 31 nm rms WFE response to a worst-case thermal slew of 0.22 K and take 14 days to passively achieve < 10 pm per 10 min stability. Obviously, this is too long for a coronagraphic exoplanet mission. HST is a cold-biased telescope heated to an ambient temperature. However, it is not a controlled thermal environment. Thus, HST's wavefront error changes by 10–25 nm every 90 min (1–3 nm per 10 min) as it moves in and out of the Earth's shadow.

The HabEx and LUVOIR mission concept study teams are expected to explore the scientific benefits and technology needs of large monolith primaries starting in 2016.

B.2.2 Large Segmented Mirrors

The development of large segmented mirrors and their structures will enable astronomy to build ever-increasing future telescopes advancing both exoplanet and general astrophysics science. However, segmented mirrors have their own challenges for reaching previously unmet contrast ratio levels of 10^{-10} at close IWAs. These challenges include: diffraction from the segmentation pattern and segment to segment rigid body motion (i.e., tip/tilt and piston).

JWST is a segmented aperture telescope scheduled for launch in 2018. Its primary aperture is 6.5 m in diameter composed of 18 gold-coated beryllium segments, each 1.32 m tip-to-tip. Working in the near- to mid-infrared, the telescope operates at a temperature below 50 K. A major cost driver of JWST was the need to verify and validate performance specifications at the 50 K operating temperature. Fortunately, by operating at a warmer temperature, due to its visible to near-infrared observational spectrum, a potential exoplanet imaging mission can use more conventional materials for its optical components and structure.

The experience of controlling 6 degree of freedom (DOF) segments can be built upon to gain a higher precision, more stable segmented aperture for exoplanet imaging. The surface figure error is required to be less than 10 nm rms and drift less than 10 pm due to thermal and dynamic instability during a wavefront control cycle. Possible design architectures include the ATLAST (Advanced Technology Large Aperture Space Telescope) design[51] and the High Definition Space Telescope (HDST) concept.[52]

To advance the understanding of coronagraph performance with segmented telescope apertures, the ExEP launched in FY16 a Segmented Coronagraph Design and Analysis task to provide a first look at current capabilities and what potential future developments may yield. Although not a down-select, five state-of-art coronagraph architectures using 6–7 segmented reference aperture architectures (**Figure 18**) will be designed by coronagraph experts and submitted to the ExEP for consistent analysis and exoplanet yield based on contrast and IWA performance. This initial study will not include telescope dynamics (e.g., jitter, thermal, segment-to-segment phasing errors) but rather study what can be achieved with a static aperture. A finite stellar angular diameter (~1 mas) will be assumed, which is expected to exceed the residual corrected telescope jitter achieved by a coronagraph's low-order wavefront sensor and control. The coronagraph architectures to be studied in the initial analysis will be:

1. PIAA CMC (University of Arizona/NASA-Ames/JPL)
2. APLC/SPC (Space Telescope Science Institute/Princeton)
3. Vortex (Caltech/JPL)
4. Hybrid Lyot (Caltech/JPL)
5. Visible Nulling Coronagraph (NASA–GSFC)

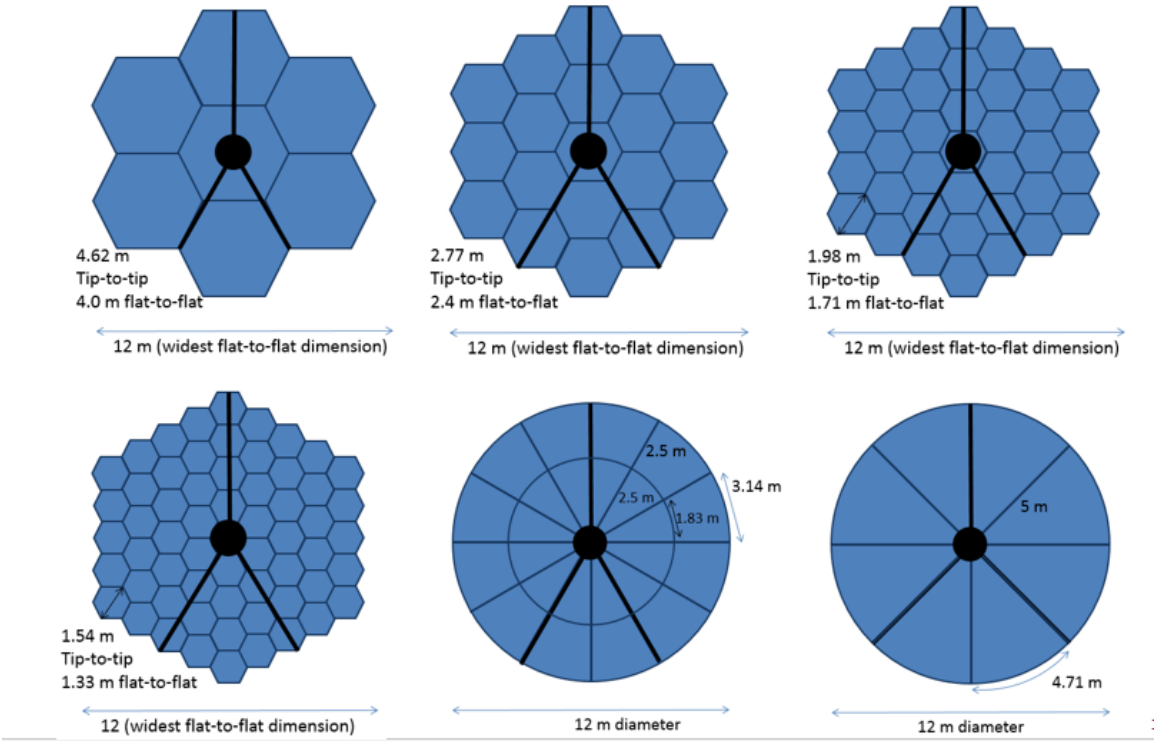

Figure 18: 12 m aperture designs being considered for the ExEP Segmented Coronagraph Design and Analysis study.

The HabEx and LUVOIR mission study teams will explore the science benefits and technology challenges of segmented primary mirrors starting in 2016.

B.3 Ultra-Low Noise, Large-Format Detectors

The collected photon rate from exo-Earths is expected to be about one per tens of minutes. Consequently, the imaging detectors for both the detection and spectrometer channels of a coronagraph instrument must be highly sensitive, have ultra-low noise, and must be radiation hardened. In addition, the need for low spectral-crosstalk spectroscopy and large outer working angles to carry out disk science and imaging of the nearest exoplanets lead to the requirement for large format focal plane array—2k×2k pixels or larger.

Proposals for the development of ultra-low noise, large format visible detectors are not solicited under the TDEM element of the SAT 2015 call, largely due to the ongoing WFIRST investments funding electron multiplying charge coupled device (EMCCD) development. Although crucial for the implementation of a future exo-Earth imaging and spectroscopy missions, proposals for the development of ultra-low noise, large-format near-infrared detectors are also not solicited under the TDEM element of the SAT 2015 call. Such proposals may be suitable under the TCOP element of the SAT 2015 solicitation or the APRA 2015

solicitation. Proposers should contact the cognizant program officer to confirm the suitability of their investigation for those programs in advance of submitting a proposal.

B.3.1 Visible Detectors (CG-8)

The leading candidate detector technology in the visible is the silicon EMCCD detector, which can provide dark current noise of order 5×10^{-4} e-/px/sec while operating at 165 K after lifetime irradiation and clock induced charge (CIC) of order 3×10^{-3} e-/pix/frame. The effective read out noise can be < 1 e-rms using EM gain; the level of EM gain, or amplification, will depend on the native read out noise of the output amplifier that is being used. These detectors can operate in three modes: conventional CCD, EM gain with analog output, and EM gain with photon counting output.

The WFIRST-AFTA coronagraph study has baselined the e2v CCD201-20 detector (1024×1024; 13 ×13 µm pixel pitch) for both of the coronagraph science cameras (imaging and IFS) and is carrying out full characterization and displacement damage dose (DDD) radiation testing. In 2015, this detector was characterized by WFIRST at the JPL Detector Lab using a NüVü EM N2 camera and found to meet the WFIRST beginning-of-life performance requirements (see **Figure 19**).

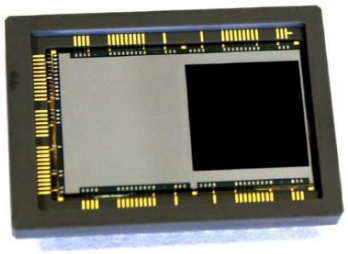

WFIRST Detector Performance Requirements

Specification	Goal	Requirement	Measurement	Unit
Effective read noise w/gain	0.2	0.2	<0.2	e^-
Dark current	1×10^{-4}	5×10^{-4}	1.01×10^{-4} *	e^-/pix/sec
Clock induced charge (CIC) @ 5.5σ threshold	0.0010	0.0018	0.0017	e^-/pix/fr

Figure 19: e2V CCD201-20 (1k×1k) detector and its characterization results conducted at the JPL CCD Detector Lab in 2015; data is beginning of life.

As part of the WFIRST coronagraph technology development program, the EMCCD 201-20 underwent a two phase DDD radiation test in 2015 simulating an L2 orbit of 6 years duration. In the first phase, a single radiation dose equivalent to six years at L2 was directed at two devices at ambient temperature to quickly assess the survivability of the EMCCD and to lay the ground work for an extended cryo-test. In Phase II, a single device was irradiated in four separate doses cumulatively simulating six years in an L2 orbit. The device was in the powered state and held at a fixed cryo temperature during the entire four-dose campaign. The cumulative six-year DDD equivalent dose was 7.5×10^{9} protons/cm^2 assuming a specific camera shielding design. Radiation for test Phases I and II were conducted at the Scherrer Institute Beamline facility in Switzerland and Harwell Helios 3 Beamline in the U.K., respectively. The data analysis is nearly complete. Preliminary results are positive—negligible change to EM gain and read noise; less than an order of magnitude degradation in the CIC and dark current. The dark current increased to only 8×10^{-4} e-/pix/s, easily mitigated with thicker or different material shielding (Rick Demers, private communication). Effects of degraded charge transfer efficiency are being assessed and will be integrated into the coronagraph detector model. Final results are expected as part of WFIRST Milestone #7, scheduled in August 2016. This is expected to bring the detector to TRL 6.

In 2014, e2V began development of the larger format 4k×4k EMCCD sponsored by a single customer.[53] At the time this Appendix was released, the company was still debugging the detectors and the larger device is unlikely to be considered for WFIRST. Given the current state of technology, a closely butted 2×2 mosaic of 1k×1k EMCCDs is far more mature than this larger format. The only drawbacks to the

mosaic architecture are 1) the physical gap between the individual CCDs (they can be butted together but there is still a small gap) and 2) the extra mass of discrete electronics for each of the four CCDs.

Alternative photon-counting visible detector technology work was funded through a TDEM-09 award[54] (Donald Figer, Rochester Institute of Technology) looked at raising the technology readiness of silicon Geiger-mode Avalanche Photodiode arrays (480–1060 nm). A silicon 256×256 diode array was fabricated, hybridized to a CMOS readout integrated circuit, hybridized, and tested. This device has a 100% fill factor and a good response from 300–1000 nm. However, performance degradation after radiation testing led to only 3 of the 5 success criteria being met.

MKID and TES arrays are cryogenics alternatives capable of performing at visible wavelengths. Both are considered less mature than the EMCCDs (more about these two promising detectors in Section B.3.2).

B.3.2 Infrared Detectors (CG-9)

Near infrared detectors with high sensitivity in the spectral region of 900 nm to 2.5 µm (and maybe greater) are critical for the spectral characterization of exoplanets and identification of possible biosignatures. Future exo-Earth missions (HabEx, LUVOIR) will consider infrared spectroscopy capabilities to detect hydrocarbons such as methane (1.00 µm, 1.69 µm, and 2.32 µm). The presence of methane in an oxygen-rich atmosphere like Earth's is one of the few known spectral combinations that point to a biotic origin with small probability of false positives.

Spectral characterization of exo-Earths in the infrared requires sub-electron read noise and the dark current noise < 0.001 e-/pix/s, in a space radiation environment over mission lifetime. These properties in a larger array, such as 2k×2k or 4k×4k, are desirable.

HgCdTe photodiode arrays hybridized to astronomy readout integrated circuits are the state of the art with a read noise < ~ 2 e- rms with multiple non-destructive reads, dark current of < 0.001 e-/s/pix. These detectors have flown in Earth orbit and have proven to be very radiation tolerant. Two large format 4k×4k pixel arrays offered by Teledyne Imaging Sensors, with 10 and 15 µm pixel pitch are at TRL 4 (H4RG-10™ and H4RG-15™).

Reducing the spurious count rate should be the top priority of non-cryogenic photon-counting detectors followed then by radiation hardening tests. Although conventional HgCdTe photodiode arrays may never function as photon-counting detectors due to leakage current at non-cryogenic temperatures, it is possible that today's H2RG and H4RG detectors are not yet approaching the fundamental physical noise limits of the photodiodes themselves.[55] Work distinguishing the contributions from the photodiode, interconnects, field-effect transistor, etc. would be valuable.

Other candidate detector technologies are currently less mature but worth watching. With appropriately optimized process, the HgCdTe avalanche photodiode (APD) array offers the possibility of the high gain and low effective read noise of EMCCDs while being capable of the same QE performance as the JWST arrays. Because gain is built into each pixel—unlike the EMCCD—they promise photon counting if the dark current is sufficiently suppressed.[56] The state-of-the-art Selex SAPHIRA arrays have reported ~10–20 e-/pix/s dark current[57]. More work is needed to determine the actual noise floor and understanding the noise contributions from the HgCdTe photodiode versus the integrated readout circuit.

Cryogenic (superconducting) detectors such as microwave kinetic inductance detectors (MKIDs) have essentially no read noise or dark current solving the spurious count rate problem associated with the non-cryogenic devices.[58] These devices are scalable to large arrays. Transition edge sensor (TES) arrays are also candidate cryogenic detectors with built-in energy resolution like the MKIDs. Both will require solutions for dynamic isolation, particularly from their cooler vibrations, and resolution (pixel number).

The immediate challenge will be providing zero vibration cooling. While cooling is not a detector technology, future telescope architectures will want to mitigate all vibrations sources to enable the coronagraph performance to reach the dual driving instrument goals of 10^{-10} contrast ratios at <3 λ/D. Also, their radiation tolerance is unknown. NASA's PICTURE-C balloon experiment is baselined to include a 10–20 kpix MKIDs device in 2019. NASA-GSFC is considering maturing TES devices for future exoplanet imaging missions.[59]

The built-in energy resolution capabilities of the MKIDs and the TES devices are currently R ≤ 20, short of the R ≥ 70 desired by future biosignature-seeking spectrographs. Of course, these detectors could be positioned after the spectrograph.

Bernard Rauscher et al.[60] present a nice summary on the state-of-art and potential detector candidates for low-flux environments (see **Figure 20**):

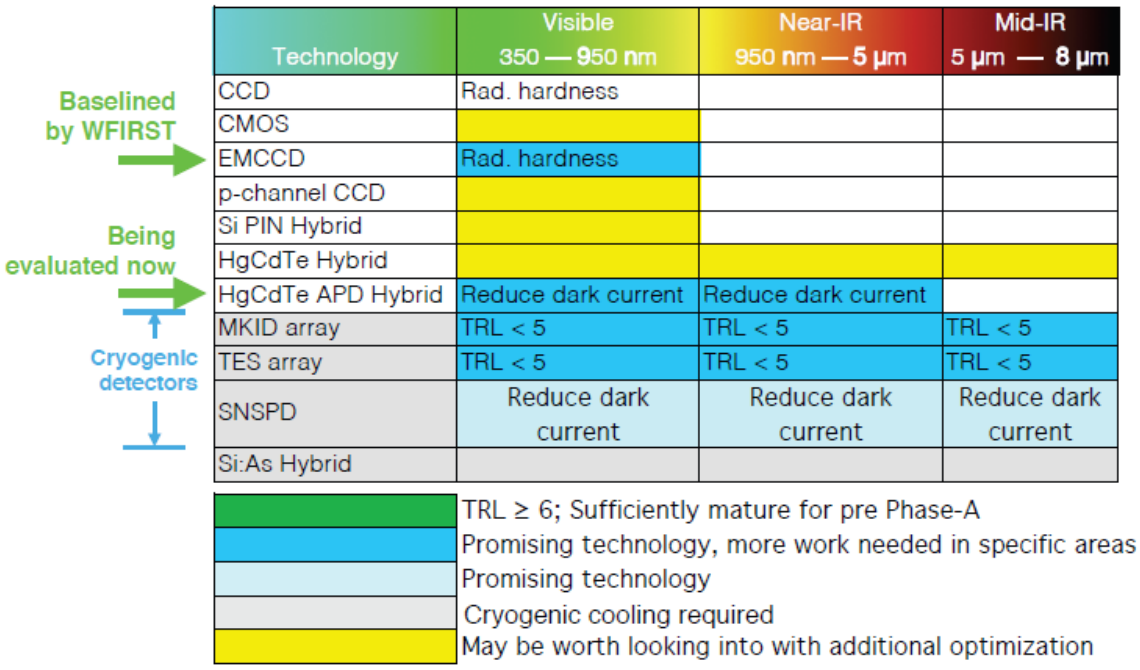

Figure 20: Summary of visible to mid-IR detectors for exoplanet science (Rauscher et. al. 2015).[61]

If future mission concepts do indeed require near-infrared spectral detections, then much work is needed in advancing the technology readiness of ultra-low noise infrared detectors.

B.4 Segment Phasing Sensing and Control (CG-6)

Unlike a traditional monolithic telescope mirror, a multisegment large-aperture mirror will require phasing and rigid-body sensing and control of the segments to achieve tight static and dynamic wavefront errors at visible wavelengths. Segment wavefront errors, such as those caused by rigid body positioning errors, dynamic vibrations, and slow thermal drifts can significantly impact coronagraph coherent imaging and hence contrast. For example, a coronagraph working with a segmented mirror, to avoid speckle noise brighter than typical exoplanets, requires a segment-to-segment dynamic cophasing error of under 10 pm rms between WFSC updates (from a few minutes to many tens of minutes depending on the host star's brightness). A tertiary DM could also provide segment phasing and jitter control. Segment position and phase errors sensed by a wavefront sensor can be sent to the segment

rigid body actuators (for coarse correction) and to the DMs of the coronagraph, or a segmented DM dedicated to fine segment tip/tilt and phasing control (for fine correction).

The Keck ground-based telescope and JWST sense and control the rigid-body positions of their segments by utilizing wavefront sensing and control, such as phase retrieval, Shack-Hartman sensing, and dispersed fringe sensing.[62] Keck also uses edge sensors. JWST's optical error budget includes 6 nm rms for rigid body positioning and 49 nm rms stability. While these methods are proven for phasing diffraction-limited segmented optical systems, such as JWST and Keck, they are probably insufficient for achieving the picometer-level stability required for exoplanet imaging at visible wavelengths.

A potential solution is a laser metrology truss to measure positional changes to the expected pm-level stability. Picometer accuracy laser metrology was demonstrated by the Space Interferometry Mission (SIM) with large beam launchers. More compact beam launchers, lightweight enough to mount to the edge of a segment, have been developed over the last few years for non-NASA customers but were designed to operate at the nanometer-precision level. Additional development in laser metrology is needed if a laser metrology truss is to be used for sensing segment positioning. An alternative to laser metrology is more precise edge sensors than those used by Keck or are planned for the Thirty Meter Telescope. Another potential solution is to isolate the telescope (see Section B.5) such that segment to segment and line-of-sight pointing errors are kept below the required amplitude.

Future work defining requirements and architectures is expected to be explored by the HabEx and LUVOIR mission concept studies commencing in 2016. While critical to the success of such a mission, proposals for the development of segment phasing sensors and control algorithm are not solicited under the TDEM element of the SAT 2015 solicitation.

B.5 Telescope Vibration Control (CG-7)

Isolation and damping of spacecraft and payload vibrational disturbances is critical in enabling a coronagraph to reach 10^{-10} contrast levels at IWAs less than 3 λ/D. Leakage of starlight due to pointing instability or jitter and vibration in the telescope that cannot be controlled by a low-order wavefront sensor and controller (LOWFS/C) will potentially scatter light onto the detector and decrease the detection contrast within the dark hole. Precision pointing stability needed by the telescope during integration to keep the star inside the suppressed region of the coronagraph may need to be better than a few mas[63] (depends on LOWFS/C capability; see Section B.7). Typical expected attenuations for monolith primary mirrors are 120 dB end-to-end attenuation at frequencies larger than 20 Hz; segmented primary mirrors are 140 dB end-to-end attenuation at frequencies greater than 40 Hz.[64,65] "End-to-end" implies isolation between disturbance source and the optical telescope element.

Several aerospace companies have demonstrated systems that allow for active dynamic isolation candidates. A noncontact isolation system by Lockheed Martin[66] demonstrated 68 dB of broadband isolation in a testbed and is assessed at TRL 5 for large observatories. The payload and spacecraft bus are separate bodies that fly in close-proximity, allowing precision payload control and simultaneous isolation from spacecraft disturbances. Micropropulsion thrusters for fine pointing, used exclusively or in a hybrid fashion with reaction wheels, is another option. Active vibration dampening and hybridizing the LOWFS/C fast steering mirror system with the fine guidance system are also credible.[67]

Telescope stability, like wavefront stability in general, is a systems-level challenge and is most efficiently addressed by a reference design that includes selected coronagraph and telescope architectures. Future work in defining requirements is expected within both the LUVOIR and HabEx mission concept studies commencing in 2016. In addition, characterizing the WFIRST transmitted disturbances to the coronagraph instrument will be valuable for understanding the threshold disturbance the coronagraph LOWFS/C can attenuate.

Although crucial for the implementation of a future exo-Earth imaging and spectroscopy mission, proposals for the development of telescope vibration control technologies are not solicited under the TDEM element of the SAT 2015 call. Proposals in this area may be suitable under the APRA 2015 solicitation. Proposers should contact the cognizant program officer to confirm the suitability of their investigation for that program in advance of submitting a proposal.

B.6 Deformable Mirrors (CG-3)

Deformable mirrors are critical components for both coronagraph starlight suppression and contrast stability. High-contrast stellar coronagraphs depend on deformable mirrors to modulate and remove the residual starlight in the region of interest creating "dark hole" control regions. In the process, the DMs can compensate for wavefront errors due to the imperfections of the telescope and coronagraph optics.

The next generation of high-contrast coronagraphs will rely even more on DMs as they play critical roles in achieving two-sided symmetric dark regions (improving exoplanet search space), correcting for low-order wavefront errors due to slow moving thermal drifts, and, in some cases, shaping the incoming wavefront to mitigate the diffraction effects of obscured apertures.[68,69]

Future DM needs include larger format sizes to allow larger outer working angles for debris disk science as well as the closest exoplanetary systems. Format needs for 4 m-class telescopes may be 96×96 actuators and 10m-class telescopes may even request 128×128 actuators or larger. Wavefront aberrations less than 1/10,000th of a wave will have to be maintained in a coronagraph if contrasts of 10^{-10} contrast are to be achieved. At visible wavelengths, this implies wavefront control at sub-angstrom levels. There is also interest in smaller pitch (< 1 mm) to reduce the size of the optical beam and hence the optical train and in larger stroke (> 500 nm) devices.

To achieve two-sided symmetric dark regions in the focal plane, two DMs will be operated in series allowing for both amplitude and phase error corrections. This was first achieved in the HCIT by Jeremy Kasdin's TDEM[70] in 2013 reaching raw contrasts of 3.6×10^{-9}. In 2015, the WFIRST study used two DMs in both their coronagraph testbeds (shaped pupil and hybrid Lyot) achieving broadband contrasts less than 10^{-8} with the obscured telescope pupil.

The WFIRST coronagraph will use two 48×48 element electrostrictive lead magnesium niobate (PMN) DMs made by Adaptive Optics Associates Xinetics in Devens, MA, a subsidiary of Northrop Grumman. These mirrors have been routinely used in the HCIT vacuum testbeds since 2003. With a 500 µm actuator stroke, they have participated in all the HCIT demonstrations better than 10^{-9} with unobscured pupils. These DMs are built up from electroceramic blocks with actuators separated by 1 mm (see **Figure 21**). These blocks can be assembled into modules covered by a single-mirror facesheet and driven by a Gen 5 voltage supply (not multiplexed) with 100V range and 16-bit resolution. One Xinetics DM has already successfully undergone a 3-axis random vibration test to 10.8 G rms at JPL.

WFIRST will help advance the DM state-of-the-art over the next few years. Expected activities include:

- Flight qualifying the drive electronics
- Redesigning the electronic interconnects to the actuators
- Miniaturizing the drive electronics
- Improving the facesheet surface figure error so as to gain more stroke
- Life test the DM actuators
- Complete environment testing including thermal, dynamic, and radiation testing

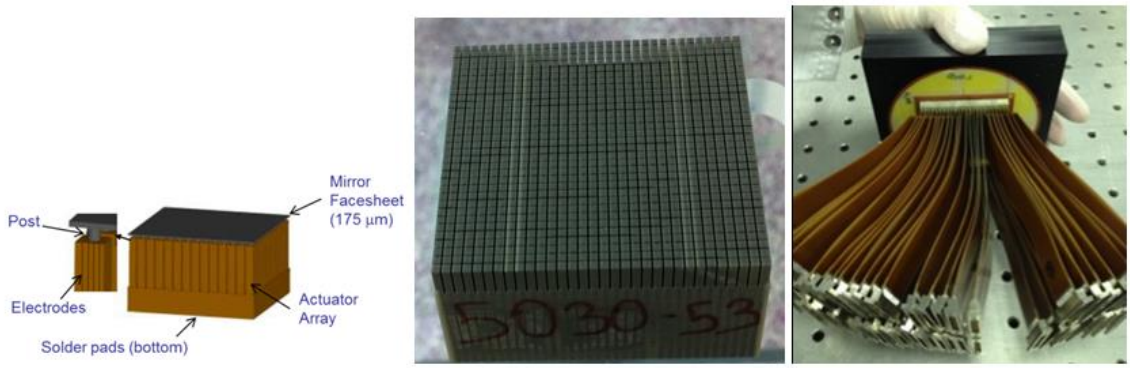

Figure 21: (Left) Schematic of the bulk ceramic block with cut actuators mounted to a facesheet. (Center) Bulk block with 1 mm cut posting actuators. (Right) Connector cables extending from the back of the DM.

WFIRST is also upgrading an existing ExEP facility, the Vacuum Surface Gauge, which will characterize all project DMs. The Vacuum Surface Gauge is an interferometer testbed that can measure both accuracy and stability of DMs along with other key parameters such as wavefront stability, cyclic errors, cross talk, and hysteresis. This testbed, when completed in early CY16, will have the ability to measure surface figure errors and wavefront changes to sub-nanometer levels becoming a premier ExEP facility instrument. It will be also be capable of characterizing other DMs such as MEMS devices.

Larger Xinetics DMs have been built through mosaicking smaller units. A 64×64 actuator device has operated successfully in the HCIT for over a decade. This larger format was achieved by mosaicking four 32×32 ceramic blocks. A 66×66 unit has also been mosaicked from 11×11 units for the Palm 3000 adaptive optics system at the Palomar Observatory. It is expected that the same technique could be used to meet future large format DM needs although no investments have been made. The technology challenge is believed to not be the mosaicking of 48×48 devices or 32×32 devices (to reach 128×128) but rather dealing with the enormous number of interconnects and their electronics.[71] In addition, Xinetics is currently developing sub-mm-pitch DMs.

Alternative DMs are the MEMS devices fabricated by Boston Micromachines Corp (BMC). These DMs are made of a polysilicon membranes coated with one or more layers for the reflective surface and are actuated by 32×32 or 64×64 electrostatic actuators on the backside. BMC offers both continuous face-sheet and segmented mirrors. Pitch sizes come less than 0.5 mm and maximum stroke is about 5 µm for 250 V drive voltage.

There are currently no plans to advance MEMS DMs with WFIRST further than what is being done through the TDEM program. Two separate TDEM awards were funded to BMC, and to another DM fabricator, Iris AO, to continue environmental testing of continuous facesheet DMs as well as segmented DMs, respectively. The goal of these TDEMs is to better characterize their failure modes, and thus raise the TRL of the respective DM models. Both efforts have been hampered by manufacturing issues delaying the commencement of characterization and environmental testing. BMC is expected to complete environment dynamic testing and present their results in CY16. In the past, they have undergone partial environmental testing[72] and have flown on a sounding rocket experiment,[73] although in the latter case, no performance data was acquired. A new sounding rocket experiment (PICTURE-B) with a MEMS DM is scheduled for CY16.

Iris AO DMs are MEMs devices with three electrostatic actuators underneath a segmented mirror surface. The three actuators provide piston, tip, and tilt to a segment. The hexagonal segments are 700 microns wide, vertex to vertex. The actuators are long stroke (8 µm or 5 µm, depending on the model)

over 200 V. The small step precision is limited by electronics digital/analog bit depth. The current Iris AO built electronics are 14 bits, but 20 bit super-resolution electronics are in development. Their environmental testing TDEM is expected to complete in CY17. An Iris AO MEMS DM has demonstrated a monochromatic raw contrast of 5×10^{-9} over angular separations of 1.5–2.5 λ/D using a Visible Nulling Coronagraph at GSFC.[74]

The development of segmented DMs to be used in conjunction with segmented apertures may provide additional wavefront error control. A segmented DM can provide pure segmented mode correction for segment tip-tilt-piston errors with large stroke and without cross-talk or aliasing (which may occur when using a continuous face sheet DM to do the segment mode correction). Segmented DMs can also be adapted with figure control to further drive wavefront errors down and potentially relax other telescope stability requirements. This will require a systems-level trade study. A segmented DM could be a third DM in the optical train or replace one of the two in series.

B.7 Low-Order Wavefront Sensing & Control (CG-5)

The coronagraph's low-order wavefront sensor and control is the critical component for contrast stability during science measurements. It utilizes the bright starlight rejected by the coronagraph optics as the source of information to sense and maintain the state of the optical wavefront established by the high contrast imaging wavefront control (WFC). The starlight wavefront is sensed at high temporal frequency to suppress vibration-induced fast line-of-sight errors and control system pointing drift as well as to correct low-order wavefront aberrations due to telescope thermal drifts.

Future space missions for direct exo-Earth imaging will likely require wavefront stability of 10s of pm over update rates around 10 minutes to achieve a dark hole contrast close to 10^{-10}. They will have to be able to sense and correct fast line of sight jitter (tip/tilt), and, with a large segmented telescope, fast segment mirror tip/tilt/piston jitter, as well as several low-order, thermally-induced wavefront error modes. Alternatively, or in addition, future missions will need to be able to passively isolate or dampen such motions below the required wavefront stability (see Section B.5).

A first step in this direction was accomplished with the development of the PIAA coronagraph system in the HCIT- 2 in 2013. Sub-mas pointing stability was demonstrated in vacuum with a servo system, with the intent of eventually expanding it to demonstrate low-order wavefront sensing and control.[75]

WFIRST is conducting a laboratory demonstration of a LOWFS/C architecture which uses a Zernike wavefront sensor (ZWFS) that provides information for tip/tilt control using a fast steering mirror and low-order wavefront correction using the coronagraph DMs.[76] The LOWFS/C's sensor is designed to have line of sight sensitivity of better than 0.4 mas and low order wavefront, focus (Z4) to spherical (Z11), sensitivity on the order of 10s of pm. Performance against focus, tip, and tilt errors was demonstrated in 2015 by the WFIRST coronagraph team (Milestone #6) where a 14 mas line of sight input error was attenuated to a residual error below 0.5 mas rms per axis (**Figure 22**). WFIRST coronagraph technology milestone 9 scheduled for mid-2016 will be integrating the ZWFS with the WFIRST coronagraphic modes and demonstrating that they can achieve contrast levels below 10^{-8} at WA ≤ 3-9 λ/D while the optical input delivered to the coronagraph includes simulated flight environment disturbance.

Since the advancement of LOWFS/C technologies that will enable future coronagraphic missions is currently included in the WFIRST-AFTA technology development program, investigations in this area are not solicited under the TDEM element of the SAT 2015 call.

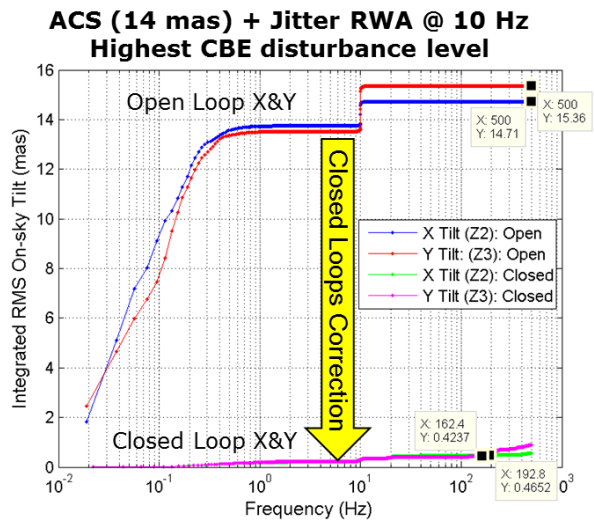

Figure 22: WFIRST coronagraph results from their Milestone #6 Technical Assessment Committee review. Sensor and correction was for tip/tily disturbances only using a fast steering mirror and a simulated WFIRST telescope aperture.

B.8 Post-data Processing (CG-4)

The removal of quasi-static speckle noise from imagery data can further improve the final contrast and inner working angle capabilities achieved by coronagraphs. Post-processing activities can help reduce not just the overall performance of the coronagraph but also relax system-level requirements throughout the observatory. For example, counting on an order of magnitude improvement in the final contrast may loosen both wavefront control and telescope stability requirements. Some post-processing techniques require angular diversity by rolling the instrument (and spacecraft) azimuthally with respect to the star, or by observing a reference star. The specifics of the post-processing technique, however, levy operational requirements and calibration requirements on the spacecraft system and should be understood from the system level and early in the design process.

Applying state-of-art post-processing techniques onto image data already at 10^{-9}-level contrasts in the visible are unprecedented. This is a regime where amplitude wavefront errors may become as important as phase errors. In addition, most of the post-processing algorithms and applications have been conducted in the near-infrared.

Remi Soummer et al.[77] applied ground-based techniques to HST NICMOS data and achieved signal-to-noise (SNR) improvements of 100 times for data with an initial contrast of 10^{-5} in the near-infrared. The use of similar techniques to improve contrast 10–100 times in the visible is under study via simulation in the WFIRST study. Initial results are promising with expected contrast improvement of 10–30×[78, 79] for initial contrasts of around 10^{-8}, depending on angular separation and actual post-processing method, as shown in **Figure 23**.

The WFIRST post-processing efforts will continue during the mission preparation and pave the way for future contrast gain studies. They will eventually provide fully optimized algorithms and even more realistic predictions of contrast gain as the coronagraph instrument gets assembled and closer to its final flight design conditions (spectral bandwidth, dynamical perturbations, etc.).

Since the advancement of algorithms for improved post-processing of coronagraphic data is currently being addressed under the WFIRST-AFTA technology development program, investigations in this area are not solicited under the TDEM element of the SAT 2015 call.

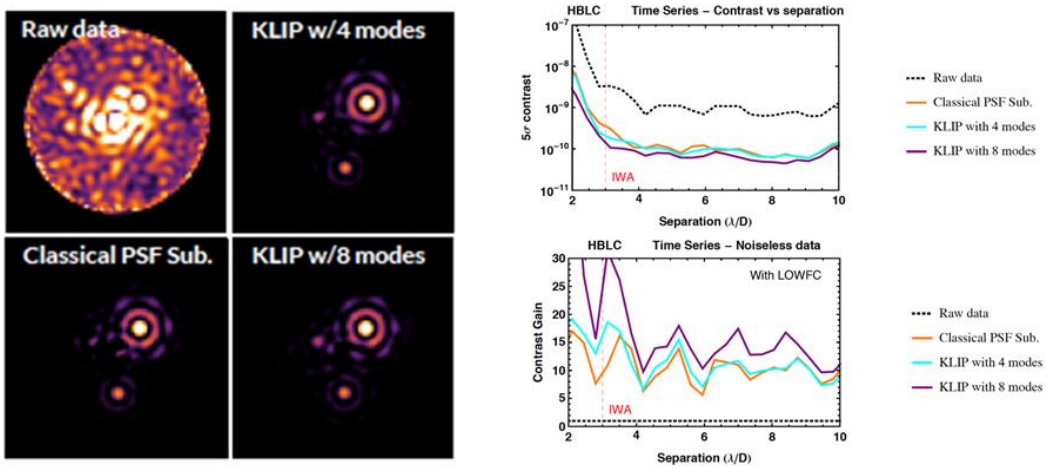

Figure 23: Post-processing improvements to simulated WFIRST HLC data. Realistic sequences of raw speckles fields are derived from full end-to-end simulations of a representative observing sequence. These include wavefront perturbations from expected thermal and structural disturbances.

C STARSHADE TECHNOLOGY NEEDS

External occulters, or starshades, block starlight by shadowing the entrance pupil of a telescope using a physical separation between the starshade and the telescope sufficient to provide the needed inner working angle. This typically requires the starshade to be tens of meters in diameter and located tens of thousands of kilometers from the telescope (**Figure** 24).

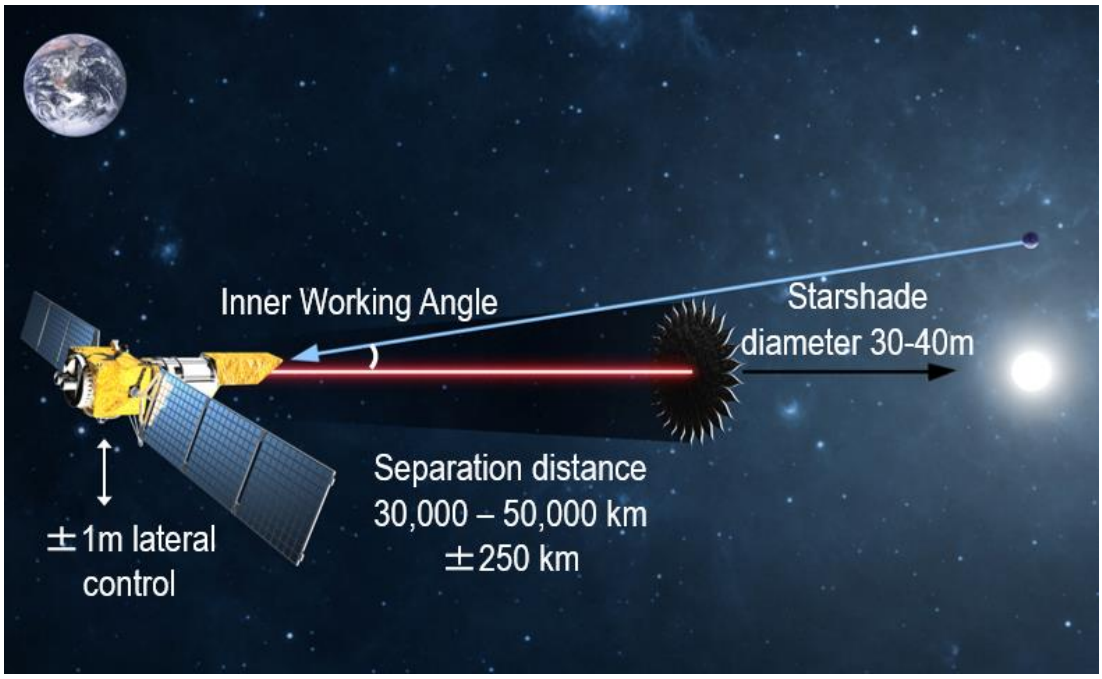

Figure 24: A typical starshade/telescope configuration. The starshade blocks starlight from reaching the telescope pupil, but allows light from the exoplanet.

A starshade suppresses on-axis starlight so that off-axis planets can be imaged. It consists of an inner disk and flower-like petals shaped to create an apodization function to control diffracted starlight. It must also be opaque and limit the amount sunlight scattered from the petal edges into the telescope.

If a circular occulter were used rather than one with numerous petals, a Poisson spot would result in the telescope's focal plane ruining the ability to image faint exoplanets. Independent optical modeling predictions have shown excellent agreement concerning the contrast sensitivity to petal shape errors,[80] and detailed preliminary error budgets have been proposed.[81]

The six starshade technology gaps are listed in **Table 4**. They target a starshade capable of flying on a probe-class mission, a possible rendezvous mission to L2 with the WFIRST telescope, and/or possible LUVOIR/HabEx missions. While no reference mission has yet been adopted, the technology needs are largely based on the architecture of the NASA Exo-S probe study with additional consideration to Northrop Grumman's architecture for larger starshades. The NASA Exo-S study, sponsored by NASA's Astrophysics Division, concluded in 2015 and demonstrated the valuable science return of a starshade mission with a 1.1-m telescope and the 2.4-m WFIRST-AFTA telescope. While the possible starshade needs of the LUVOIR and HabEx mission concepts have not yet been defined, many of the needs listed in **Table 4** will remain applicable.

The six technology gaps listed in **Table 4** fall into three categories (as shown in **Figure 25**).

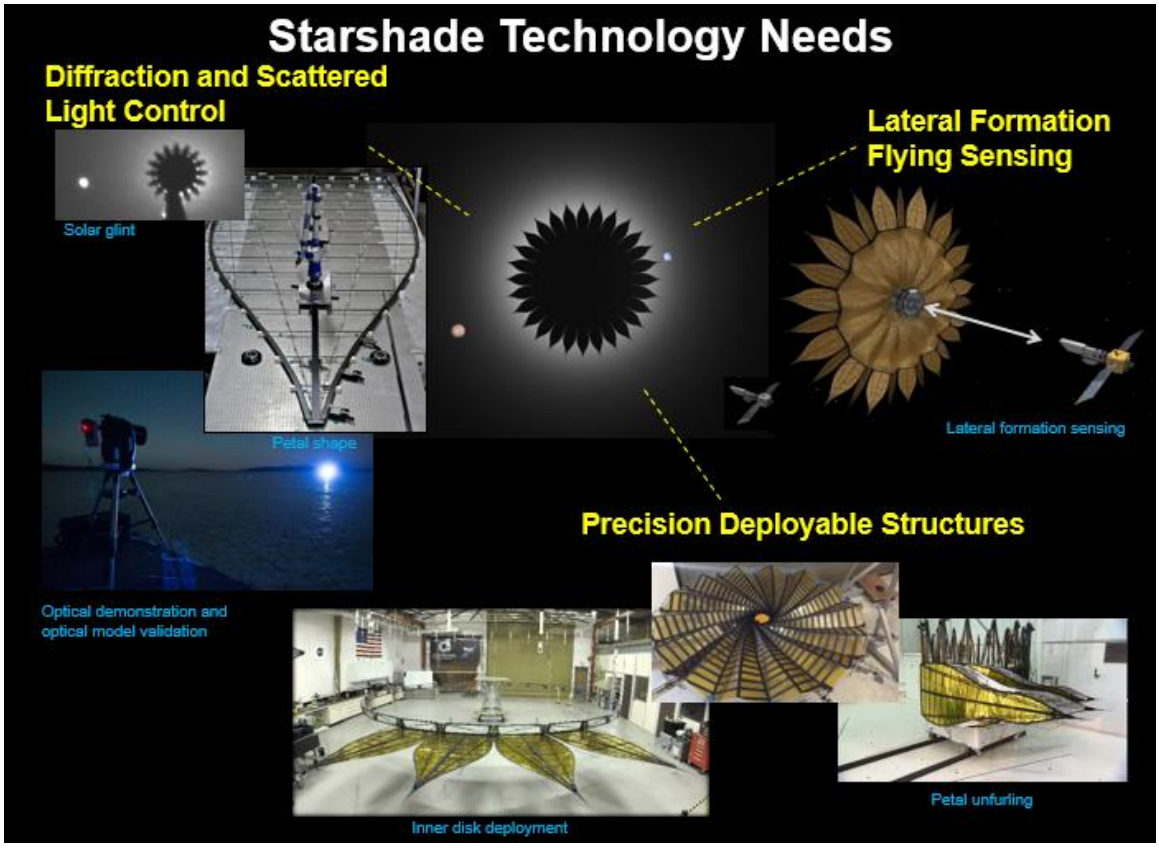

Figure 25: The three categories of starshade technology needs (in yellow font) to directly image and characterize exo-Earths around Sun-like stars.

1. **Diffraction and Scattered Light Control** – the ability to fabricate petals and their integrated optical edges to the design tolerances needed to create contrasts near the petal edges to better than 10^{-10} at the image plane. Fabricated petals that meet design requirements will minimize the diffraction from on-axis starlight and scatter/diffraction from off-axis Sun light detected at the science focal plane. The starlight suppression capabilities of the starshade must be demonstrated to validate optical models so that the models can predict performance in a space environment.
2. **Precision Deployable Structures** – the ability to stow, survive launch, and deploy the petals and inner disk to within the deployment tolerances budgeted to meet the contrast requirements. The optical shields within both the petals and the inner disk fully deploy intact with no damage.
3. **Lateral Formation Sensing** – the ability to sense and control the lateral offset between the starshade and the telescope maintaining the desired contrast long enough for full science integration.

The criteria and rationale of the prioritization of the technology gaps can be found in Section A.3; the results of the prioritization can be found in Section D.

The SAT-TDEM program has done well in funding all of the three key areas of starshade technology needs shown in **Figure 25**. Only the "petal deployment" technology (Section C.3) has remained unfunded by the TDEM program largely because it was only recognized as a technology gap in 2015. As described in the pages to follow, many of the starshade TDEMs are underway and are typically 2–3 years

away from completion. To minimize redundancy between investigations, individuals who wish to propose investigations in any area where existing work is ongoing should discuss their plans with the ExEP Chief Technologist prior to preparing their proposal, and should be careful to clearly differentiate their investigation from ongoing work in their proposal.

One area that would benefit from advancing starshade technology development to TRL 5 would be systems engineering. While not itself a technology gap, systems engineering would perform the necessary work to ensure the various component developments would work together (interface definitions), develop a system error budget and allocations, and conduct the necessary systems performance trades. Thus "system performance assessments" are permissible TDEM proposals. The challenge, however, is that a design reference must be assumed.

Table 4: ExEP Starshade Technology Gap List. Gaps are listed in order of their prioritization scores according to the criteria in Section A.3**.**

ID	Title	Description	Current Capabilities	Needed Capabilities
S-2	**Optical Performance Demonstration and Model Validation**	Experimentally validate the equations that predict the contrasts achievable with a starshade.	3×10^{-10} contrast at 632 nm, 5-cm mask, and ~500 Fresnel number; validated optical model 9×10^{-10} contrast at white light, 58 cm mask, and 210 Fresnel number	Experimentally validated models of contrast to $\leq10^{-10}$ in scaled flight-like geometry with Fresnel numbers ≤20 across a broadband optical bandpass.
S-1*	**Solar Glint**	Limit edge-scattered sunlight and diffracted starlight with optical petal edges that also handle stowed bending strain.	Machined graphite edges meet all specs but edge radius (≥10 µm); etched metal edges meet all specs but in-plane shape tolerance (Exo-S design).	Integrated petal optical edges maintain precision in-plane shape requirements after deployment trials and limit solar glint contributing $<10^{-10}$ contrast at petal edges.
S-6	**Petal Deployment**	Demonstrate petals deploy without edge contact.	Model simulations predict uncontrolled petal unfurling produces edge contact (Exo-S design).	Full-scale controlled petal deployment mechanism demonstrated to secure petals throughout launch and deploy with no edge contact.
S-3**	**Lateral Formation Flying Sensing**	Demonstrate lateral formation flying sensing accuracy consistent with keeping telescope in starshade's dark shadow.	Centroid star positions to ≤1/100th pixel with ample flux. Simulations have shown that sensing and GN&C is tractable, though sensing demonstration of lateral control has not yet been performed.	Demonstrate sensing lateral errors ≤0.30 m accuracy at scaled flight separations (mas bearing angle). Estimated centroid positions to ≤1/40th pixel with limited flux from out of band starlight. Control algorithms demonstrated with scaled

ID	Title	Description	Current Capabilities	Needed Capabilities
				lateral control errors corresponding to ≤1 m.
S-5*	**Inner Disk Deployment**	Demonstrate that a starshade can be autonomously deployed to within its budgeted tolerances after exposure to relevant environments.	Petal deployment tolerance (≤1 mm) verified with low fidelity 12 m prototype and no optical shield; no environmental testing (Exo-S design).	Demonstrate deployment tolerances are met to ≲1 mm with flight-like, minimum half-scale inner disk, with simulated petals, optical shield, and interfaces to launch restraint after exposure to relevant environments.
S-4*	**Petal Shape**	Demonstrate a high-fidelity, flight-like starshade petal meets petal shape tolerances after exposure to relevant environments.	Manufacturing tolerance (≤100 µm) verified with low fidelity 6-m prototype and no environmental tests. Petal deployment tests conducted but on prototype petals to demonstrate rib actuation; no shape measurements.	Fabricate a flight-like, full-scale petal (~7 m) fabricated to within 200 µm tolerance and maintains shape after multiple deployments from stowed configuration.

* New proposals for these gaps should be careful to clearly differentiate their investigation from ongoing work in their proposal.

** Proposals for funding are not requested under the TDEM program at this time.

C.1 Optical Performance Demonstration and Model Validation (S-2)

Starshades must demonstrate experimentally they can reach ≤ 10^{-10} contrasts in scaled flight-like geometry with Fresnel numbers ≤ 20 across a broadband optical bandpass. The challenge is that the large starshade-telescope separation distances required prohibit ground-based optical performance verifications of large starshades. Instead performance will need to be verified in a two-step process. First, subscale tests will demonstrate contrast performance consistent with imaging an exo-Earth and validate the optical models, upon which full-scale shape tolerances are based. The scaling approach is to match the flight design in terms of the number of Fresnel zones across the starshade such that the diffraction equations defining the dark shadow are identical. Second, the shape tolerances will be verified on a full-scale petal. Key capabilities have already been demonstrated via early prototypes, however, only a limited number of tests have been conducted at a flight-like Fresnel number (<20).

Several experiments over the last decade demonstrate the viability of creating a dark shadow with a starshade to contrasts better than 10^{-10} just outside the petal edge. They include lab demonstrations at the University of Colorado,[82,83] Northrop-Grumman,[84,85] Princeton University,[86,87] larger scale tests in a dry lakebed by Northrop Grumman as part of their TDEM-12,[88] and larger scale night-time tests using the McMath Pierce solar observatory on astronomical objects. Each of these experiments has been limited in contrast performance to some extent by a subset of the following test environment issues:

- Wavefront errors due to collimating optics

- Dust in open air testing
- Diffraction effects due to the finite extent of the optical enclosure
- Diffraction off starshade support struts
- Imperfections in shade due to small dimensions
- Diffraction from imperfections in optics

The TDEM-12 activity led by Tiffany Glassman and Steve Warwick of NGAS was completed in 2015. It tested 58 cm starshades in open air on a dry lakebed with a starshade-telescope distance of 1 km and a "star"-starshade separation of 1 km (see **Figure 26**). The light source was a 1W white-light LED.

The configuration parameters compared to flight are shown in **Table 5**.

Figure 26: Optical demonstration setup in a Nevada dried lake bed. A 4 cm Celestron telescope is positioned 1 km from the 58-cm starshade prototype. A 1W white light lamp simulating a distant star is positioned an additional km from the starshade. LEDs of various intensity simulating exoplanets are positioned near the lamp (photo: Northrop Grumman).

Table 5: Configuration parameters for Northrop Grumman's desert tests.

Test	Starshade to Telescope Separation (km)	Starshade Diameter (m)	Telescope Aperture (m)	Resolution (arcsec)	Resolution Elements	Inner Working Angle (arcsec)	Fresnel Number
1	1	0.58	0.04	3.8	26.8	51	210
2a	0.4	0.29	0.12	1.5	82.7	62	87
2b	0.4	0.20	0.08	1.9	43.2	41	42
2c	0.4	0.10	0.04	3.8	11.1	21	10
3	2.4	0.29	0.04	3.8	4.0	12	14
Space	~ 50,000	~ 40	2.4	0.08	2	0.065	< 20

Northrop Grumman was able to reach a contrast result of 9×10^{-10} near a petal edge (**Figure 27**).

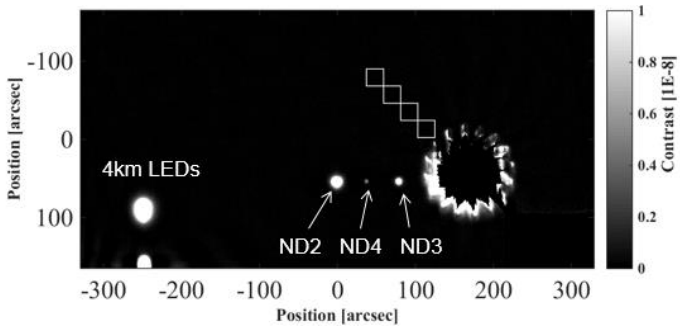

Figure 27: Combined 112 images; 3σ standard deviation in box closest to the starshade is 9.09×10^{-10}. Planet LEDs have neutral density (ND) filters in front; ND4 planet ~ 8×10^{-9} below main source. Light scatter from dust is modelled and subtracted from the image. (credit: Northrop Grumman)

During the TDEM-12 tests, flawed starshades were measured and compared to predicted results generated using Northrop Grumman, JPL, and University of Colorado models. In general, model predictions were within a factor of 5 of measured values. This level of disagreement between model predictions and measurements was expected, given the uncertainties in the measured results. However, significant differences between the different model predictions were seen, likely due to the modifications to the models to handle the spherical wavefront due to the light source at 1 km, rather than infinity (**Figure 28**). The differences between models are higher than expected based on previous model comparisons. Further field tests and model case studies are underway in CY16 to better understand these model discrepancies.

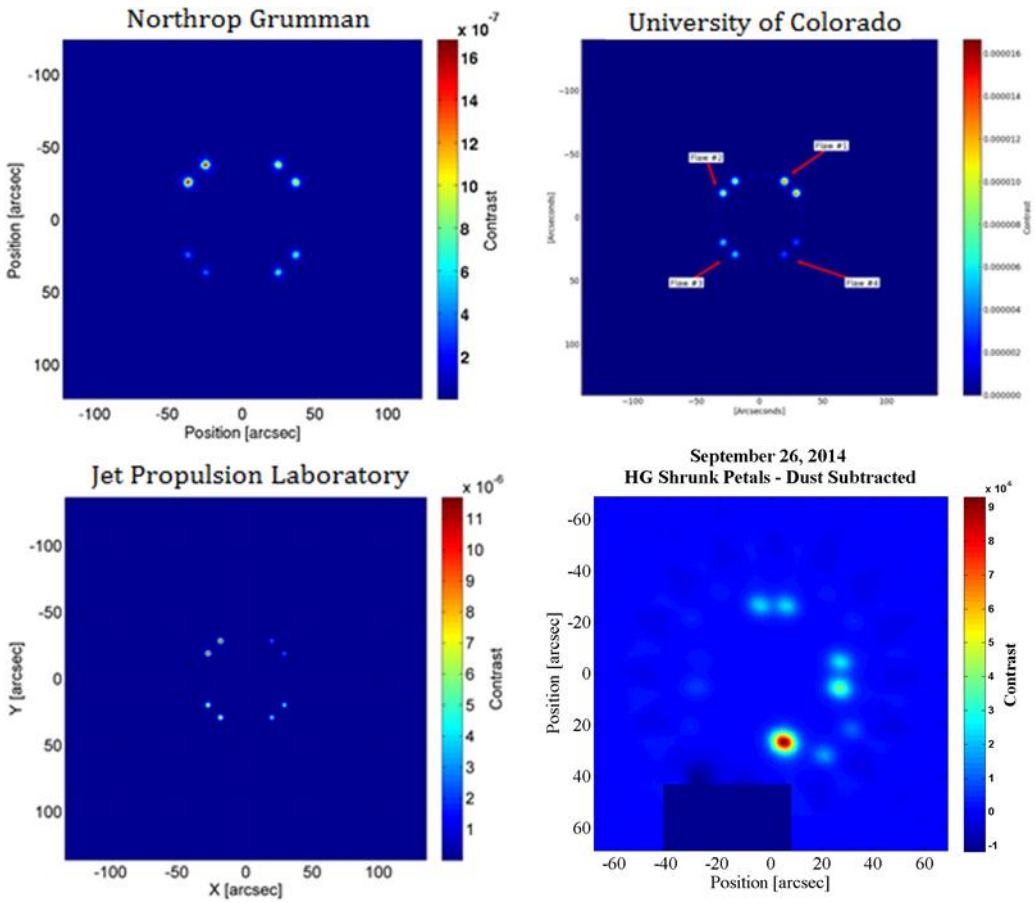

Figure 28: Figure Model Verification. Three independent models predicted the impact of intentional flaws on the optical performance of the starshade. Shrunk Petal model results (top, bottom-left) and actual measurement (bottom-right) are shown here. Qualitative similarities between the contrast features in the model and the measurement are clear. Quantitatively they agree to within an order of magnitude. The bright peak and dark mask at the bottom of the measured image are due to the starshade stand and should be ignored. (credit: Northrop Grumman)

Northrop Grumman has also carried out optical testing of the starshade at the McMath Pierce solar observatory outside of Tucson (**Figure 29** and **Figure 30**). This testing allows the starshade optics to be tested at close to the flight-like Fresnel numbers and uses parallel light from actual astronomical sources rather than the diverging source used in the desert. Use of a heliostat to track the position of the stars allows long integration times (~1 hr of stacked images).

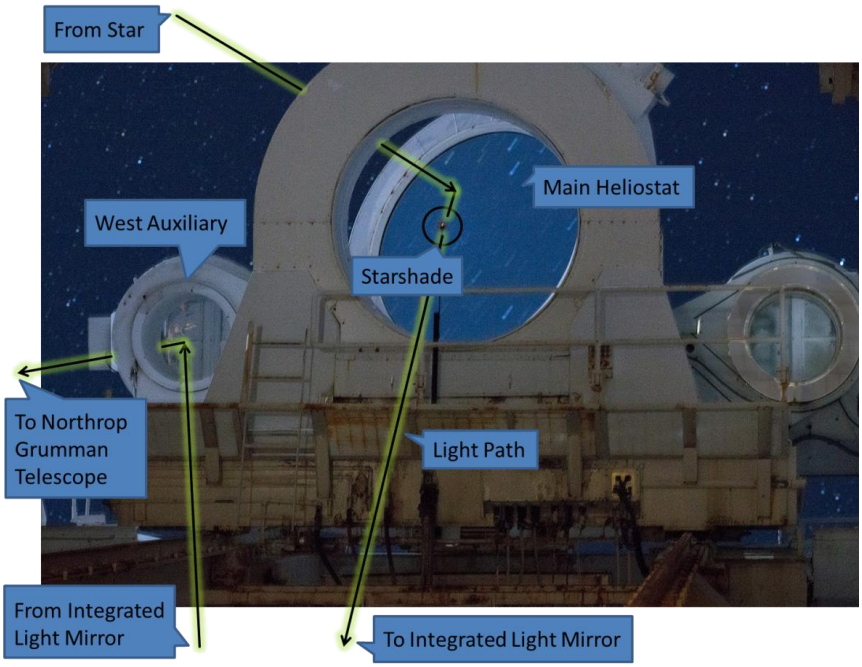

Figure 29: Light from a bright star or planet is reflected off the main heliostat and interacts with a small (~10 cm) starshade mounted directly after the heliostat. That light is shone off the integrated light mirror approximately 80 m down the McMath tube and back up onto the West Auxillary heliostat (**Figure 30**) where it is directed over to a different collection site on the mountain. (credit: Northrop Grumman)

Figure 30: The Northrop Grumman collection telescope points at the west heliostat mirror approximately 250 m away collecting the light from the bright star and the starshade. The total optical separation of the starshade and collecting telescope is approximately 420 m. (credit: Northrop Grumman)

Demonstrations using this setup have been carried out against a number of astronomical objects (**Figure 31**) and sizes of starshades, covering Fresnel numbers of ~90 to 10, as shown in **Table 5** for Tests 2a-2c. A further collection site at 2.4 km has been tested (Test 3) and has been shown to be viable for future tests in 2016, allowing another step closer to flight like Fresnel numbers and inner working angles.

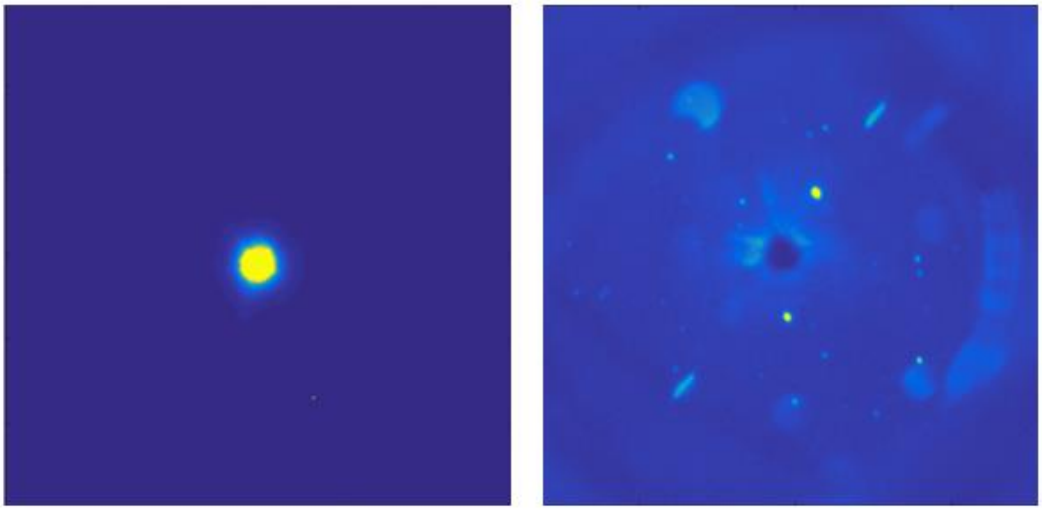

Figure 31: The 20 cm starshade (Test 2b) against the star Vega. A 1 sec exposure on the left is completely saturated. A 20 min exposure of Vega obscured by a starshade on the right allows much dimmer stars in the proximity of Vega to be seen. The two bright stars close to the center at ~10,000 times dimmer than Vega, with angular separation of ~2 arcmin. Dimmer stars in the image are approximately 10^{-6} of the brightness of Vega. All other optics are the same between the two images. (credit: Northrop Grumman)

The first demonstration to be conducted at a flight-like Fresnel number (<20) is planned for 2016.[89] A 78-m starshade optical testbed being constructed at Princeton University as part of their TDEM-12 addresses the limitations identified above to hopefully yield the darkest shadow produced by a starshade to date (PI is Jeremy Kasdin; see **Figure 32**).

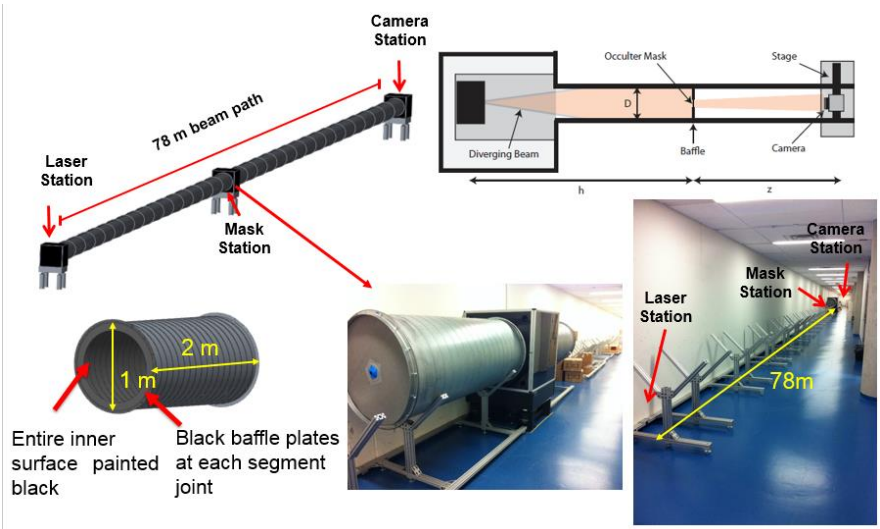

Figure 32: Schematic diagrams and pictures of the Princeton University starshade performance testbed (TDEM-12; PI Kasdin). Tubes are each 2 m in length and 1 m in diameter. They are painted with low reflectivity black paint and will include baffles to suppress stray light.

An expanding beam will be used to eliminate collimating optics and the testbed length is constrained to an available indoor facility with an optical enclosure that limits dust effects. Diffraction effects from the optical enclosure and support struts are mitigated with an innovative mounting scheme whereby the

starshade is supported by an outer ring with an apodization profile optimized in similar fashion to the starshade profile (see Figure 33). This introduces a nonflight outer working angle limit at the tip of the outer ring. The demonstration is expected to match the flight Fresnel number (14.5) and first light of the testbed is expected in early CY16.

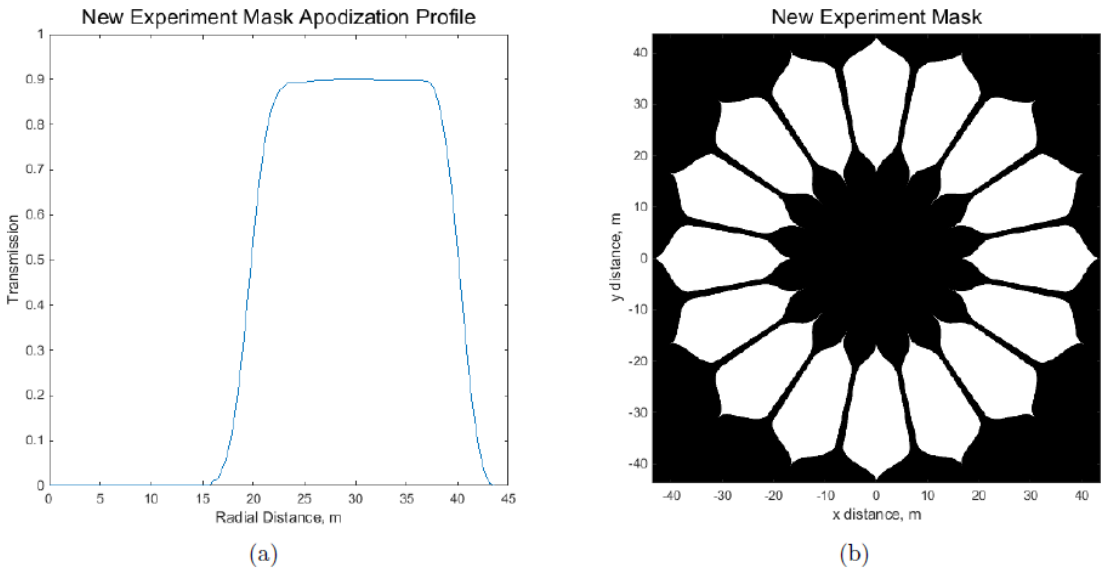

Figure 33: (a) Kasdin TDEM-12 designed apodization profile including outer ring and struts. (b) Binary realization of mask profile.

In 2015, JPL's Microdevices Laboratory, in support of Kasdin's TDEM-12, was able to reduce their starshade manufacturing resolution from 500 nm to 250 nm. This improvement is expected to reduce contributing contrast noise from the 26-mm-scaled shade. Significantly, the test results match well with analytical predictions for the shape resolution and defects.

C.1.1 Contrast vs Suppression

As part of their TDEM-12, PI Glassman and Warwick from Northrop Grumman were asked to address their demonstration's enhanced contrast performance due to a disproportionately larger telescope aperture.[90] Contrast ratio was selected as the figure of merit as that it correctly reflects the ability to detect light from a dim source at an angular separation from a bright source. Contrast ratio is defined as the ratio of signal brightness at a location offset from the shaded star to the peak brightness of the unblocked star. It is measured in the focal plane. Suppression, alternatively, measuring the intensity in the pupil plane, is defined as the ratio of the total starlight that enters the telescope with the starshade in place to that without the starshade.

Suppression is primarily affected by the starshade performance. Contrast ratio, on the other hand, gets better (decreases) with telescope resolution. As the PSF of the star gets narrower and the peak higher, the contrast relative to the peak of the star gets better. In the flight configuration, where the telescope resolution element is about half the radius of the starshade in the image plane, the telescope resolution contributes a factor of 10–100 to the contrast ratio (relative to the total suppression) at locations just beyond the edge of the starshade. For the field test configuration, they over-resolved the starshade by a factor of about 8. The telescope resolution element is about 1/16 the radius of the starshade in the image plane. In this case, the telescope resolution contributes a factor 10^4-10^5 to the contrast ratio at the radius of the starshade tips compared with a flight-like telescope contribution of 10^1–10^2 (see **Figure 34**).

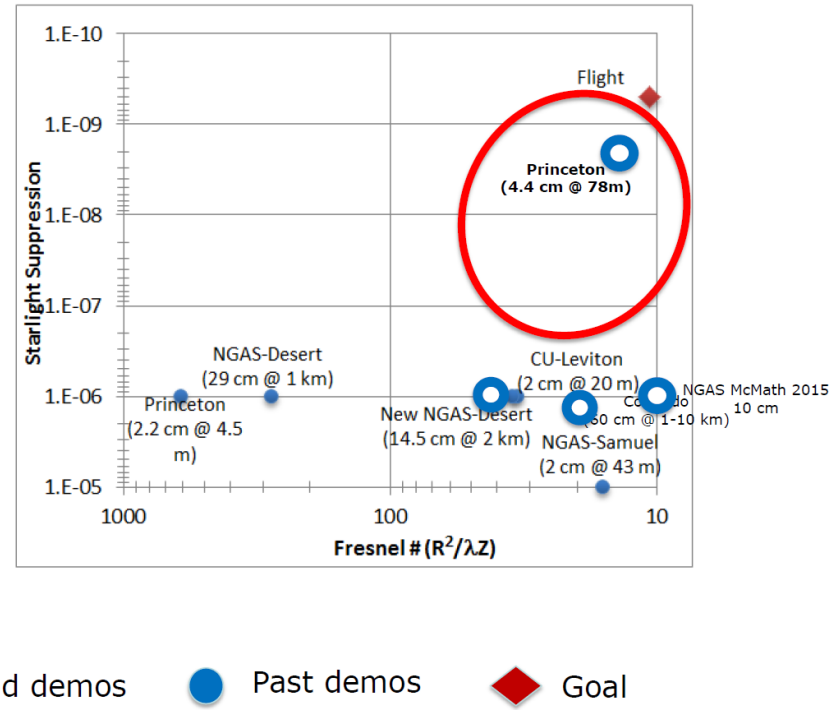

Figure 34: Draft chart comparing light suppression versus Fresnel number. The red diamond indicates the parameter space expected for a flight starshade. It is distinct from past demonstrations shown by the solid blue circles. The "new" Princeton demo will be the closest to replicating a flight configuration of starshade size, starshade-telescope distance, and wavelength. Most of the previous demos did not measure suppression but rather contrast and we are estimating the suppression. The red circle indicates the region where a demonstration gap has existed before the Kasdin TDEM-12.

For the desert field tests, uncontrollable effects such as dust and background scattered light introduce errors that would make it very difficult to accurately calculate the total suppression of the measurement. While the effects of these error sources are not particularly large, they swamp the ~10^{-8} effect attempting to be measured. In other words, these effects would need to be modeled to extremely high accuracy to allow accurate subtraction of background light and therefore allow accurate full suppression measurements. Avoiding the uncertainty of this correction Northrop Grumman used contrast as the best figure of merit for these tests.

C.2 Solar Glint (S-1)

Starshade optical edges will scatter or diffract a small fraction of sunlight into the telescope. A starshade to be effective must both minimize starlight diffraction at and mitigate reflected and diffracted sunlight away from the telescope. This solar glint appears primarily as two large lobes, spread by the telescope PSF, originating from a few petals oriented with edges broadside to the Sun. Solar glint can be effectively calibrated with a spinning starshade, but this requires limiting the flux to below the level of the exozodiacal light.

The required need is an identified material that can be integrated to the petal's structural edge to (1) meet and maintain precision in-plane shape requirements after deployment trials and (2) limit solar glint enabling 10^{-10} contrast at the petal edges. Analyses for an Exo-S petal architecture show[91] that this optical edge should have a sharp beveled edge (≤ 1 µm radius) and precisely shaped (≤ 20 µm rms) edges that also handle stowed bending strain. This requires limiting the product of edge radius and

reflectivity to less than 12 µm-%, while maintaining a precise in-plane shape, limiting thermal deformation of the petal and accommodating stowed bending strain.

The current capability for optical edges less than 10 µm in radius is machined graphite edges that satisfy all requirements except edge radius, and chemically etched amorphous metal edges that satisfy all requirements except the in-plane shape tolerances.

Northrop Grumman has a different architecture for the starshade and its petals require looser optical edge requirements. In 2015, a TDEM-12[92] led by Suzy Casement progressed towards developing a stray light model to understand the amount of Sun light that may contaminate the image due to scattering and/or diffracting off of the edge of the starshade, depending on the material and geometry of the edge. They are working with three coated metals—aluminum, titanium, and BeCu—which will be tested by the company ScatterWorks to see if the stray light requirements are met. To support the final analyses, scatter measurements will be taken of both the flat surface for an optical engineering model and the edge as a direct measurement. These values will then be compared using the simple test model[93] developed by early CY16. The TDEM will also conduct in CY16 environment tests on two samples (humidity exposure, thermal cycling, cyclic abrasion, adhesion test).

In 2015, a similar effort funded by JPL internal research and technology developed prototype optical edges by chemically etching thin strips of amorphous metal and then bonding them to a graphite substrate of matching shape. The in-plane shape error exceeded the allocated tolerance due to the redistribution of internal stresses upon the removal of material.

The ongoing Kasdin TDEM-12 effort is focused on mounting the edge material to a relatively stiff carrier to hold the in-plane shape through the chemical etching process and then transferring the edge to a stiff graphite substrate. The team intends to revisit several candidate metals, including stainless steel, through scatter testing of etched coupons. Another effort within the TDEM is dedicated to characterizing the sensitivity of edge scatter performance to dust that can be attracted to statically charged optical edges. The dust environment in the launch vehicle fairing during launch will be evaluated and compared to the laboratory environment. One of the TDEM-12 milestones is proposed to verify solar glint performance at the petal level after testing to all relevant environments.

An alternative approach to controlling solar glint is to not spin the starshade and apply a specific edge shape to select petals to eliminate the surface area presented broadside to the Sun. This approach has large system implications and is under careful evaluation.

To minimize redundancy between investigations, individuals who wish to propose investigations in any area where existing work is ongoing should discuss their plans with the ExEP Chief Technologist prior to preparing their proposal, and should be careful to clearly differentiate their investigation from ongoing work in their proposal.

C.3 Petal Deployment (S-6)

Full-scale controlled petal deployment mechanism must be designed and demonstrated to secure petals throughout launch and deploy with no edge contact. The Exo-S starshade mechanical architecture stows the petals for launch in a very small volume by wrapping, or furling, them around a central hub (**Figure 35**; left). They deploy, or unfurl, by releasing the stored strain energy. The challenge is to control this energy release, ideally in quasi-static fashion. Computer-simulated petal releases conducted by Roccor (JPL's SBIR partner) showed unstable motion and physical contact between the unfurled petals.

Northrop Grumman's deployment architecture, based in part on non-NASA heritage, relies on simultaneous telescopic booms to deploy both the inner disk and the petals—one boom per petal (**Figure 35**, right).

Figure 35: On the left is a schematic of the Exo-S controlled petal unfurling approach compared to the Northrop Grumman approach on the right using simultaneous deployable telescopic booms.

To close this technology gap requires a demonstration of petals deploying without any unwanted interpetal contact and no optical edge contact. There is no apparent state-of-art for this problem.

Part of any petal deployment mechanism must include a method to restrain the petals during launch, withstand the expected dynamic launch loads, and unlatch and deploy them in a controlled manner. One solution being developed by JPL and Roccor is to tension radial cords through the petal stack and then cut the cords and close the openings. The interface to this mechanism is built into the current petal design. A specific launch restraint issue is to avoid any optical edge contact during launch. This issue is made tractable by the vibration damping provided by the open cell foam of the petal optical shields.

In 2015, several mechanical solutions for unfurling the petals were studied via a SBIR with ROCCOR and their subcontractor Tendeg. The current effort is focused on producing a full-scale Petal Unfurling Testbed that will be used to develop the mechanical solution in CY16. The simulated petals are specifically designed for adaptation to the specific mechanical solution. A second generation testbed is also planned.

This unfurling mechanism concept requires additional investment to complete and there may be other architectures to deploy wrapped petals.

C.4 Lateral Formation Flying Sensing (S-3)

The rapid decline in contrast as one moves radially from the center of the starshade's shadow places a tight constraint on the lateral position of the starshade relative to the telescope-star line of sight. Maintaining alignment is imperative to achieving the science goals of an Earth-finding mission. According to the Exo-S and New Worlds Observer studies,[94] the starshade spacecraft must control its lateral position to within about ±1 m of the telescope boresight to keep the telescope within the dark shadow. The benign disturbance environment at either Earth-Sun L2 or an Earth Drift-Away orbit makes the control function straightforward with conventional chemical thrusters. The challenge, however, is to sense the lateral position error to within ± 30 cm at distances of tens of thousands of kilometers. While the control requirements of formation flying at L2 may not be beyond current capabilities, the accuracy of position sensing at such large separations is unprecedented (**Figure 36**). Closing this gap requires demonstrating this capability.

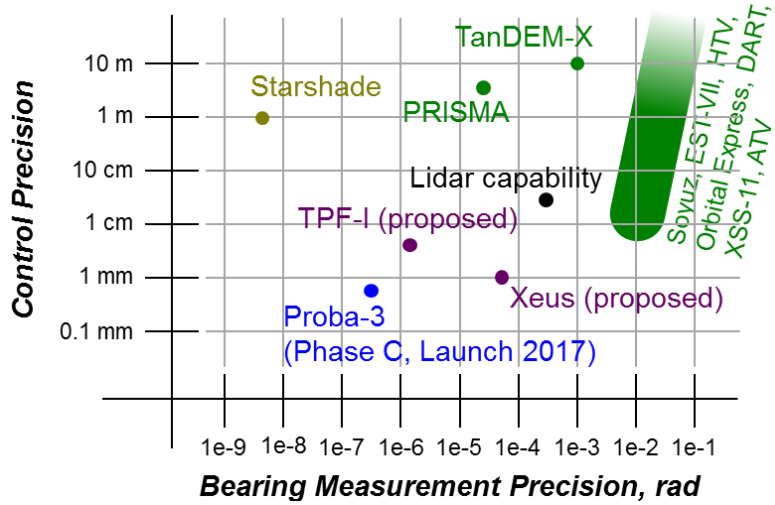

Figure 36: Precision of formation flying control versus precision of bearing angle. The ±1 m offset control between the starshade and the telescope is not unique to spacecrafts. However, the bearing angle, due to the 30,000–50,000 km separations are unprecedented. More details can be found in the Exo-S report as well as Scharf et al. (2015).[95]

The axial separation distance, or range, between the starshade and telescope is loosely controlled to within ±250 km, with sensing knowledge to within ±1 km. The range is measured by a proximity radio with two-way ranging. These tolerances are well within the state of the art.

The lateral formation sensing challenge is made tractable by employing the large aperture science telescope to feed a guide camera that can be a channel within the exoplanet science instrument. Out-of-band starlight leaks around the starshade to indicate the stars position relative to the starshade position that can be indicated by a flashing laser beacon. The guide camera can image both signals onto the same focal plane and measure the difference between their centroided PSFs. For a preliminary camera design the sensing accuracy requirement equates to about 1/40th of a pixel. By comparison, conventional cameras have demonstrated less than 1/100th of a pixel accuracy. However, the star flux is relatively low and this adds to the challenge.

In 2015, formation guidance studies within the Exo-S Probe Study focused on a Rendezvous Mission with WFIRST, and specifically the use of existing focal planes in the coronagraph instrument for both science and formation guidance. This moves the guide camera wavelengths from the NIR to within the available visible band.

A TDEM-13 activity led by Jeremy Kasdin of Princeton University was awarded to demonstrate the technology of a focal-plane imaging formation flying sensor at visible wavelengths.[96] A science instrument and guide camera simulator will be produced and tested with simulated PSFs and flux levels that match the flight condition. An integrated computer will run algorithms to compute the lateral error. This signal is fed to a separate computer that runs the control algorithm for a closed loop simulation. The optical simulation will be verified by comparison to test data from the Princeton Optical Testbed (same as the 78-m testbed being used for optical demonstrations described in Section C.1). This TDEM activity will also demonstrate retargeting and acquisition performance via simulations.

Another TDEM-13 activity, this one led by Webster Cash of the University of Colorado-Boulder, plans to investigate lateral sensing using long wavelength light diffracted around the starshade to provide accurate position information using a pupil-imaging formation flying sensor,[97] a phenomenon known as the spot of Arago. This technique will map the distribution of light at the aperture and to guide to the

center of the shadow. Recovered intensity from behind the starshade of greater than 1% at wavelengths outside of the science bandpass will be measured, and the measured wavefronts at different wavelengths and starshade configurations will be used to validate model predictions. This will be the first demonstration of starshades at wavelengths greater than 1 µm and will provide a new wavelength regime in which to investigate the starshade's performance and validate the state of the art diffraction codes.

Results from the two demonstrations are expected in CY17. With these two TDEM-13 just commencing their investigations no TDEM-15 proposals in lateral formation sensing are being sought.

C.5 Inner Disk Deployment (S-5)

To function as an occulter and create a dark shadow for the formation-flying telescope, the inner disk must (a) deploy petals to an in-plane position tolerance (±1 mm for the Exo-S design where contrast performance is predicted to be relatively insensitive to out-of-plane errors) and (b) deploy a large optical shield without incidence (snagging, ripping). Deployment tolerances must be demonstrated with flight-like, minimum half-scale inner disk, with simulated petals, optical shield, and interfaces to launch restraint.

Several different implementations are possible for the packaging and deployment of a starshade. One example for the inner disk and petal deployment is the use of telescopic deployable booms (**Figure 37**, right); another is the use a deployable perimeter truss (**Figure 37**, left). The latter, inspired by Northrop Grumman's flight-heritage Thuraya communications satellite and most recently flown with NASA's Soil Moisture Active Passive mission, was the approach taken by the Exo-S study for 30–40 m-class starshades. The required size of starshades for 10-m-class telescopes has not yet been finalized nor whether they would be scalable from the Exo-S architecture. These remain important open issues and should be part of the HabEx/LUVOIR mission concept studies.

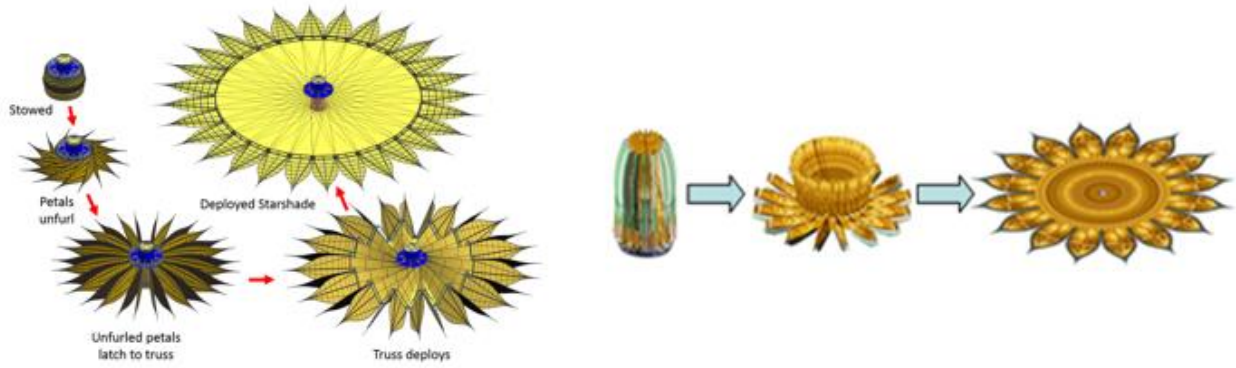

Figure 37: (Left) Exo-S petal unfurling and inner disk deployment approach[98]; (Right) Northrop Grumman petal and inner disk deployment approach[99].

A TDEM-10 activity[100] led by Jeremy Kasdin (Princeton) successfully demonstrated the allocated deployment tolerances using a retrofitted 12m diameter Astromesh Antenna (NGAS-Astro) that is representative of perimeter trusses in terms of deployment repeatability (**Figure 38**).

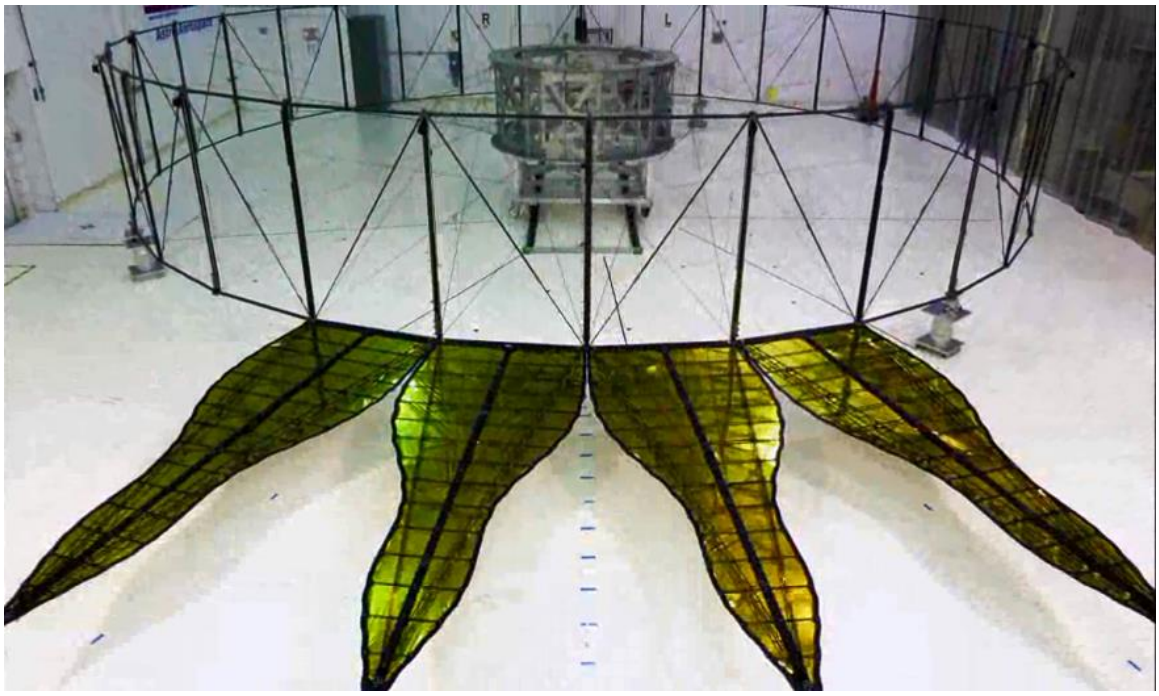

Figure 38: Kasdin TDEM-10 inner disk demonstration with an off-the-shelf Astro-Aerospace antenna deployment demonstrating petal positioning tolerances. Astro-Aerospace is a subsidiary of Northrop Grumman.

This TDEM activity also produced an inner disk design that was tailored to accommodate petals. In 2014, the ExEP invested in designing and building a 10 m diameter testbed per this new design. **Figure 39** shows this testbed fully deployed with four mockup petals.

Figure 39: Starshade Deployment Testbed at JPL has 10-m-diameter perimeter truss with gravity compensation fixtures.

In 2015, the ExEP produced a second-generation perimeter truss testbed that included a more flight-like truss design removing a model-predicted static buckling mode, again following the Exo-S approach. This

testbed remains to be fully integrated. A separate SBIR (Small Business Innovation Research) activity by a Louisville, Colorado-based company (Roccor) is now producing the spokes for this testbed, removing the cross-laced architecture of the previous testbed.

Also in 2015, an inner disk optical shield concept was developed that incorporates an origami fold pattern, considered to be ideal for stowage and deployment. A 2-m testbed was developed by JPL and Roccor allowing for early prototype development (see **Figure 40**). The most recent origami design included panelized sections. Demonstrations were conducted both with paper and later acrylic prototypes. A 5-m-diameter inner disk prototype is being designed and built in FY16 to support more mature development of the origami concept on the way towards a TRL 5 half-scale Exo-S–based inner disk.

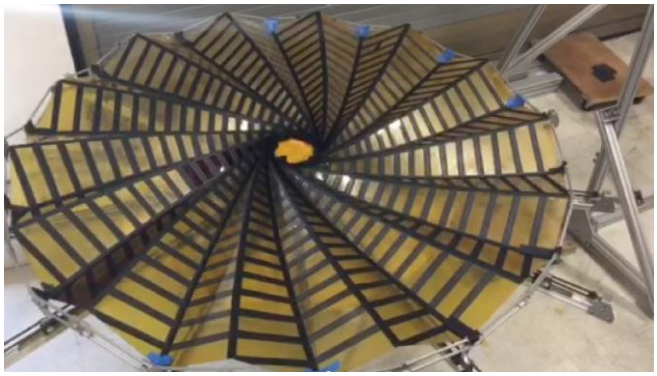

Figure 40: 2m Optical Sheet Testbed allows for early optical shield prototype design demonstrations. This figure shows an early panelized acrylic panelized design constructed by 2015 summer students at JPL.

A TDEM-14 activity[101] led by Mark Thomson of JPL is underway to develop the inner disk optical shield design, produce a prototype that integrates with the 10-m-diameter Starshade Deployment Testbed, and demonstrate the requisite deployment tolerances, including thermal loads from the optical shield. In addition to stowing in a very compact volume, the key challenge is to attach the optical shield in a fashion that limits thermal deformation of the inner disk.

To minimize redundancy between investigations, individuals who wish to propose investigations in any area where existing work is ongoing should discuss their plans with the ExEP Chief Technologist prior to preparing their proposal, and should be careful to clearly differentiate their investigation from ongoing work in their proposal.

C.5.1 Micrometeoroid Holes

Micrometeoroids will create holes in the starshade optical shield. Some will pass all the way through and others will not. The multiple spaced layers of an optical shield mitigate the impact of through holes, as only a small fraction will create a light path to the telescope. Preliminary modeling[102] of the starshade design and micrometeoroid flux environment indicates a cumulative through hole area less than 1 cm^2 that will add contrast of 10^{-12}.

In 2015, the transmission of sunlight through micrometeoroid holes was modeled. It was shown that the open cell foam currently used to separate the optical shield layers is effective at dissipating sunlight. None the less, an additional layer of Kapton is now planned as per the Exo-S architecture.

The new Thomson TDEM-14 activity to develop the inner disk optical shield includes a study of micrometeoroid requirements by Northrop Grumman Co-Investigators (Co-Is). The goal is to leverage any relevant experience gained on JWST.

C.6 Petal Shape (S-4)

Starshade petals are responsible for re-directing the diffraction pattern of the on-axis starlight away from the aligned formation-flying telescope and mitigate reflection and diffraction of light from the off-axis Sun. Consequently, they must be fabricated to a precise shape. This remains to be verified. A flight-like, full-scale petal (~7 m) must be fabricated to within 200 µm of shape tolerances and to maintain shape after multiple deployment cycles from stowed configuration.

Two similar approaches to the design of external occulters have been studied, differing by whether an analytical petal shape is used[103,104] or whether it derives from a mathematical optimization.[105,]**Error! Reference source not found.**[106] The TDEM-09 activity led by Jeremy Kasdin of Princeton adopted the latter approach and successfully demonstrated the allocated manufacturing tolerance (≤100 µm) of an early 6-m petal prototype, but without optical shields that make the petal opaque, optical edges, and environmental testing (**Figure 41**).

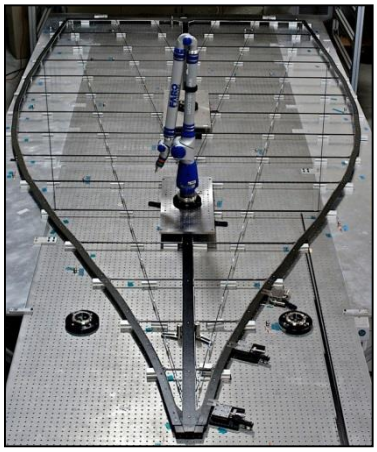

Figure 41: TDEM-09 6-m prototype petal designed and fabricated to meet 100 µm design tolerances (PI Kasdin/Princeton with his JPL Co-Is).

In 2015, a TDEM-12 activity led by Kasdin developed a new preliminary petal design that incorporates flight-like optical edges and optical shields and includes interfaces to proposed launch restraint and petal deployment control mechanisms. Ongoing activities will complete the detailed petal design, produce a flight-like, full-scale prototype and test it to relevant environments. The final verification will be to verify petal shape multiple times with deployment testing in between. This will require an in-situ petal metrology tool.

To minimize redundancy between investigations, individuals who wish to propose investigations in any area where existing work is ongoing should discuss their plans with the ExEP Chief Technologist prior to preparing their proposal, and should be careful to clearly differentiate their investigation from ongoing work in their proposal.

D PRIORITIZATION

The technology gaps were prioritized by members of the ExEP technology team and presented at ExoPAG 13 (January 2016) for feedback. The sum of the three prioritization criteria scores is shown in **Table 6**. No weighting was applied to any of the criteria. Definitions of the criteria and their relative values are described in Section A.3.

Table 6: Coronagraph and Starshade Technology Gap Prioritizations.

Coronagraph Technology Gap Prioritization

Gap ID	Gap Title	Impact	Urgency	Trend	Total
CG-2	Coronagraph Architecture	4	4	3	11
CG-1	Large Aperture Mirrors	4	2	4	10
CG-8	Visible Ultra-Low Noise Detector	4	3	2	9
CG-9	NIR Ultra-Low Noise Detector	4	2	3	9
CG-6	Segment Phasing Sensing & Control	4	2	3	9
CG-7	Telescope Vibration Control	4	2	3	9
CG-5	Deformable Mirrors	4	2	2	8
CG-3	Low-Order Wavefront Sensing and Control	4	2	2	8
CG-4	Post-Data Processing	4	2	2	8

Starshade Technology Gap Prioritization

Gap ID	Gap Title	Impact	Urgency	Trend	Total
S-2	Optical Performance Demonstration and Optical Modeling	4	4	3	11
S-1	Control Edge-Scattered Sunlight	4	4	3	11
S-6	Petal Unfurling	4	3	3	10
S-3	Lateral Formation Flying Sensing	4	3	2	9
S-5	Inner Disk Deployment	4	3	2	9
S-4	Petal Shape	4	3	1	8

E CONCLUSION

The 2010 Astrophysics Decadal Survey recommended the creation of a technology development program for a potential future exoplanet mission to mature starlight-suppression technology for the detection of spectra of Earth-like exoplanets. The ExEP supports a community-based process to help NASA identify the needed technologies to achieve this goal and to mature the selected concepts to inform the 2020 Decadal Survey committee. This Appendix outlines technology development plans and activities that will lead toward that goal.

A new ExEP Technology Development Plan Appendix will be released each year to update the progress made in each technology area and to identify new SAT-TDEM and APRA opportunities.

F DOCUMENT CHANGE LOG

This section contains a log of changes to the ExEP Technology Development Appendix.

Date	Version	Author	Description
Jan. 27, 2016	Initial	N. Siegler	Initial signature version of this document.

G ACRONYMS

ACAD	Adaptive Correction of Aperture Discontinuities
AFTA	Astrophysics Focused Telescope Assets
AMTD	Advanced Mirror Technology Development
APLC	Apodized Pupil Lyot Coronagraph
APRA	Astrophysics Research and Analysis
ATLAST	Advanced Technology Large Aperture Space Telescope
BMC	Boston Micromachines Corporation
CIC	Clock-induced Charge
CTE	Coefficient of Thermal Expansion
DM	Deformable Mirror
EMCCD	Electron Multiplying Charge Couple Device
ExEP	Exoplanet Exploration Program
ExoPAG	Exoplanet Program Analysis Group
HabEx	Habitable Exoplanet Imaging Mission
HCIT	High Contrast Imaging Testbed
HDST	High Definition Space Telescope
HiCAT	High Contrast Imager for Complex Aperture Telescopes
HST	Hubble Space Telescope
IWA	Inner Working Angle
JWST	James Webb Space Telescope
LOWFS/C	Low-order Wavefront Sensor and Controller
LTF	Low-temperature Fusion
LTS	Low-temperature Slumping
LUVOIR	Large Ultra-Violet Optical Infrared
MEMS	Micro Electro Mechanical Systems
MKID	Microwave Kinetic Inductance Detectors
NG-VNC	Next Generation Visible Nulling Coronagraph
NICMOS	Near-Infrared Camera and Multi-Object Spectrometer
NWNH	New Worlds, New Horizons
PIAACMC	Phase-Induced Amplitude Apodization Complex Mask Coronagraph
PMN	Lead Magnesium Niobate
PSF	Point Spread Function
ROSES	Research Opportunities in Space and Earth Sciences
SBIR	Small Business Innovation Research
SIM	Space Interferometry Mission
SLS	Space Launch System
SOA	State of Art
SP	Shaped Pupil
SPLC	Shaped Pupil Lyot Coronagraph
STScI	Space Telescope Science Institute
TCOP	Technology Development for the Cosmic Origins Program
TDEM	Technology Development for Exoplanet Missions
ULE	Ultra-Low Expansion

VNC	Visible Nulling Coronagraph
WFC	Wavefront Control
WFIRST	Wide-Field Infrared Survey Telescope
WFSC	Wavefront Sensing and Control

H REFERENCES

[1] National Research Council. *New Worlds, New Horizons in Astronomy and Astrophysics*. Washington, DC: The National Academies Press, 2010, http://science.nasa.gov/astrophysics/special-events/astro2010-astronomy-and-astrophysics-decadal-survey/

[2] 2014 update to the Astrophysics Implementation Plan, http://science.nasa.gov/media/medialibrary/2015/01/16/ImpPlan_Rev2_15Apr2013_LL_150107TAGGED.pdf

[3] Exo-C and Exo-S Final Reports (2015); http://exep.jpl.nasa.gov/stdt/

[4] WFIRST-AFTA Home Page: http://wfirst.gsfc.nasa.gov/index.html

[5] NSPIRES APRA past awards: https://nspires.nasaprs.com/external/solicitations/solicitations.do?method=closedPastIni&stack=push

[6] ExEP Technology Website; http://exep.jpl.nasa.gov/technology/.

[7] Macintosh, B. et al. 2014, "First light of the Gemini Planet Imager", PNAS 111(35) 12661-12666 http://adsabs.harvard.edu/abs/2014PNAS..11112661M

[8] Project 1640: Gautam Vasisht, private comm (December 31 2015)

[9] Vigan, A., Gry, C., Salter, G., Mesa, D., Homeier, D., Moutou, C., and Allard, F., 2015, "High-contrast imaging of Sirius A with VLT/SPHERE: looking for giant planets down to one astronomical unit." MNRAS, 454, 129-143; http://adsabs.harvard.edu/abs/2015MNRAS.454..129V

[10] Lawson, P. R., Belikov, R., Cash, W., et al. 2013, "Survey of experimental results in high-contrast imaging for future exoplanet missions," Proc. SPIE 8864, 88641F, http://spiedigitallibrary.org/proceeding.aspx?articleid=1744192&resultClick=1.

[11] Moody, D. C., Gordon, B. L., & Trauger, J. T. 2008, "Design and demonstration of hybrid Lyot coronagraph masks for improved spectral bandwidth and throughput," Proc. SPIE 7010, 70103P, http://spiedigitallibrary.org/proceeding.aspx?articleid=787868&resultClick=1

[12] Trauger, J., Moody, D., Gordon, B., Krist, J., Mawet, D. 2011, "A hybrid Lyot Coronagraph for the direct imaging and spectroscopy of exoplanet systems," Proc. SPIE 8151, 81510G, http://spiedigitallibrary.org/proceeding.aspx?articleid=1342401&resultClick=1.

[13] Trauger, J. et al, TDEM-09 Final Report: http://exep.jpl.nasa.gov/files/exep/Lyot_TDEM_Report_121215_signed.pdf

[14] John Trauger; Dwight Moody; John Krist; Brian Gordon, 2015, "Hybrid Lyot coronagraph for WFIRST-AFTA: coronagraph design and performance metrics", J. Astron. Telesc. Instrum. Syst. 2016; 2(1):011013. doi: 10.1117/1.JATIS.2.1.011013, http://astronomicaltelescopes.spiedigitallibrary.org/article.aspx?articleid=2482759

[15] Eric Cady; Camilo Mejia Prada; Xin An; Kunjithapatham Balasubramanian; Rosemary Diaz; N. Jeremy Kasdin; Brian Kern; Andreas Kuhnert; Bijan Nemati; Ilya Poberezhskiy; A. J. Eldorado Riggs; Robert Zimmer; Neil Zimmerman, 2015, "Demonstration of high contrast with an obscured aperture with the WFIRST-AFTA shaped pupil coronagraph", J. Astron. Telesc. Instrum. Syst; 2(1):011004. doi: 10.1117/1.JATIS.2.1.011004, http://arxiv.org/pdf/1511.01882v1

[16] Neil T. Zimmerman; A. J. Eldorado Riggs; N. Jeremy Kasdin; Alexis Carlotti; Robert J. Vanderbei, 2016, "Shaped pupil Lyot coronagraphs: high-contrast solutions for restricted focal planes", J. Astron.

Telesc. Instrum. Syst; 2(1):011012. doi: 10.1117/1.JATIS.2.1.011012, http://astronomicaltelescopes.spiedigitallibrary.org/article.aspx?articleid=2482760

[17] Soummer, R. ApJ 618, L161 (2005); http://adsabs.harvard.edu/cgi-bin/nph-data_query?bibcode=2005ApJ...618L.161S&db_key=AST&link_type=ABSTRACT&high=5697e4cafa06758

[18] Pueyo & Norman ApJ 769, 31 (2013); http://adsabs.harvard.edu/cgi-bin/nph-data_query?bibcode=2013ApJ...769..102P&db_key=AST&link_type=ABSTRACT&high=5697e4cafa03070

[19] N'Diaye, M., Pueyo, L., & Soummer, R., ApJ 799, 13 (2015); http://adsabs.harvard.edu/cgi-bin/nph-data_query?bibcode=2015ApJ...799..225N&db_key=AST&link_type=ABSTRACT&high=5697e4cafa16543

[20] N'Diaye, M., Pueyo, L., Soummer, R. (2016, submitted)

[21] Neil T. Zimmerman; A. J. Eldorado Riggs; N. Jeremy Kasdin; Alexis Carlotti; Robert J. Vanderbei, 2016, "Shaped pupil Lyot coronagraphs: high-contrast solutions for restricted focal planes", J. Astron. Telesc. Instrum. Syst; 2(1):011012. doi: 10.1117/1.JATIS.2.1.011012, http://astronomicaltelescopes.spiedigitallibrary.org/article.aspx?articleid=2482760

[22] Kasdin, N. J., et al ApJ 582, 1147 (2003); http://adsabs.harvard.edu/cgi-bin/nph-data_query?bibcode=2003ApJ...582.1147K&db_key=AST&link_type=ABSTRACT&high=5697e4cafa23140

[23] Vanderbei, R. J., Spergel, D. N., Kasdin, N. J. ApJ 599, 686 (2003); http://adsabs.harvard.edu/cgi-bin/nph-data_query?bibcode=2003ApJ...599..686V&db_key=AST&link_type=ABSTRACT&high=5697e4cafa23140

[24] Carlotti, A., Vanderbei, R., Kasdin, N. J. Opt. Expr. 19, 26796 (2011), https://www.osapublishing.org/oe/viewmedia.cfm?uri=oe-19-27-26796&seq=0

[25] N'Diaye, M., Pueyo, L., & Soummer, R., ApJ 799, 225 (2015); http://adsabs.harvard.edu/cgi-bin/nph-data_query?bibcode=2015ApJ...799..225N&db_key=AST&link_type=ABSTRACT&high=5697e4cafa18208

[26] N'Diaye, M., Pueyo, L., Soummer, R. (2016, submitted)

[27] Ibid

[28] Ibid

[29] Guyon, O. 2003, "Phase-induced amplitude apodization of telescope pupils for extrasolar terrestrial planet imaging," Astron. Astrophys. 404, pp. 379–387, http://arxiv.org/pdf/astro-ph/0301190v2

[30] Guyon, O., Kern, B., Belikov, R., et al. 2012, "Phase Induced Amplitude Apodization (PIAA) coronagraphy: Recent results and future prospects," Proc. SPIE 8442, 84424V, http://spiedigitallibrary.org/proceeding.aspx?articleid=1362336&resultClick=1

[31] Kern, B., Guyon, O., Give'on, A., Kuhnert, A., Niessner, A. 2011, "Laboratory testing of a Phase-Induced Amplitude Apodization (PIAA) coronagraph," Proc. SPIE 8151, 815104, http://spiedigitallibrary.org/proceeding.aspx?articleid=1342434&resultClick=1

[32] Erkin Sidick; Brian Kern; Ruslan Belikov; Andreas Kuhnert; Stuart Shaklan; 2014, "Simulated contrast performance of Phase Induced Amplitude Apodization (PIAA) coronagraph testbed ", Proc. SPIE. 9143, 91430W, http://spiedigitallibrary.org/proceeding.aspx?articleid=1894760&resultClick=1

[33] Olivier Guyon et al., TDEM-09 Final Reports: http://exep.jpl.nasa.gov/technology/

[34] Olivier Guyon et al., TDEM-10 Final Report: http://exep.jpl.nasa.gov/technology/Guyon-PIAA-Milestone-3.pdf

[35] Dalcanton, J. et al. (2015) 2015arXiv150704779D; http://www.hdstvision.org/s/hdst_report_final_072715.pdf

[36] Serabyn et al. 2013, "High-contrast imaging with the vortex coronagraph," Proc. SPIE 8864, 8864–32, http://proceedings.spiedigitallibrary.org/proceeding.aspx?articleid=1744178&resultClick=1

[37] Eugene Serabyn, et al., "Demonstrations of Deep Starlight Rejection with a Vortex Coronagraph", TDEM-10 Final Report: http://exep.jpl.nasa.gov/technology/Serabyn_Final_2010.pdf

[38] Mawet, D. et al., 2011, "Recent results of the second generation of vector vortex coronagraphs on the high-contrast imaging testbed at JPL", Proc. SPIE 8151, 81511D, http://proceedings.spiedigitallibrary.org/proceeding.aspx?articleid=1268318&resultClick=1

[39] Mawet, D. et al., 2013, "The multistage and ring-apodized vortex coronagraph: two simple, small-angle coronagraphic solutions for heavily obscured apertures", 886411, http://proceedings.spiedigitallibrary.org/proceeding.aspx?articleid=1744180&resultClick=1

[40] Carlotti, A., et al., 2013, "Shaped pupil coronagraphy with WFIRST-AFTA", Proc. SPIE 8864, 886410, http://spiedigitallibrary.org/proceeding.aspx?articleid=1744179&resultClick=1

[41] Fogarty, K., Pueyo, L., and Mawet, D., 2014, "Optimal apodizations for on-axis vector vortex coronagraphs ", Proc. SPIE 9143, 914326, http://proceedings.spiedigitallibrary.org/proceeding.aspx?articleid=1894796&resultClick=1

[42] Mawet, D. et al., (2014), "Demonstration of vortex coronagraph concepts for on-axis telescopes on the Palomar Stellar Double Coronagraph", Proc. SPIE 9143, 91432T http://proceedings.spiedigitallibrary.org/proceeding.aspx?articleid=1894816&resultClick=1

[43] Mazoyer, J., et al, 2015, "Active correction of aperture discontinuities (ACAD) for space telescope pupils: a parametic analysis", Proc. SPIE 9605, 96050M, http://proceedings.spiedigitallibrary.org/proceeding.aspx?articleid=2443263&resultClick=1

[44] Ruane, G.J. et al, 2015, "Lyot-plane phase masks for improved high-contrast imaging with a vortex coronagraph", A&A 583 A81R http://www.aanda.org/articles/aa/abs/2015/11/aa26561-15/aa26561-15.html

[45] Clampin, M., et al, 2013, TDEM-9 Technology Milestone #1 Final Report, "Visible Nulling Coronagraph Technology Maturation: High Contrast Imaging and Characterization of Exoplanets", Jet Propulsion Laboratory Doc. D-68671 http://exep.jpl.nasa.gov/technology/Clampin_Report_FINAL.pdf

[46] Matt Bolcar, et al., TDEM-14 Abstract: "Next Generation Visible Nulling Coronagraph ", http://exep.jpl.nasa.gov/technology

[47] Chris Stark et al. 2015, "Lower Limits on Aperture Size for an ExoEarth Detecting Coronagraphic Mission", ApJ 808 149S, http://adsabs.harvard.edu/abs/2015ApJ...808..149S

[48] John W. Zinn; George W. Jones, 2007, "Kepler primary mirror assembly: FEA surface figure analyses and comparison to metrology"; Proc. SPIE 6671 667105, http://spiedigitallibrary.org/proceeding.aspx?articleid=816022&resultClick=1

[49] Gary W. Matthews ; Robert Egerman ; Steven P. Maffett et al, 2014, "The development of stacked core technology for the fabrication of deep lightweight UV-quality space mirrors";Proc. SPIE 9143, http://spiedigitallibrary.org/proceeding.aspx?articleid=1894787&resultClick=1

[50] Stahl, H. P., Postman, M., Smith, W. S. 2013, "Engineering specifications for large aperture UVO space telescopes derived from science requirements," Proc. SPIE 8860 06,

http://spiedigitallibrary.org/proceeding.aspx?articleid=1762023&resultClick=1

[51] Postman, M., et al., 2009, "Advanced Technology Large-Aperture Space Telescope (ATLAST): A Technology Roadmap for the Next Decade," http://www.stsci.edu/institute/atlast/documents/ATLAST_NASA_ASMCS_Public_Report.pdf

[52] Dalcanton, J. and Seager, S., et al. [From Cosmic Birth to Living Earths], Association for Universities for Research in Astronomy, Washington, DC, (2015).

[53] Gach et al. 2014, "Development of a 4k×4k frame transfer electron multiplying CCD for scientific applications", SPIE 9154 91540A, http://spiedigitallibrary.org/proceeding.aspx?articleid=1891356&resultClick=1

[54] Figer, D. 2010, et al., TDEM9 "Technology Milestone Final Report: A Photon-Counting Detector for Exoplanet Missions," Jet Propulsion Laboratory. D-93392; http://exep.jpl.nasa.gov/technology/TDEMReportFiger.pdf

[55] Rauscher, B. et al. 2015, "ATLAST detector needs for direct spectroscopic biosignature characterization in the visible and near-IR", SPIE 9602, 96020D, http://spiedigitallibrary.org/proceeding.aspx?articleid=2444184&resultClick=1

[56] Rauscher, B. et al. 2015, "ATLAST detector needs for direct spectroscopic biosignature characterization in the visible and near-IR", SPIE 9602, 96020D, http://spiedigitallibrary.org/proceeding.aspx?articleid=2444184&resultClick=1

[57] Atkinson, D., Hall, D., Baranec, C., Baker, I., Jacobson, S., and Riddle, R., 2014, "Observatory deployment and characterization of SAPHIRA HgCdTe APD arrays," SPIE 9154, 915419, http://spiedigitallibrary.org/proceeding.aspx?articleid=1891378&resultClick=1

[58] Mazin, B. A., et al., "A superconducting focal plane array for ultraviolet, optical, and near-infrared astrophysics," Opt. Express 20, 1503-1511 (2012), http://arxiv.org/pdf/1112.0004v1.pdf

[59] Private communications with Bernie Rauscher (December 2015)

[60] Rauscher, B. et al. 2015, "ATLAST detector needs for direct spectroscopic biosignature characterization in the visible and near-IR", SPIE 9602, 96020D, http://spiedigitallibrary.org/proceeding.aspx?articleid=2444184&resultClick=1

[61] Rauscher, B. et al. 2015, "ATLAST detector needs for direct spectroscopic biosignature characterization in the visible and near-IR", SPIE 9602, 96020D, http://spiedigitallibrary.org/proceeding.aspx?articleid=2444184&resultClick=1

[62] Albanese, M., et al. 2006, "Verification of the James Webb Space Telescope coarse phase sensor using the Keck Telescope," Proc. SPIE 6265 05, http://spiedigitallibrary.org/proceeding.aspx?articleid=1326681&resultClick=1

[63] Stahl, H. P., Postman, M., Smith, W. S. 2013, "Engineering specifications for large aperture UVO space telescopes derived from science requirements," Proc. SPIE 8860, http://spiedigitallibrary.org/proceeding.aspx?articleid=1762023&resultClick=1

[64] Stahl, M. T., Shaklan, S. B., Stahl, H. P. 2015, "Preliminary Analysis of effect of random segment errors on coronagraph performance," Proc SPIE 9605 0P, http://spiedigitallibrary.org/proceeding.aspx?articleid=2446862&resultClick=1

[65] Stahl, H. P., Postman, M., Smith, W. S. 2013, "Engineering specifications for large aperture UVO space telescopes derived from science requirements," Proc. SPIE 8860 06, http://spiedigitallibrary.org/proceeding.aspx?articleid=1762023&resultClick=1

[66] Gonzales, M. A., et al., "Unprecedented Vibration isolation Demonstration using the Disturbance Free

Payload Concept," AIAA 2004-5247, (2004), http://arc.aiaa.org/doi/pdf/10.2514/6.2004-5247

[67] Feinberg, L.D., et al. 2009, "Large segmented UV-optical space telescope using a Hybrid Sensor Active Control (HSAC) architecture," Proc. SPIE 7436 08, http://spiedigitallibrary.org/proceeding.aspx?articleid=785987&resultClick=1

[68] Pueyo, L, and Norman, C. 2013, "High-contrast Imaging with an Arbitrary Aperture: Active Compensation of Aperture Discontinuities ", ApJ 769, 102, http://adsabs.harvard.edu/cgi-bin/nph-data_query?bibcode=2013ApJ...769..102P&db_key=AST&link_type=ABSTRACT&high=5697e4cafa22878

[69] John Trauger; Dwight Moody; John Krist; Brian Gordon, *J. Astron. Telesc. Instrum. Syst.* 2016; 2(1):011013. doi: 10.1117/1.JATIS.2.1.011013

[70] Jeremy Kasdin, et al., TDEM-10 Final Report, "Integrated Coronagraph Design and Wavefront Control using Two Deformable Mirrors", http://exep.jpl.nasa.gov/technology/TDEM_Kasdin_D-93928.pdfhttp://exep.jpl.nasa.gov/technology/

[71] Private communication with John Trauger (December 2015).

[72] Enya, K., Abe, L., Takeuchi, S., et al., 2011, "A high dynamic-range instrument for SPICA for coronagraphic observation of exoplanets and monitoring of transiting exoplanets," Proc. SPIE 8146, 81460Q, http://spiedigitallibrary.org/proceeding.aspx?articleid=1342223&resultClick=1

[73] Mendillo, C. B., Hicks, B. A., Cook, T. A., et al. 2012, "PICTURE: a sounding rocket experiment for direct imaging of an extrasolar planetary environment," Proc. SPIE 8442, 84420E, http://spiedigitallibrary.org/proceeding.aspx?articleid=1362201&resultClick=1

[74] Clampin, M., et al, 2013, TDEM-9 Technology Milestone #1 Final Report, "Visible Nulling Coronagraph Technology Maturation: High Contrast Imaging and Characterization of Exoplanets", Jet Propulsion Laboratory Doc. D-68671, http://exep.jpl.nasa.gov/technology/Clampin_Report_FINAL.pdf

[75] Guyon, O., Schneider, G., Close, L., et al. 2011, "Technology Milestone #2 Whitepaper: Instrument Tip-Tilt Control Demonstration at the sub-Milliarcsecond Level," Jet Propulsion Laboratory Doc. D-71066. http://exep.jpl.nasa.gov/files/exep/Guyon_Milestone_WP2.pdf

[76] Shi, F. et al. 2015; "Low Order Wavefront Sensing and Control for WFIRST-AFTA Coronagraph", SPIE 9605 960509, http://spiedigitallibrary.org/proceeding.aspx?articleid=2443256&resultClick=1

[77] Soummer, R., et al., 2014, "Five Debris Disks Newly Revealed in Scattered Light from the Hubble Space Telescope NICMOS Archive," The Astrophysical Journal Letters 786 (23S), http://adsabs.harvard.edu/cgi-bin/nph-data_query?bibcode=2014ApJ...786L..23S&db_key=AST&link_type=ABSTRACT&high=5697e4cafa04593

[78] Menesson, D., 2015, "AFTA coronagraph performance feedback from post-processing studies to overall design," Proc. SPIE 9605, http://spiedigitallibrary.org/proceeding.aspx?articleid=2443259&resultClick=1

[79] Ygouf, M., et al., 2015, "Data processing and algorithm development for the WFIRST-AFTA coronagraph: reduction of noise free simulated images, analysis and spectrum extraction with reference star differential imaging" Proc. SPIE 9605 9605 0S, http://spiedigitallibrary.org/proceeding.aspx?articleid=2443266&resultClick=1

[80] Shaklan, S. B., Noecker, M. C., Glassman, T., et al. 2010, "Error budgeting and tolerancing of starshades for exoplanet detection," Proc. SPIE 7731, 77312G, http://spiedigitallibrary.org/proceeding.aspx?articleid=749972&resultClick=1

[81] Shaklan, S. B., Marchen, L., Lisman, P. D., et al. 2011, "A starshade petal error budget for exo-earth detection and characterization," Proc. SPIE 8151, 815113, http://spiedigitallibrary.org/proceeding.aspx?articleid=1268343&resultClick=1

[82] Schindhelm, E., Shipley, A., Oakley, P., et al. 2007, "Laboratory studies of petal-shaped occulters" Proc. SPIE 6693, 669305, http://spiedigitallibrary.org/proceeding.aspx?articleid=817922&resultClick=1

[83] Leviton, D. B., Cash, W. C., Gleason, B., et al. 2007, "White-light demonstration of one hundred parts per billion irradiance suppression in air by new starshade occulters." Proc. SPIE 6687 66871B, http://spiedigitallibrary.org/proceeding.aspx?articleid=817377&resultClick=1

[84] Lo, A. S., Glassman, T., Dailey, D., Sterk, K., Green, J., Cash, W., Soummer, R. 2010, "New Worlds Probe," Proc. SPIE 7731, 77312E, http://spiedigitallibrary.org/proceeding.aspx?articleid=749969&resultClick=1

[85] Samuele, R., Varshneya, R., Johnson, T. P., et al. 2010, "Progress at the starshade testbed at Northrop Grumman Aerospace Systems: comparisons with computer simulations," Proc. SPIE 7731, 773151, http://spiedigitallibrary.org/proceeding.aspx?articleid=750104&resultClick=1

[86] Cady, E. et al. 2010, "Broadband suppression and occulter position sensing at the Princeton occulter testbed." Proc. SPIE 7731, 77312F, http://spiedigitallibrary.org/proceeding.aspx?articleid=749970&resultClick=1

[87] Sirbu, D., Kasdin, N. J., Vanderbei, R. J., 2013, "Progress on optical verification for occulter-based high contrast imaging," Proc. SPIE 8864, 886419, http://spiedigitallibrary.org/proceeding.aspx?articleid=1744187&resultClick=1

[88] Glassman, T. et al., TDEM-12 Final Report, "Demonstration of Starshade Starlight-Suppression Performance in the Field"; http://exep.jpl.nasa.gov/files/exep/GlassmanTDEM2012_FinalReport.pdf

[89] Kasdin et al., TDEM-12 White Paper "Optical and Mechanical Verification of an External Occulter for Starlight Suppression", http://exep.jpl.nasa.gov/files/exep/Kasdin_OcculterTDEM_12_Milestone_signed.pdf

[90] Glassman et al., TDEM-12 Final Report, "Demonstration of Starshade Starlight-Suppression Performance in the Field"; http://exep.jpl.nasa.gov/files/exep/GlassmanTDEM2012_FinalReport.pdf

[91] Martin, S. R., Shaklan, S. B., Crawford, S. L., et al. 2013, "Starshade optical edge modelling, requirements, and laboratory tests," Proc. SPIE 8864, 88641A, http://spiedigitallibrary.org/proceeding.aspx?articleid=1744188&resultClick=1

[92] Casement et al., TDEM-12 Whitepaper "Starshade Stray Light Mitigation through Edge Scatter Modeling and Sharp-Edge Materials Development"; http://exep.jpl.nasa.gov/technology/casement_whitepaper.pdf

[93] John C. Stover, 2015, "Measuring and quantifying scatter from a variety of sample types ", Proc. SPIE. 9628, 96280K, http://spiedigitallibrary.org/proceeding.aspx?articleid=2443968&resultClick=1

[94] Cash, W., Kendrick, S., Noecker, et al., 2009, "The New Worlds Observer: the astrophysics strategic mission concept study," Proc. SPIE 7436, http://spiedigitallibrary.org/proceeding.aspx?articleid=785984&resultClick=1

[95] Scarf, D. et al. 2015 Precision Formation Flying at Megameter Separations for Exoplanet Characterization, 8th International Workshop on Satellite Constellations and Formation Flying, 8-10 June, 2015 (journal coming out in early CY16).

[96] Kasdin, J. et al., TDEM-13 Abstract "Formation Flying for External Occulters", http://exep.jpl.nasa.gov/technology/20013tdemabstractKasdin/

[97] Cash, W. et al., TDEM-13 Whitepaper "Development of Formation Flying Sensors", http://exep.jpl.nasa.gov/files/exep/CU_Whitepaper_v2.pdf

[98] Exo-S Final Report, http://exep.jpl.nasa.gov/stdt/

[99] Cash, W., Kendrick, S., Noecker, et al., 2009, "The New Worlds Observer: the astrophysics strategic mission concept study," Proc. SPIE 7436. http://spiedigitallibrary.org/proceeding.aspx?articleid=785984&resultClick=1

[100] Kasdin, J., TDEM-10 Final Report, "Verifying Deployment Tolerances of an External Occulter for Starlight Suppression", http://exep.jpl.nasa.gov/technology/KasdinTDEM10FinalReport.pdf

[101] Thomson, M., et al., TDEM-14 Abstract "Optical Shield for the Starshade Inner Disc Subsystem", https://exep.jpl.nasa.gov/files/exep/2014_tdem_thompson.pdf

[102] Exo-S Final Report, p.6-26, http://exep.jpl.nasa.gov/stdt/

[103] Cash, W. 2006, "Detection of Earth-like planets around nearby stars using a petal-shaped occulter," Nature 442, pp. 51–53, http://www.nature.com/nature/journal/v442/n7098/full/nature04930.html

[104] Vanderbei, R. J., Cady, E., & Kasdin, N. J. 2007, "Optimal Occulter Design for Finding Extrasolar Planets," Astrophys. J. 665, pp. 794–798, http://adsabs.harvard.edu/cgi-bin/nph-data_query?bibcode=2007ApJ...665..794V&db_key=AST&link_type=ABSTRACT&high=5697e4cafa02790

[105] Cady, E. 2011, "Nondimensional representations for occulter design and performance evaluation," Proc. SPIE 8151, 815112, http://spiedigitallibrary.org/proceeding.aspx?articleid=1268342&resultClick=1

[106] Lo, A., Cash, W., Hyde, T., Polidan, R., & Glassman, T. 2009, "Starshade Technology Development: Astro2010 Technology Development Whitepaper," ArXiv Astrophysics e-prints 2010, pp. 44+, http://www8.nationalacademies.org/astro2010/DetailFileDisplay.aspx?id=525